VUF-1035

VELA UNIFORM PROGRAM

STERLING EVENT

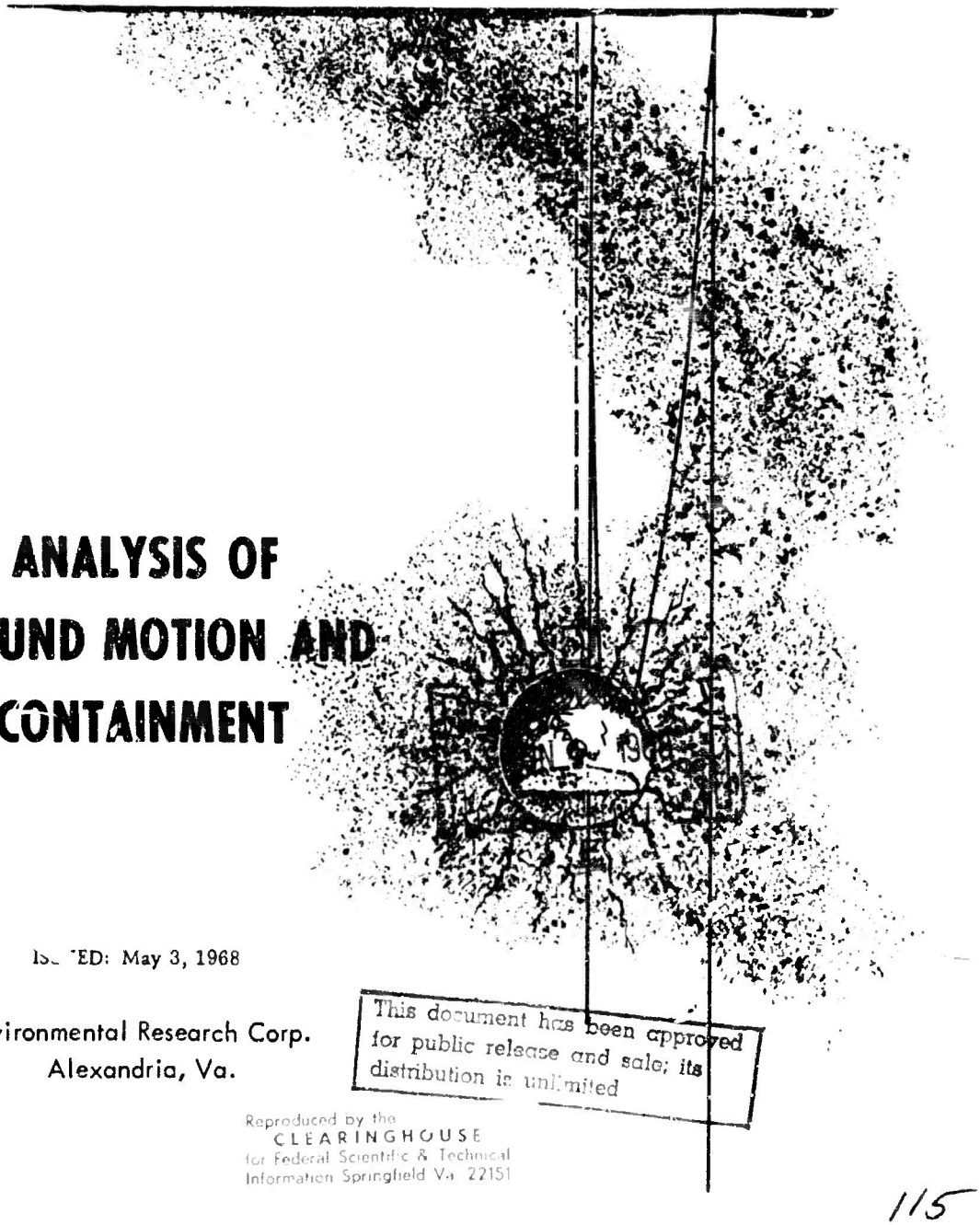

ANALYSIS OF GROUND MOTION AND CONTAINMENT

ISSUED: May 3, 1968

Environmental Research Corp.
Alexandria, Va.

ANALYSIS OF GROUND MOTION AND CONTAINMENT, STERLING EVENT,

by

Lawrence L. Davis

January 26, 1968

Environmental Research Corporation
813 North Royal Street
Alexandria, Virginia

Prepared under
Contract AT(29-2)-1163
for the
Nevada Operations Office
U. S. Atomic Energy Commission

LEGAL NOTICE

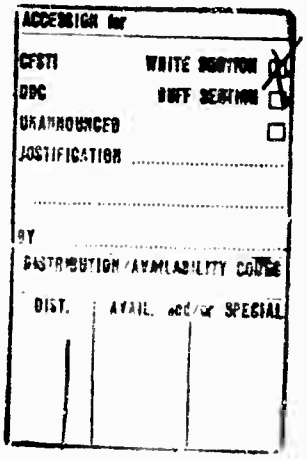

TABLE OF CONTENTS

TABLE OF CONTENTS (Continued)

INDEX OF TABLES

INDEX OF FIGURES

INDEX OF FIGURES (Continued)

INDEX OF FIGURES (Continued)

ABSTRACT

The pre-shot predictions and evaluations of ground motion, stemming and containment are presented and compared with the available observed data.

The analysis of seismic data included corrections for frequency response of the instruments, derivation of non-recorded motions by differentiation and integration, and filtering of the seismic signals to derive amplitude-frequency relationships. Seismic data were available from stations located between 2 to 32 kilometers from surface zero. Observed ground motions were lower than expected from a coupled (fully tamped) explosion of equal size. The peak accelerations and velocities displayed high rates of attenuation compared to Salmon. Relatively small azimuthal variations were observed. Peak motions were associated with frequencies between 3 and 80 hz. A noticeable decrease in frequency with increasing distance was observed. The purpose of Sterling was to test decoupling theory which predicts that seismic signals can be reduced by detonating a nuclear device in a large cavity. The observed decoupling effects were strongly frequency-dependent. At frequencies between 2 and 5 hz, particle velocities were reduced by a factor of about 200. Outside this range, observed decoupling factors decreased exponentially with frequency. The observed

frequency dependence of the decoupling factor was found to agree with decoupling theory.

The prediction of containment and evaluation of the stemming plan were substantiated by the test results. No other post-shot data were available for comparison.

CHAPTER 1

INTRODUCTION

1.1 BACKGROUND

Environmental Research Corporation, under contract to the Nevada Operations Office of the U. S. Atomic Energy Commission, is responsible to the Safety Evaluation Division of that office for providing safety evaluations of underground nuclear detonations. Specific tasks for which this organization is responsible include predictions of close-in phenomenology as it relates to containment, overall containment evaluations, predictions of ground motion, and reduction and analysis of seismic data.

The Sterling event took place on December 3, 1966 at 06:15 hours CST in the Tatum Salt Dome in Lamar County, Mississippi. The nuclear device was designed to have a yield of 0.36 kilotons and a maximum probable yield of 0.44 kilotons. The actual yield was estimated to be 0.35 kt (Reference 1.1). It was located at a depth of 828 meters in the center of the cavity created by the Salmon event. Detailed descriptions of the Salmon cavity can be found in References 1.2 and 2.10.

The purpose of the Sterling experiment was to test decoupling theory which states that seismic signals can be reduced by detonation of the device in a cavity. The

decoupling factor is defined as the ratio of the ground motion amplitudes (particle acceleration, displacement, and velocity) from a tamped (fully coupled) event to the amplitudes from a decoupled event of equivalent yield. The amount of decoupling is dependent on the ratio of the yield to the cavity volume, and to some extent on the frequency of the generated seismic signals. The degree of decoupling expected from the Sterling event was calculated by the Lawrence Radiation Laboratory to be between factors of 20 and 160, depending on the amount and the effects of the Salmon-caused alteration of the material forming the cavity wall (Reference 1.2).

1.2 OBJECTIVES

The objectives of ERC's participation in Project Sterling were to provide the Safety Evaluation Division of the USAEC/NVOO with:

1. Pre-shot predictions of
   a. Close-in phenomenology affecting containment.
   b. Peak ground motions.
2. Post-shot
   a. Reduction and analysis of seismic data.
   b. Comparisons of predictions and observed results.

1.3 THEORY

The evaluation of containment was based on procedures developed as part of a Long-Range Program directed to the continuing improvement of confidence in predictions. Currently, greater dependence is placed on empirical relationships, and it is probable that experience will always be a major factor in evaluation. However, a large part of the improvement will come from greater knowledge of the pressure-time history and temperature-time history of underground explosions. This is being pursued, and some of the results were employed in the development of predictions and the evaluation for Sterling.

The predictions of ground motion were based, to a large degree, on experience gained from the Salmon event which was detonated at the same location. Except for the cavity and the alteration of the rock adjacent to the cavity, the geologic environment affecting transmission of seismic energy from the Sterling event was identical with that of the Salmon event. Therefore, the predicted attenuation of amplitude with distance was taken from the regression lines through the data from Salmon.

The Sterling yield was accounted for by use of cube-root scaling relationships to scale from Salmon (5 kt) to Sterling, .36 kt. This was considered appropriate because the predictions for Salmon (which agreed with the data)

were made using the same procedure to scale from Gnome, 3 kt, to Salmon. The remaining consideration was the amount of decoupling which might occur as a result of the Sterling event being detonated in the Salmon-created cavity. Scaling from Salmon provides predictions which would be applicable only if Sterling were fully coupled. Because the amount of decoupling was the purpose of experiment it was not possible to know in advance how much decoupling might occur. In order to make predictions which would be more realistic, the fully coupled predictions were divided by a decoupling factor. The Sterling Technical Concept (Reference 1.2) stated that the decoupling factor was estimated to be between 20 and 160, depending on the alteration of the cavity wall caused by Salmon. To provide Safety Evaluation Division, NVOO, with ground motion estimates which would account for decoupling effects and at the same time would be conservative for safety purposes, the smallest decoupling factor (20) given in the Technical Concept was used. Peak accelerations, displacements, and velocities predicted for the tamped (fully coupled) situation were divided by this decoupling factor to provide the predicted peak motions for the decoupled Sterling event. No attempt was made to consider the frequency dependence of the decoupling factor in the pre-shot predictions.

CHAPTER 2

PROCEDURE

2.1 GEOLOGIC ENVIRONMENT

2.1.1 Location and Topography

The site of the Sterling event was within the Tatum Salt Dome, Lamar County, Mississippi. The Tatum surface area is about 75 to 100 meters above sea level. The surface is moderately dissected with narrow, flat-topped ridges rising about 30 meters above intervening valleys. The hills are well drained, but usually the bottomlands are wet during most of the year. The principal streams in the area are Half Moon and Grantham Creeks which flow into Lower Little Creek about one or two kilometers north of the dome (Reference 2.1). The area immediately over the dome is a topographic low.

2.1.2 Regional Geology

Formations outcropping in the state of Mississippi are of upper Cretaceous and Tertiary age. The older formations, exposed along the northern edge of the state, are overlain to the south-southwest by progressively younger beds which outcrop in roughly parallel bands. In general, the formations thicken to the south-southwest. Younger beds dip about 1.9 meters per kilometer to the south, whereas dips on the base of the older, deeper Eocene beds are about 6.6 meters per kilometer southward (Reference 2.1).

Tatum dome is a large buried salt stock that has pierced sedimentary deposits of early Cretaceous to Oligocene (middle Tertiary) age. Sediments of Miocene age surround and overlie the dome, but are thinner over the dome than in the surrounding area. Rocks of Eocene age are absent on the crest of the dome (Reference 2.2). Regional strikes and dips are locally disturbed around the dome.

2.1.3 Local Stratigraphy and Lithology

Stratigraphic relations over and around the dome are shown in the attached cross section (Figure 2.1), which extends southwest through the dome. Figure 2.2 shows the location of this section.

Figure 2.3 is a generalized columnar section at Station 1A, the location of the Sterling event. Abbreviated lithologic descriptions of the various rock types in the dome area are given on this figure. The sediments over the dome are mainly sands, clays and silts in varying mixtures. The true caprock which underlies the Catahoula Sandstone is composed of two dominant lithologic units. The upper unit is fine- to medium-grained, crystalline limestone. The limestone contains zones of high permeability in which varying quantities of drilling fluid were reported lost while drilling. It also contains some lenses of medium-grained, calcareous, loose sand. This sand may be either contained as

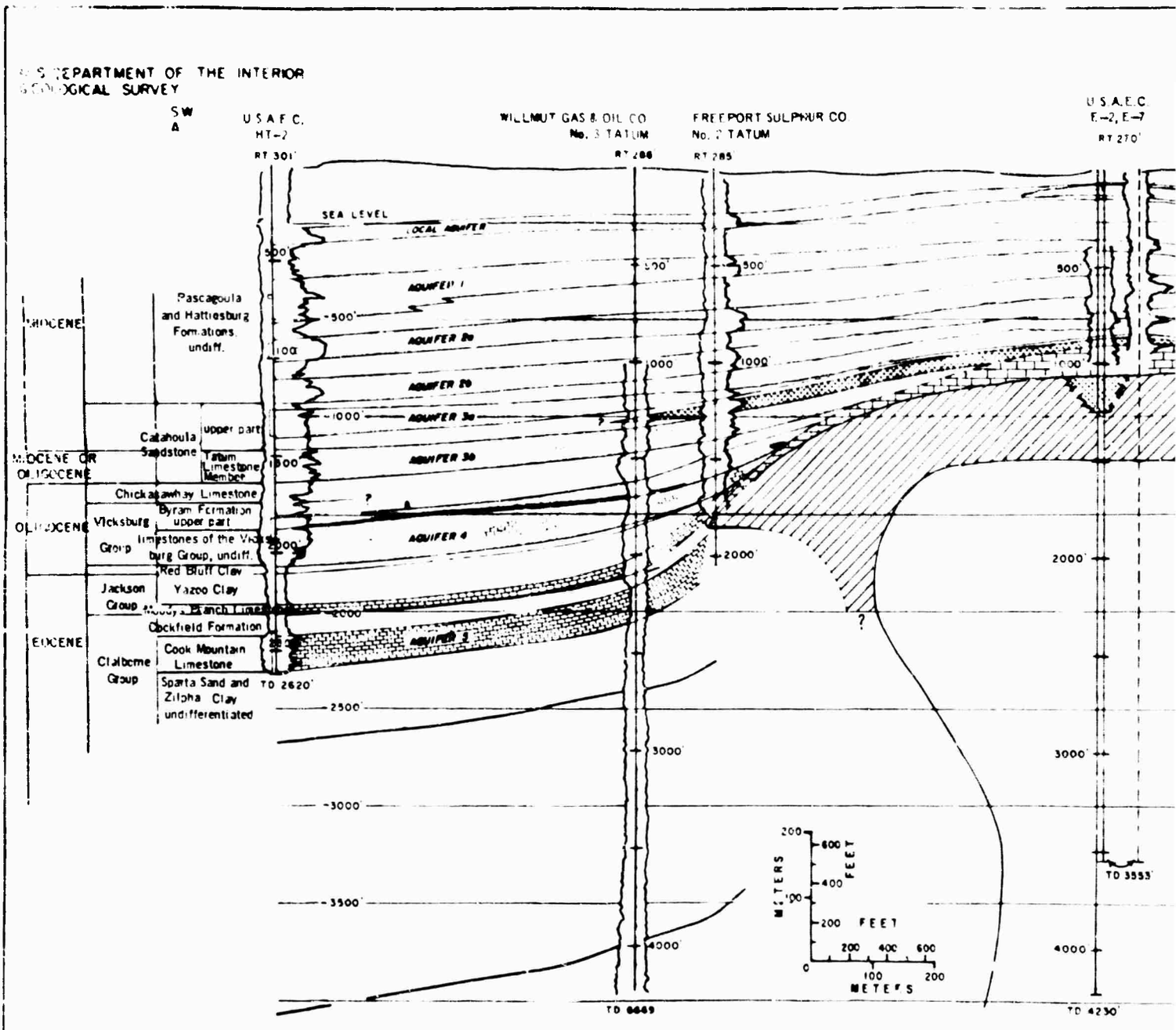

FIGURE 2.1 – SOUTH

Drafted by B. O Davis
U.S.G.S. Austin, Texas
February 26 1963

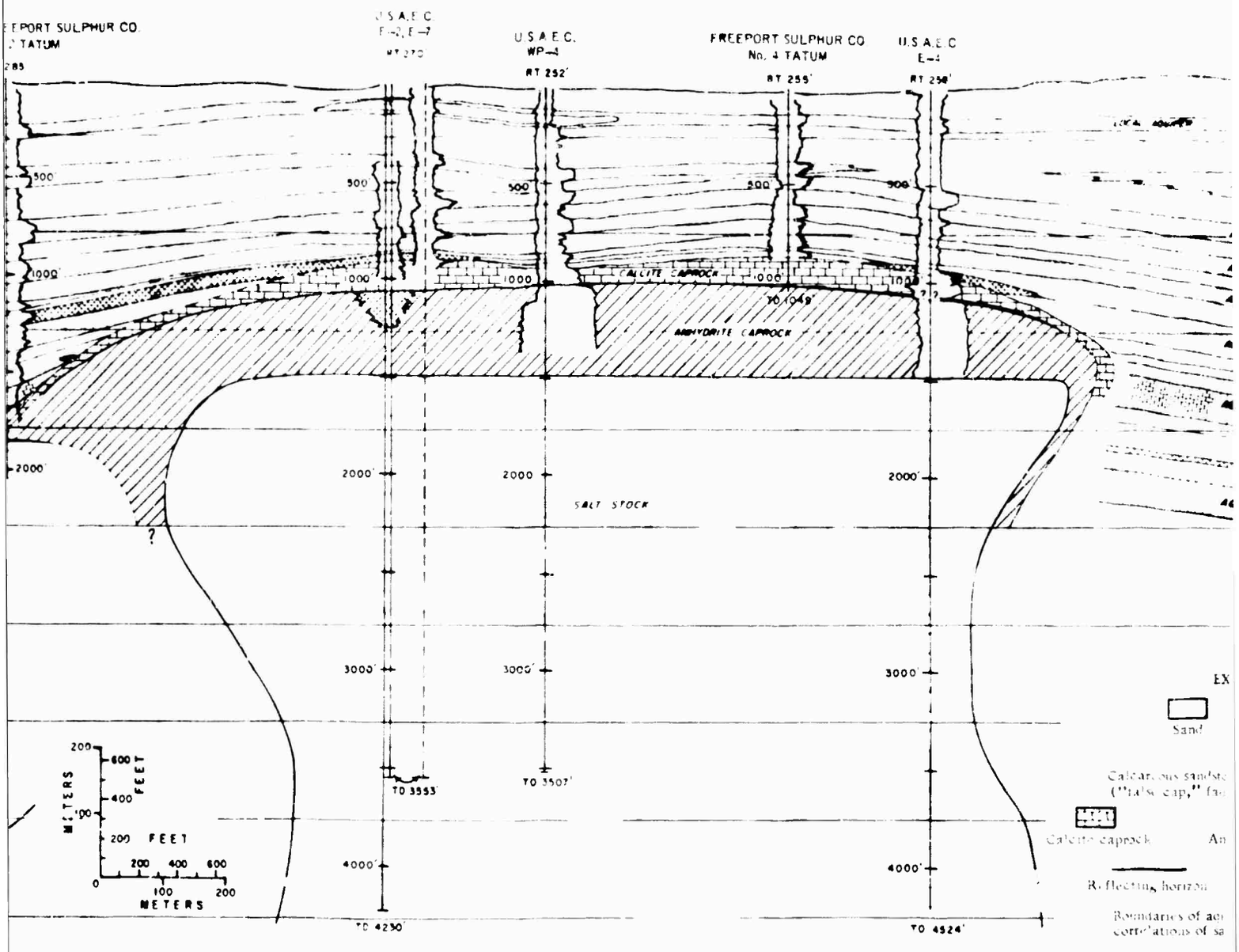

FIGURE 2.1 – SOUTHWEST–NORTHEAST SECTION THROUGH TATUM DOME

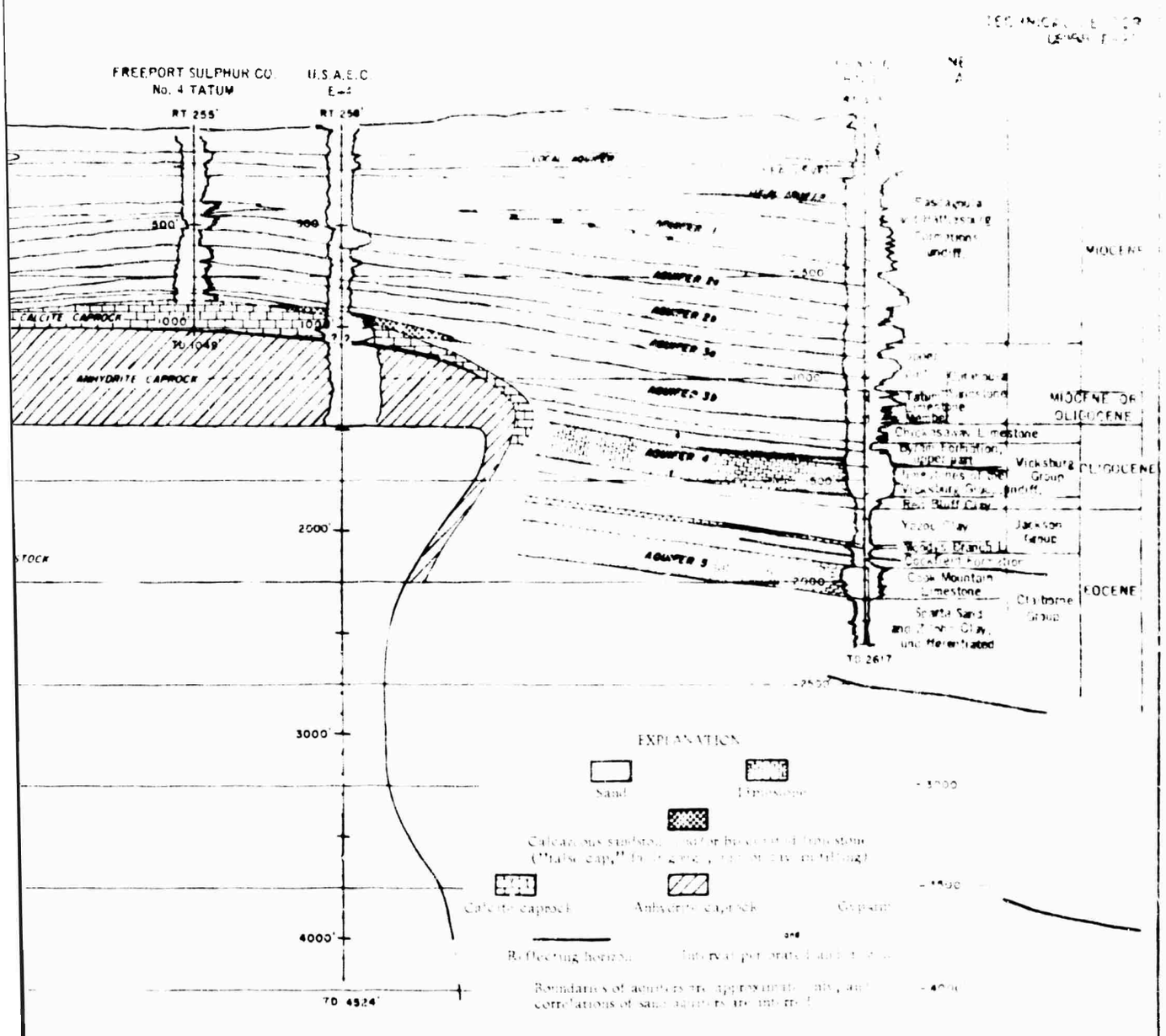

AST SECTION THROUGH TATUM DOME

Modified after Figure 2,
USGS Tech Letter,
DRIBBLE-29, April 3, 1963

B

C

BLANK PAGE

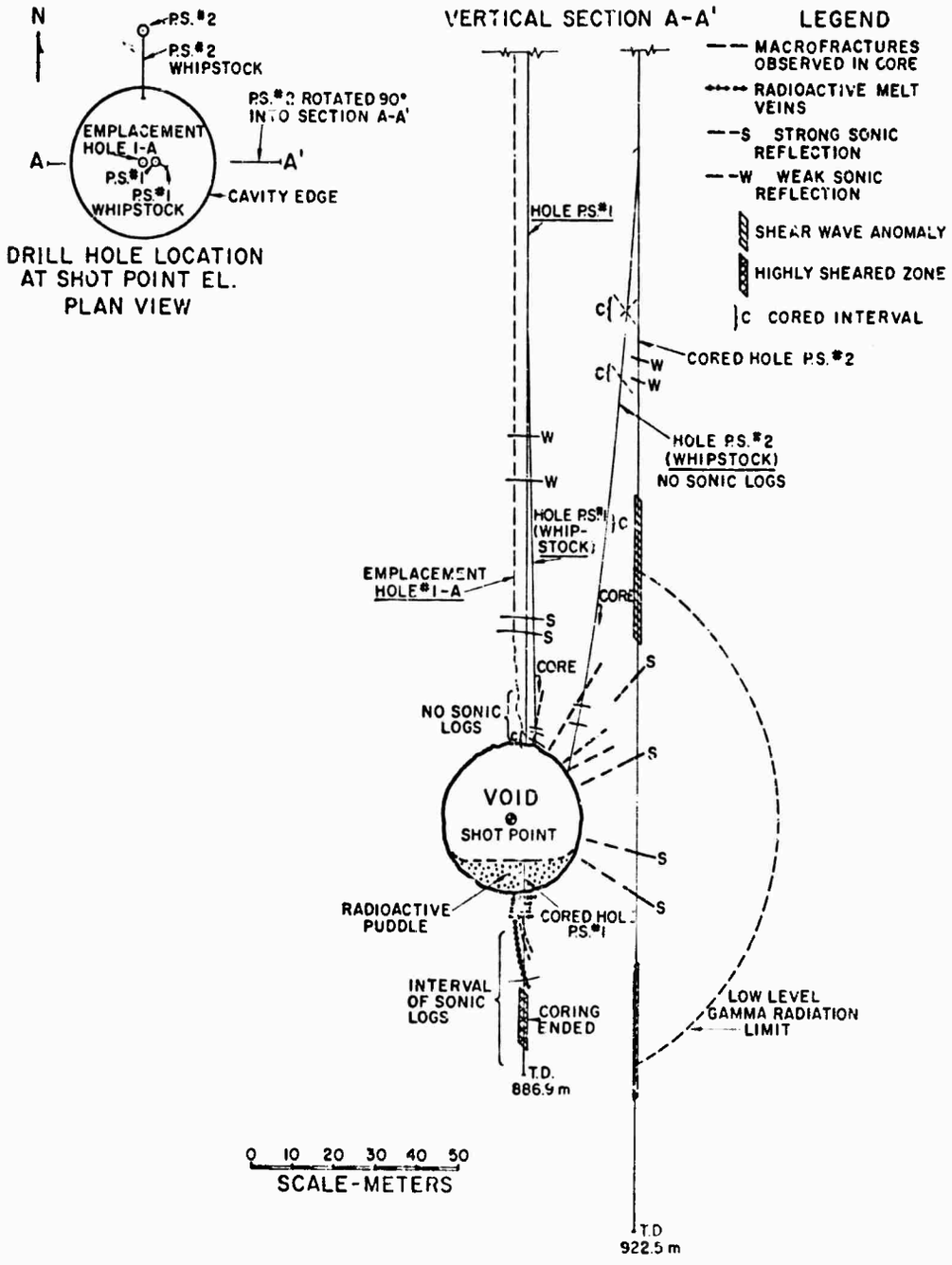

Figure 2.4 Vertical section of the Salmon postshot environment with plan view showing locations of drill holes. (Taken from Reference 2.10)

TABLE 2.1

PHYSICAL PROPERTIES: Tatum Salt Dome
Section Over Dome

Rock Unit	Compressional Velocities (meters/sec)			Natural Bulk Density (g/cc)		
	min.	max.	mean	min.	max.	mean
Coastal Terrace Deposits	--	--	365.8[d]	1.9[j]	2.05[j]	1.98
Pascagoula & Hattiesburg	1752.6[a]	1874.5[a]	1809.0	1.60[e]	2.21[e]	1.93[e]
Catahoula Sandstone	1905.0[a]	2383.5[a]	2142.7	1.88[e]	2.56[e]	2.05[e]
Limestone	2377.4[a]	4724.4[a]	3301.0	2.24[f]	2.71[f]	2.47[f]
Gypsum	2539.0[b]	2651.8[b]	2595.4	2.2[j]	2.4[j]	2.3
Anhydrite	5547.4[a]	5861.3[a]	5699.8	2.85[f]	2.92[f]	2.90[f]
Salt	4358.6[a]	4550.7[a]	4480.6[a,g]	2.13[d]	2.215[d]	2.181[j]

Porosity and Elastic Properties of Salt

	min.	max.	mean
Porosity %	1.53[h]	8.59[h]	3.61[h]
Poisson's Ratio	0.215[g]	0.267[g]	0.239[g]
Shear Modulus (kilobars)	133.[g]	149.[g]	142.[g]
Young's Modulus (kilobars)	325.[g]	371.[g]	348.[g]
Bulk Modulus (kilobars)	224.[g]	244.[g]	230.[g]
Tensile Strength (kilobars)	5860.	10140.	8280.
Compressive Strength (kilobars)			
Standard	3050.[h]	3700.[h]	3330.
L/D* = 1/1	4140.[h]	4450.[h]	4250.
L/D = 3/1	3240.[h]	3450.[h]	3393.

*L/D = Length/Diameter Ratio

References Listed on Table 2.2

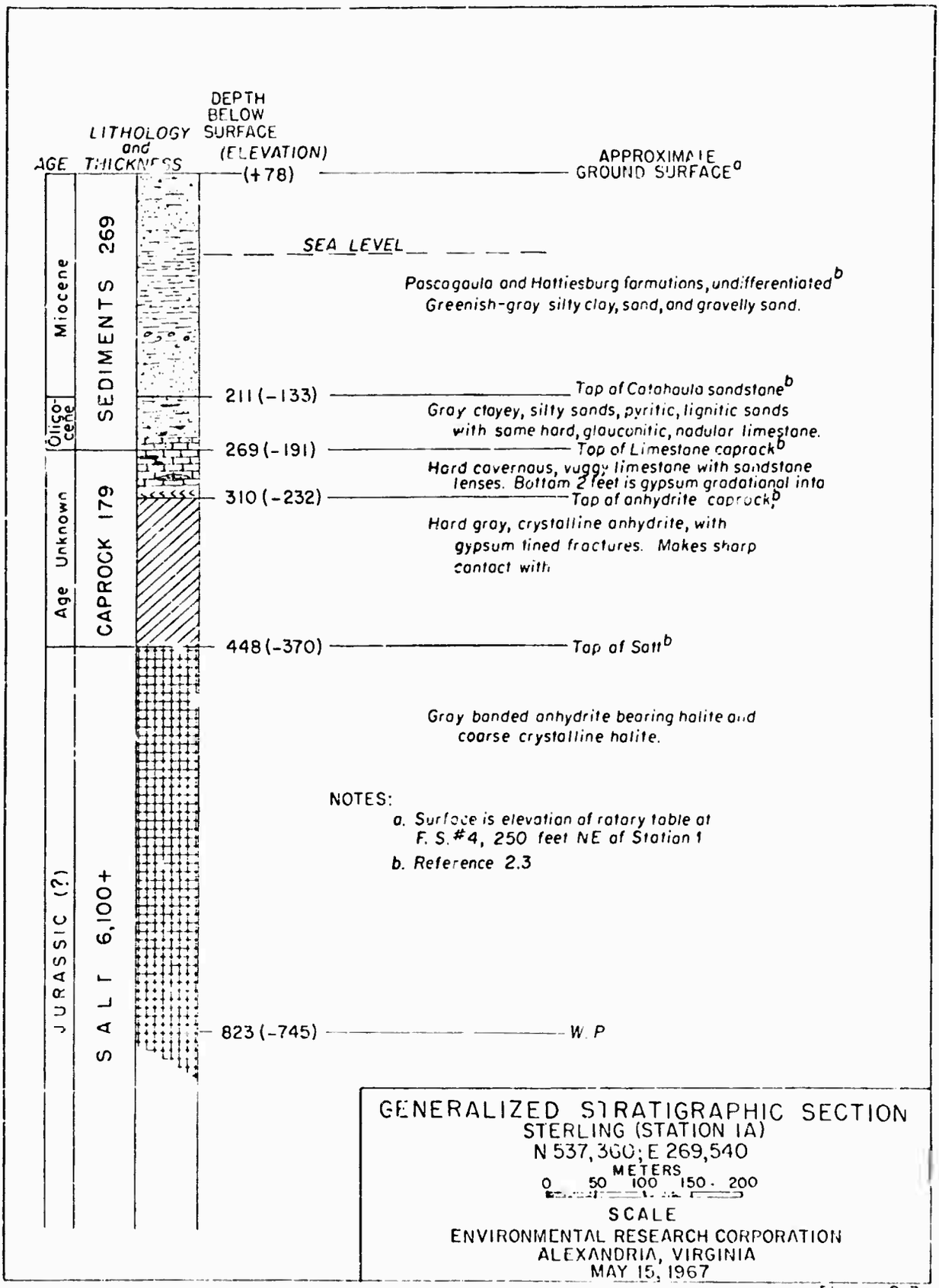
AGE
LITHOLOGY and THICKNESS
DEPTH BELOW SURFACE (ELEVATION)
(+78)
APPROXIMATE GROUND SURFACE[a]
SEA LEVEL
Miocene
SEDIMENTS 269
Pascagoula and Hattiesburg formations, undifferentiated[b]
Greenish-gray silty clay, sand, and gravelly sand.
Oligocene
211 (-133)
Top of Catahoula sandstone[b]
Gray clayey, silty sands, pyritic, lignitic sands with some hard, glauconitic, nodular limestone.
269 (-191)
Top of Limestone caprock[b]
Hard cavernous, vuggy limestone with sandstone lenses. Bottom 2 feet is gypsum gradational into
310 (-232)
Top of anhydrite caprock[b]
Age Unknown
CAPROCK 179
Hard gray, crystalline anhydrite, with gypsum lined fractures. Makes sharp contact with
448 (-370)
Top of Salt[b]
Gray banded anhydrite bearing halite and coarse crystalline halite.
JURASSIC (?)
SALT 6,100+
NOTES:
a. Surface is elevation of rotary table at F. S. #4, 250 feet NE of Station 1
b. Reference 2.3
823 (-745)
W. P
GENERALIZED STRATIGRAPHIC SECTION
STERLING (STATION 1A)
N 537,360; E 269,540
METERS
0 50 100 150 200
SCALE
ENVIRONMENTAL RESEARCH CORPORATION
ALEXANDRIA, VIRGINIA
MAY 15, 1967

Figure 2.3

lenses within the limestone or as interfingering lenses of the Catahoula Sandstone with the caprock limestone (Reference 2.3). In some places, the limestone has been leached, forming channels and vugs. The lower 6 meters of the limestone (in WP-4) consist of vuggy brecciated black calcitic limestone.

The limestone at its base grades into several feet of gypsum which in turn grades down into the anyhydrite which composes the lower dominant lithologic unit of the caprock. The anhydrite is hard and finely crystalline. In WP-4, the upper part of the anhydrite has been highly fractured, and gypsum veins line the slickensided surfaces. Its basal contact with the salt is sharp. The salt varies from anhydrite-bearing halite to transparent, very coarse crystalline, almost pure halite. The salt is banded with nearly vertical alternating thin bands of anhydrite-bearing halite and almost pure halite (Reference 2.4).

Tabulations of Pre-Salmon drill hole information and lithologic logs are shown in Tables 3.3.1 and 3.3.2 of Reference 2.5. Pre-Salmon holes are shown on Figure 2.2. Post-Salmon holes are shown on Figure 2.4 (taken directly from Reference 2.10) and are discussed in Section 2.2.

2.1.4 Physical Properties

Physical properties for the salt and surrounding sediments are compiled in Tables 2.1 and 2.2. Changes in physical

TABLE 2.2

PHYSICAL PROPERTIES: Tatum Salt Dome
Section Beside Dome

Rock Unit	Compressional Velocity (meters/sec) min.	max.	mean	Natural State Bulk Density (g/cc)
Coastal Terrace deposits	--	--	365.8[d]	1.98[j]
Pascagoula & Hattiesburg fms.	1920.2[c]	1953.8[c]	1941.6	1.93[e]
Catahoula Sandstone	2286.0[c]	2499.4[c]	2392.7	2.05[e]
Paynes Hammock & Chickasaway	2103.1[c]	2164.1[c]	2133.6	2.5[k]
Upper Vicksburg	2057.4[c]	2316.5[c]	2138.2	2.2[j]
Lower Vicksburg	3109.0[c]	3596.7[c]	3352.8	2.5[k]
Red Bluff Clay	2651.8[c]	2895.6[c]	2773.7	2.2[j]
Yazoo Clay	2103.1[c]	2255.5[c]	2145.8	2.2[j]
Moody's Branch fm.	2651.8[c]	3261.4[c]	3026.7	2.5[k]
Cockfield fm.	1981.2[c]	2240.3[c]	2133.6	2.2[j]
Cook Mountain fm.	2956.6[c]	3276.6[c]	3144.0	2.1[j]

References:
a. In hole Velocity logs on dome (see Tables 1 and 2)
b. In hole Velocity log WP-1, tabulated, in DR-19
c. In hole Velocity logs off dome (HT-1, HT-2, Humble Hibernia #1)
d. Seismic Profile of the Southeast Flank of the Tatum Salt Dome, UED Inc., Dec. '62
e. Gamma gamma density log, HT-3
f. Gamma gamma density log, E-15
g. Memo: D. M. Christensen, LRL-N May 14, 1963
Statistical Summary of Calculations from in hole Velocity logs: E-14, E-15, WP-1
h. RFB 4085, Petrographic Examination and Physical Tests of Cores, Tatum Salt Dome, Mississippi, Table 6, WES, Jan. 1963
j. Birch, Francis, 1942 Handbook of Physical Constants, GSA sp. paper 36
k. Heiland, C. A., 1946, Geophysical Exploration, Prentice-Hall

Unmarked means are by compiler.

properties in the immediate area of the existing cavity are discussed at length in Reference 2.10.

2.1.5 Structure

The enclosed cross section (Figure 2.1), extending southwest through HT-1 and HT-2, shows the structural relations across the dome.

Faulting of the caprock is indicated in the vicinity of E-7 (See Figure 2.1). There, a 41 meter section of brecciated sandstone, calcite conglomerate and black chert gravel was found here the anhydrite would normally be. As previously mentioned, numerous fractures are present in the anhydrite. For a discussion of fractures due to the Salmon event, see Reference 2.10 and Section 2.2 of this report.

Although little mention of jointing is made specifically in the literature, it seems reasonable to expect its moderate development in the more brittle lithologic types including sandstones, limestones, anhydrites and gypsum. The salt within the dome is essentially free from jointing and fracturing, with the exception of Salmon-induced fracturing as mentioned above.

2.1.6 Hydrology

A complete review of the hydrology of the dome area is contained in Reference 2.2 (Pre-Salmon) and Reference 2.7 (Post-Salmon).

Post-shot data indicate that the Salmon event was essentially contained within the salt matrix of the (Tatum) dome and no explosion-produced radioactivity had been detected in the aquifers (Reference 2.7).

2.2 PHENOMENOLOGY AND CONTAINMENT PREDICTIONS

2.2.1 Cavity Radius

The device for the Sterling event was placed in the center of the approximately spherical Salmon cavity. The horizontal radius of the cavity was about 16.5 meters (Reference 2.8).

It was assumed that the total energy for this event would be suddenly distributed uniformly throughout the volume of the chamber. Therefore, the resulting initial equilibrium pressure on the chamber walls could be estimated on the basis of the work done in an adiabatic process. Thus

$$p = \frac{(\alpha-1)W}{V} = 189 \text{ bars}$$

where $\alpha = 1.2$ for air, $W = .44$ kt and $V = 1.96 \times 10^{10}$ cm^3.

The total heat in the explosion, based on a yield of .5 kt, is 4.4×10^{11} calories. Neglecting the very small contribution from the metal of the device and any steam from contained water, the energy density was computed as follows:

$$\frac{\text{Yield}}{V \times \alpha_{air}} = \frac{4.4 \times 10^{11}}{1.96 \times 10^{10} \times 1.293 \times 10^{-3}} = 1.74 \times 10^{4} \text{ cal/gm}$$

This corresponded to a temperature of 22000°K (see Appendix A, Table A1, Internal Energy Table). An indication of the rate of temperature changes for a .5 kt explosion in a 14.2 meter radius cavity was obtained from Appendix D of Reference 2.9. Conditions for this calculation were considered to be close enough to those for Sterling to be indicative. The vaporization of the salt would cause a rapid drop in temperature. Cooling would occur at a rate such that the vaporized salt would condense in about 60 seconds, based on the vaporization temperature of 2500°K stated. From that time, continued melting would reduce the temperature to the melting point of 1059°K. Solidification would begin at about 2 hours (Figure A1, Appendix A) and from that point cooling would proceed slowly.

Computation shows that 281 cal/gm is required to raise salt to the melting point and to melt it. Deducting the internal energy in the cavity at the melting point and assuming that the remaining heat would be used in melting, it was estimated that the thickness of salt removed would be 20 cm.

At initial high pressures, some crushing and spalling of the salt in the cavity walls was anticipated. This, added to melting, was predicted to result in a total increase in cavity radius of about 30 cm.

2.2.2 Relationship of Internal and Overburden Pressure

The maximum theoretical pressure of 189 bars slightly exceeded the overburden pressure of 182 bars. However, it was felt that if this theoretical maximum were achieved, it would exceed overburden pressure only for a very short time. The temperature drop to reduce the pressure from 189 bars to 182 would be about 1600°K. Figure A2, Appendix A, indicated that such a reduction in temperature would occur within milliseconds. As further check, a calculation was made of the pressure following condensation of the salt. At this time all the metal from the canister would have condensed as well, since the vaporization temperature is higher for steel than salt. Using the energy density for air at 2500°K, namely, 554 cal/gm, the pressure was computed to be 6 bars. As indicated previously, this condition would be reached in about 60 seconds.

From the above, it was apparent that the pressure in the cavity would be reduced below overburden almost instantaneously and to a very low pressure in about one minute. Furthermore, the largest theoretical pressure was predicted without consideration for any energy loss by vaporization and melting of halite. With conservative consideration of energy loss, a realistic estimate of the peak pressure

indicated that it would probably not exceed the overburden pressure.

2.2.3 Cracking Radius

Observed fractures from the Salmon event were found to extend 120 meters from the weapon point (Reference 2.10). The fracture radius of Sterling was expected to be much less, and extension of Salmon fractures by the Sterling event was not anticipated.

2.2.4 Radius of Radiation Injection into Cracks

Radioactivity was found at 37 meters from the Salmon W.P. (Reference 2.10). Extent of Sterling radioactivity was expected to be much less.

2.2.5 Surface Spalling

The depth of spall for a tamped event of the yield of Sterling would be considerably less than the 12 meters measured at Salmon (Reference 2.11) because of the reduced motion at ground zero. With a decoupled event the motions, and consequently the depth of spall, would be reduced further. Therefore, spall depth was considered insignificant to containment for Sterling.

2.2.6 Chimney Height

Neither Gnome nor Salmon produced a chimney. Therefore, no chimney was expected from Sterling.

2.2.7 Analysis of Stemming

Stemming for the Sterling emplacement hole is shown in Figure 2.5. The hole was filled with normal sand stemming, reinforced at the bottom by a 157 meter grout plug.

Because of the length of this plug in relation to the small magnitude of close-in deformation effects, it seemed certain that the plug's integrity would be essentially unaffected by the blast. As a safeguard against the unlikely possibility of minor seepage, a 1.5 meter thick charcoal layer was placed immediately above the plug to diminish any escaping radioactivity. A similar charcoal layer was placed near the top of the stemming with 1.5 meters of impermeable polymer above it.

In light of the conservative features of its design, the stemming was considered fully adequate.

The two post-shot Salmon drill holes were completely grouted, eliminating the hazard of leakage through these holes.

2.2.8 Damage to Grout Seals and Aquifer Contamination

The results from the Salmon event indicated that, as predicted, neither grout seal damage nor aquifer contamination occurred (Reference 2.11). Because it was predicted that cracking and radioactive injection into cracks caused

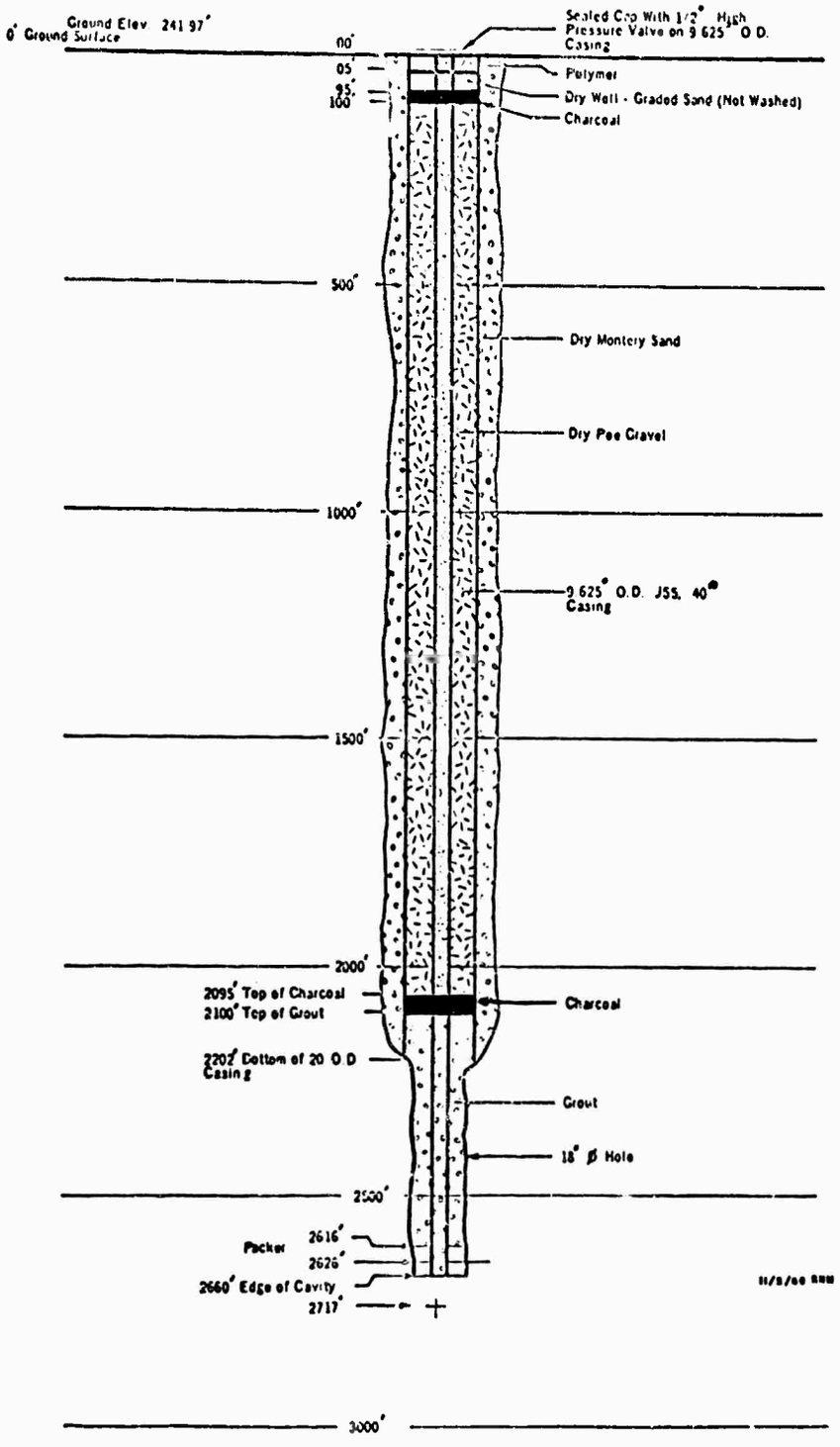

Figure 2.5 Sterling Stemming Plan
(Redrawn for Reproduction from Reference 2.6)

by the Sterling event would not exceed the effects caused by Salmon, no hazards to grout seals or aquifers were anticipated.

2.2.9 Containment Evaluation

The depth of burial of 828 meters provided a scaled depth of 1,088 meters. Peak cavity pressure was assumed to be less than overburden pressure. Even the largest theoretically calculated pressure would exceed overburden only slightly and for only a few milliseconds. With complete stemming, therefore, gross dynamic venting appeared unlikely.

Minor leakage also appeared unlikely. The device was under 366 meters of impermeable salt and significant fissuring was not anticipated. Illustrative of the impermeability of the medium was the vacuum maintained in the Salmon cavity up until drill-back several months after detonation. Accordingly, the chance of escape of cavity gases through the halite was considered to be extremely remote. Stemming, which was continuous to the surface and included concrete plugs, was considered to be adequate. Assuming effective grouting of the casing, the possibility of leakage appeared small.

On the basis of the foregoing evaluations and the assumption that construction and emplacement would be accomplished in accordance with the proposed plans, it was

predicted that the Sterling event with a yield of 44 kt would be contained.

2.3 SEISMIC PREDICTIONS

2.3.1 Transmission Model

As it was located in the Salmon post-shot cavity, the Sterling event was expected to generate seismic waves which would be transmitted through the same regional geologic environment as those generated by the Salmon event. With the exception of the immediate vicinity of the source where a cavity existed and the surrounding salt had undergone some degree of alteration, the physical properties of this environment were considered to be the same as at the time of the Salmon event. To evaluate fully the effect of these differences would have required a detailed knowledge of the degree of alteration beyond the cavity wall. Even if this information had been available, the effort required to evaluate the effects would have been out of proportion to the total effort necessary to evaluate Sterling in terms of safety hazards. Therefore, it was assumed that Salmon experience was directly applicable to the Sterling event except for the decoupling factor. The Salmon predictions fitted the observed data for that event quite well (Reference 2.11).

The Salmon predictions utilized cube root scaling relationships applied to Gnome subsurface data with application of transmission coefficients to account for the local geology and to convert subsurface predictions to surface predictions. Because Salmon surface data were available, cube root relationships were used to predict Sterling surface motions, assuming fully tamped conditions.

2.3.2 Prediction Equations

The equations discussed below were based on a fully tamped situation. To predict motions for the Sterling event under decoupled conditions all predictions were divided by the decoupling factor of 20. This factor is normally applied to peak particle displacement but was utilized here to provide predictions for all motions, i.e., peak particle surface displacement, velocity and acceleration.

Acceleration

The cube root scaling relationship for acceleration is

$$aW^{1/3} = K\left(\frac{R}{W^{1/3}}\right)^{-n} \qquad (1)$$

or algebraically rearranged

$$a = K\, W^{1/3(n-1)}\, R^{-n} \qquad (2)$$

The regression equation through the Salmon peak surface acceleration data was

$$a = 4.07 \times 10^{6} R^{-1.95} \text{ (Reference 2.11)} \qquad (3)$$

Substituting the Salmon yield of 5.3 kt into Equation (2) and letting $4.07 \times 10^6 = K\, W^{1/3(n-1)}$ gives

$$a = 2.39 \times 10^6\, W^{.32}\, R^{-1.95} \qquad (4)$$

which was the equation used to predict surface motions from Sterling in a fully tamped condition. In the above equations:

a = peak surface particle acceleration in g

W = yield in kilotons

R = slant distance in meters

Displacement

The relationship of displacement to yield and distance utilizing cube root scaling is

$$\frac{d}{W^{1/3}} = K \left(\frac{R}{W^{1/3}}\right)^{-n} \qquad (5)$$

or

$$d = K\, W^{1/3(n+1)} R^{-n} \qquad (6)$$

The peak surface displacement data observed at Salmon were fitted with the least squares regression equation,

$$d = 2.83 \times 10^5\, R^{-1.60} \text{ (Reference 2.11)} \qquad (7)$$

where d = peak surface particle displacement in cm.

This equation rewritten in the form of equation (6) becomes

$$d = 6.64 \times 10^4\, W^{.87}\, R^{-1.60} \qquad (8)$$

which was used to predict the ground motions for the tamped case.

Velocity

Peak particle velocity was predicted for Salmon using

$$u = 3.26 \times 10^6 \, W^{.55} \, R^{-1.64} \qquad (9)$$

where

u = peak surface particle velocity in cm/sec

This equation was derived from Gnome data using cube root relationships similar to those just discussed. This equation fits the Salmon data sufficiently well that no modification was required for predicting the Sterling velocity for the tamped situation.

2.3.3 Predicted Ground Motions

Ground motion predictions were made only for the maximum yield of 0.44 kt because the difference in motions anticipated from the design yield of 0.36 kt were not significantly less. The main uncertainty in predicting ground motions from the Sterling event was the degree of decoupling which would occur. The Sterling Technical Concept (Reference 1.2) estimated decoupling might vary from a factor of 20 to a factor of 160, depending on the alteration of the cavity wall which was caused by the Salmon explosion. The only previous

experiment conducted to test decoupling was Project Cowboy, an HE experiment at Winnfield Dome, Louisiana. The Cowboy data indicated that decoupling was achieved with HE explosives. However, the theory had never been tested with nuclear explosives.

To provide ground motion predictions which would be useful from the standpoint of safety, the motions anticipated from a tamped 0.44 kt explosion were calculated using Equations 4, 8, and 9 above. The predictions for selected points of interest are listed in Table 2.3. These predictions were made in order to provide an upper limit on the ground motions from the Sterling event. To account for the decoupling effects and to provide more realistic estimates of ground motion, the smallest decoupling factor, 20, given in Reference 1.1 was used. All predictions for the tamped case were divided by 20 and the resulting predictions given in Table 2.4.

Figures 2.6 through 2.8 show peak predicted motions versus slant distance. Each graph shows the predictions for Sterling assuming a decoupling factor of 20 and assuming a fully tamped (no decoupling) case.

2.3.4 Predicted Distances to Significant Ground Motions

Using the decoupling factor of 20, it was predicted that ground motion would not exceed 0.1 g acceleration beyond 1100

TABLE 2.3 PREDICTED PEAK SURFACE MOTIONS, 0.44 kt FULLY TAMPED

Location	Slant Distance (meters)	Predicted Motions		
		Acceleration (g)	Displacement (cm)	Velocity (cm/sec)
1 mile from SZ	1,810	8.0×10^{-1}	1.9×10^{-1}	9.5×10^{0}
2 miles from SZ	3,340	2.4×10^{-1}	7.3×10^{-2}	3.5×10^{0}
3 miles from SZ	4,900	1.2×10^{-1}	4.0×10^{-2}	1.8×10^{0}
Baxterville	6,000	7.7×10^{-2}	2.9×10^{-2}	1.3×10^{0}
Baxterville Oil Field	9,600	3.1×10^{-2}	1.4×10^{-2}	5.9×10^{-1}
Purvis	14,500	1.4×10^{-2}	7.3×10^{-3}	3.0×10^{-1}
Lumberton	17,700	9.4×10^{-3}	5.2×10^{-3}	2.1×10^{-1}
Columbia	27,800	3.9×10^{-3}	2.6×10^{-3}	1.0×10^{-1}
Hattiesburg	32,000	2.9×10^{-3}	2.0×10^{-3}	8.0×10^{-2}

TABLE 2.4 PREDICTED PEAK SURFACE MOTIONS, 0.44 kt WITH DECOUPLING OF 20

Location	Slant Distance (meters)	Predicted Motions		
		Acceleration (g)	Displacement (cm)	Velocity (cm/sec)
1 mile from SZ	1,810	4.0×10^{-2}	9.5×10^{-3}	4.7×10^{-1}
2 miles from SZ	3,340	1.2×10^{-2}	3.6×10^{-3}	1.8×10^{-1}
3 miles from SZ	4,900	5.9×10^{-3}	2.0×10^{-3}	9.0×10^{-2}
Baxterville	6,000	3.9×10^{-3}	1.4×10^{-3}	6.5×10^{-2}
Baxterville Oil Field	9,600	1.6×10^{-3}	6.9×10^{-4}	3.0×10^{-2}
Purvis	14,500	7.0×10^{-4}	3.6×10^{-4}	1.5×10^{-2}
Lumberton	17,700	4.7×10^{-4}	2.6×10^{-4}	1.1×10^{-2}
Columbia	27,800	2.0×10^{-4}	1.3×10^{-4}	5.0×10^{-3}
Hattiesburg	32,000	1.5×10^{-4}	1.0×10^{-4}	4.0×10^{-3}

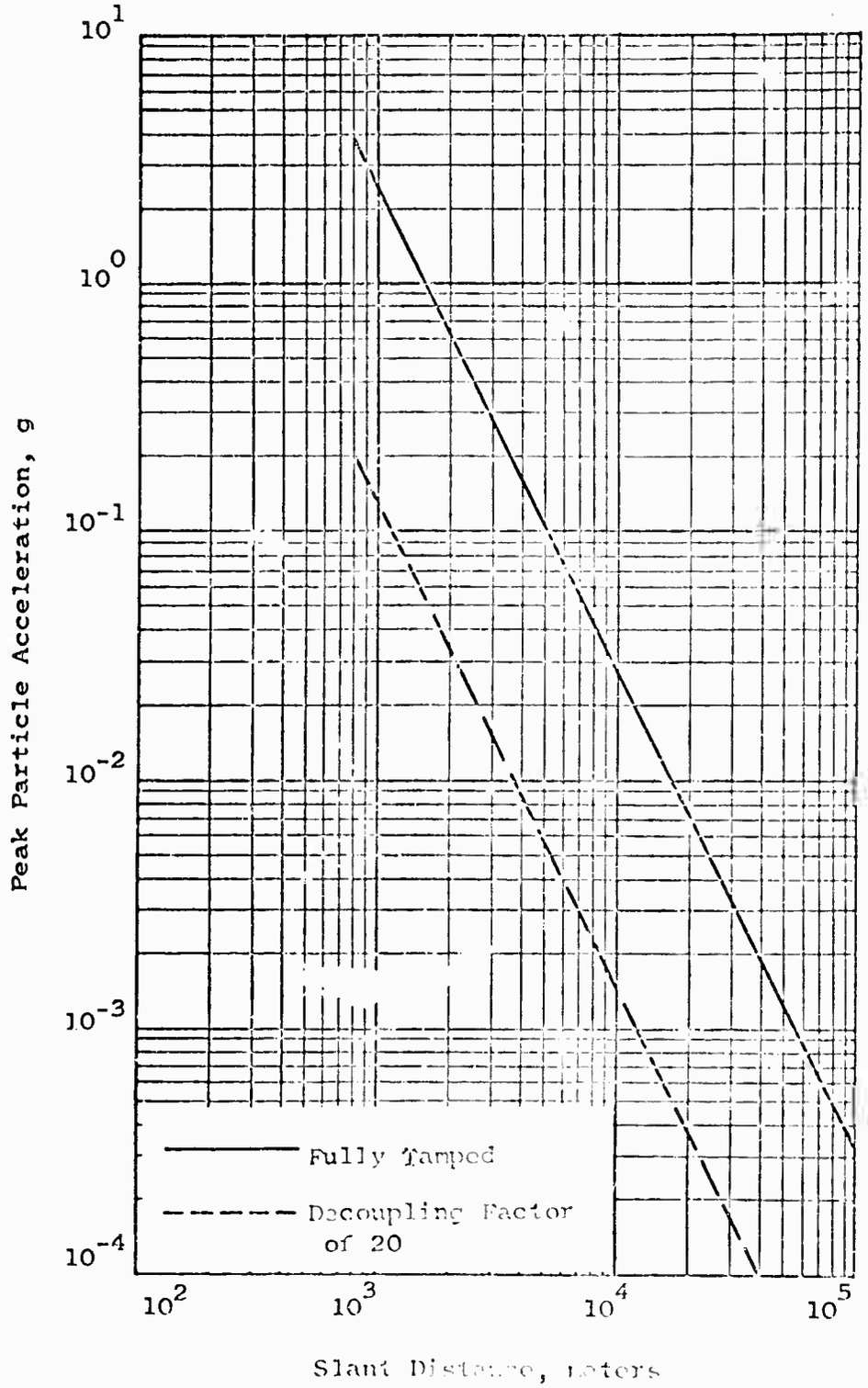

Figure 2.6. Predicted Peak Surface Particle Acceleration versus Slant Distance, 0.44 kt.

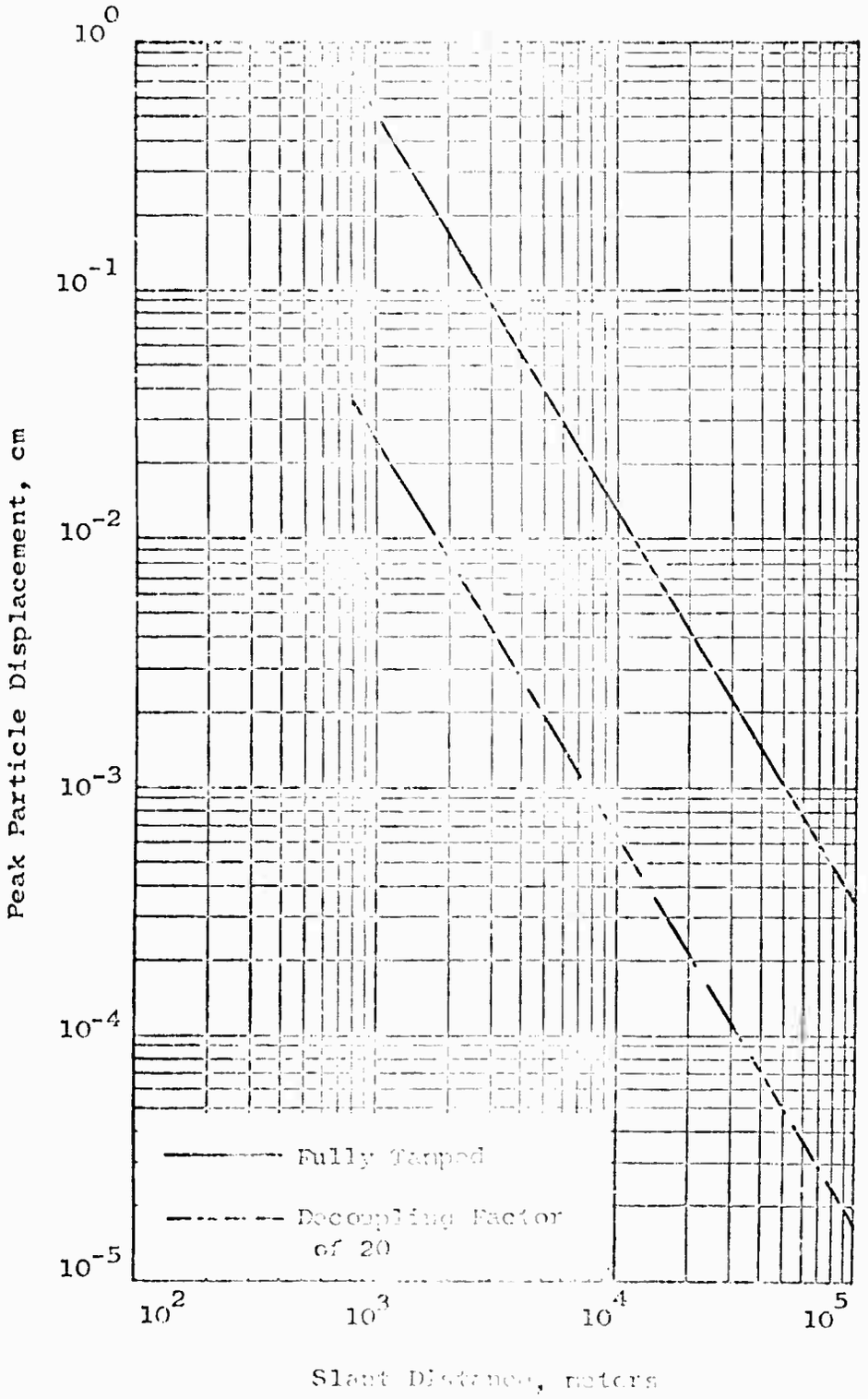

Figure 2.7. Predicted Peak Surface Particle Displacement versus Slant Distance, 0.44 kt.

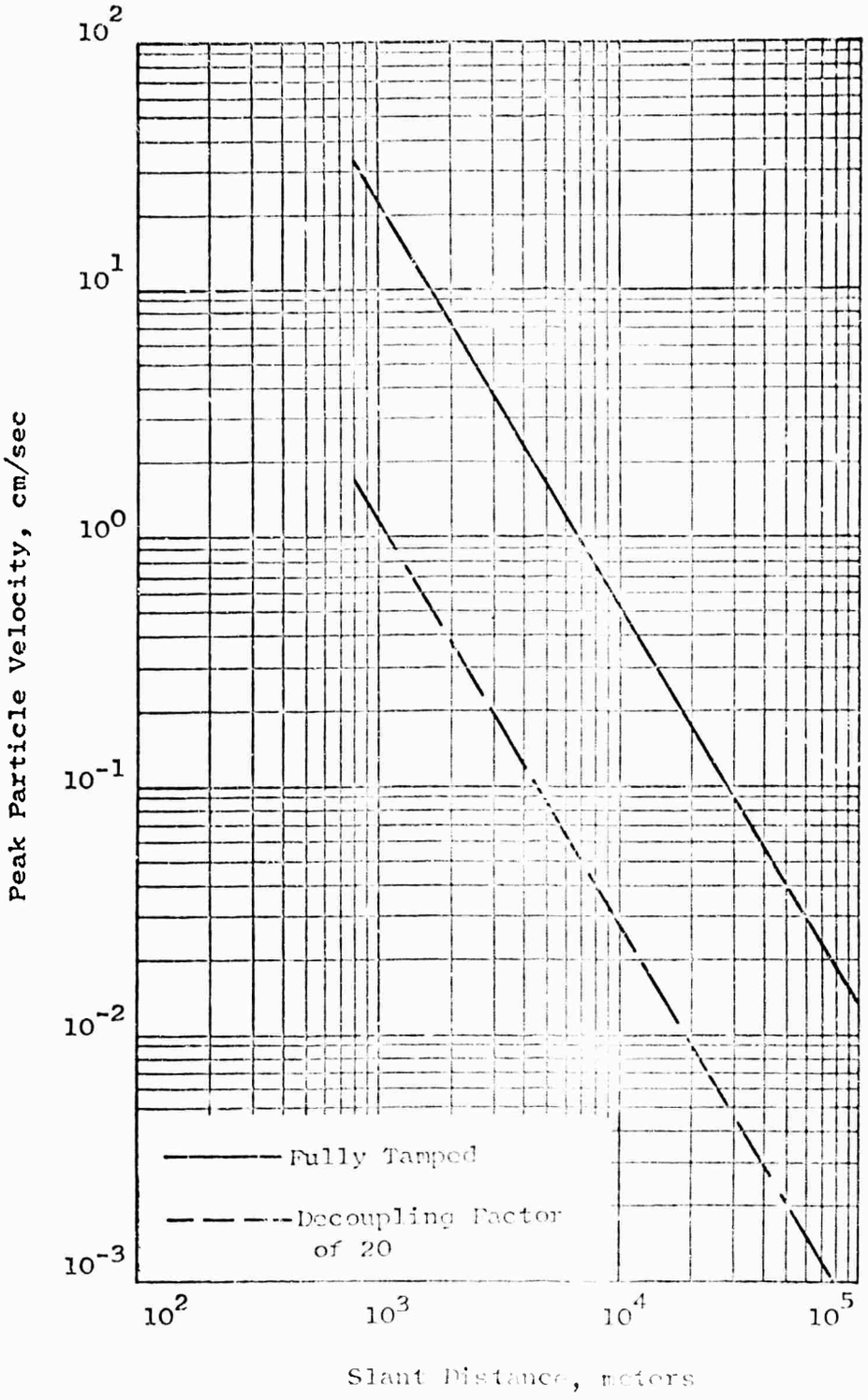

Figure 2.8. Predicted Peak Surface Particle Velocity versus Slant Distance, 0.44 kt.

meters slant distance, which is a horizontal distance of 730 meters from surface zero. If no decoupling occurred, 0.1 g was predicted to extend to a slant distance 5.3 km (5.1 km from surface zero).

The predicted distance to a particle velocity of 1 cm/sec was 1150 meters slant distance or 800 meters horizontal from surface zero for Sterling using a decoupling factor of 20. If no decoupling was achieved and Sterling effects were similar to a tamped event, the distance to 1 cm/sec was predicted to be 7.0 kilometers.

The distance to 0.001 g for the Sterling event was predicted to be 12 km assuming a decoupling factor of 20. If no decoupling occurred, peak accelerations of 0.001 g were predicted to occur as far as 55 km from the Sterling surface zero. These predicted distances were average values. Azimuthal variation in ground motion was observed for the Salmon event and was expected to occur for Sterling. However, it was thought that the variations observed at Salmon would not be applicable to Sterling because of the close-in environmental differences. Consequently, no attempt was made to incorporate the observed Salmon azimuthal variation into the Sterling predictions.

The pertinent distances are summarized below and shown graphically with respect to surrounding towns on Figures 2.9 and 2.10.

	Distance from Surface Zero, km	
Motion	Fully Tamped	Decoupling of 20
0.1 g	5.1	0.73
1 cm/sec	7.0	0.80
0.001 g	55	12

2.3.5 Hazards to Subsurface Facilities

There was no known damage to any of the oil or gas wells in the vicinity or to the closest pipeline as a result of the Salmon event. Therefore, it was concluded that Sterling, at a much smaller yield and decoupled, would not present any hazard to these facilities.

2.4 INSTRUMENTATION

Seismic instrumentation was installed and operated by the Special Projects Party of the U.S. Coast and Geodetic Survey. Instrumentation consisted of 1) Accelerographs which record three orthogonal components of particle acceleration and displacement on photographic paper, 2) National Geophysical Co. Type 21 seismometers (NC-21) which record three components of particle velocity on magnetic tape and, 3) Wood-Anderson

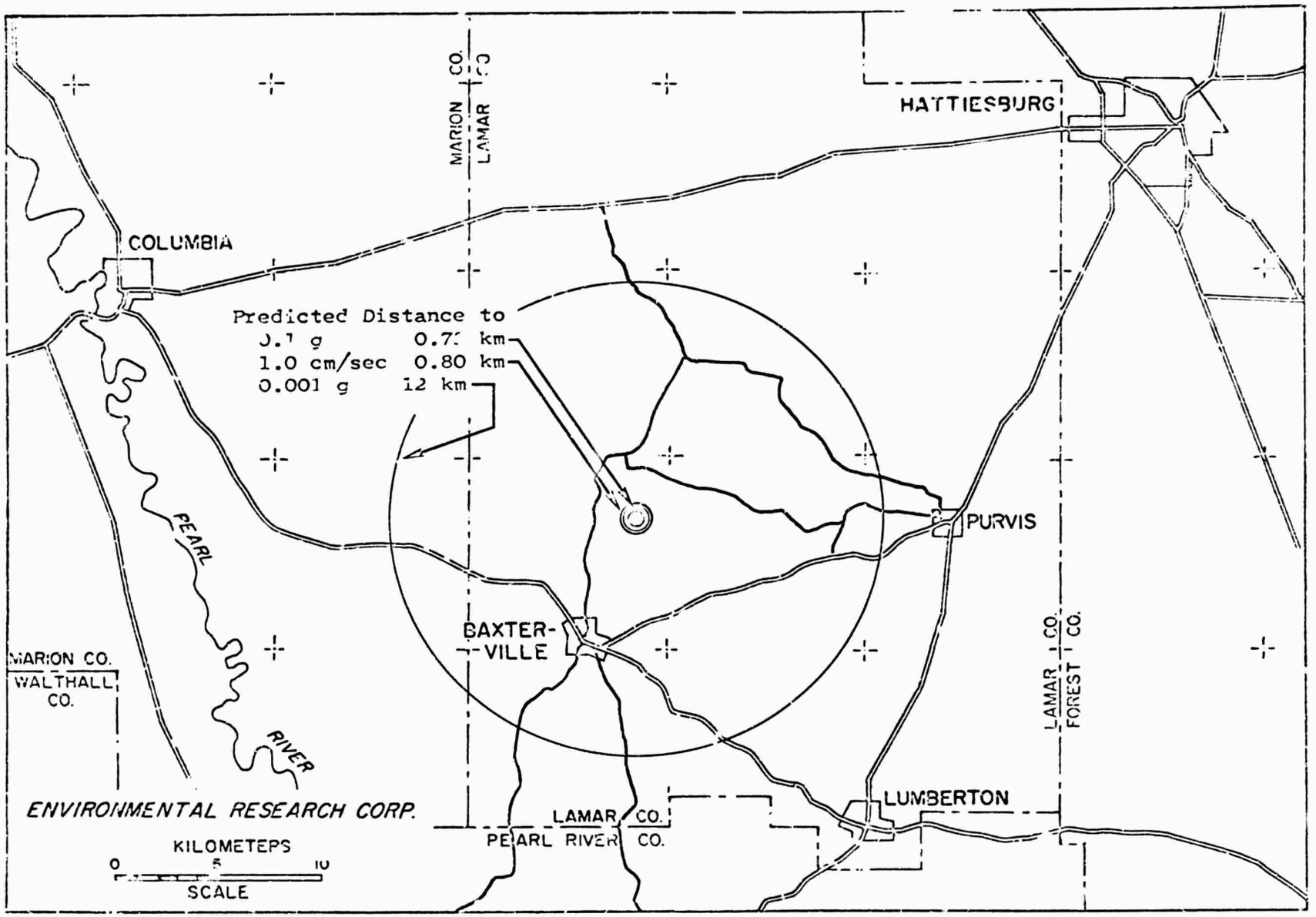

Figure 2.9. Predicted Distances to Significant Motions, Sterling Event with a Decoupling Factor of 20

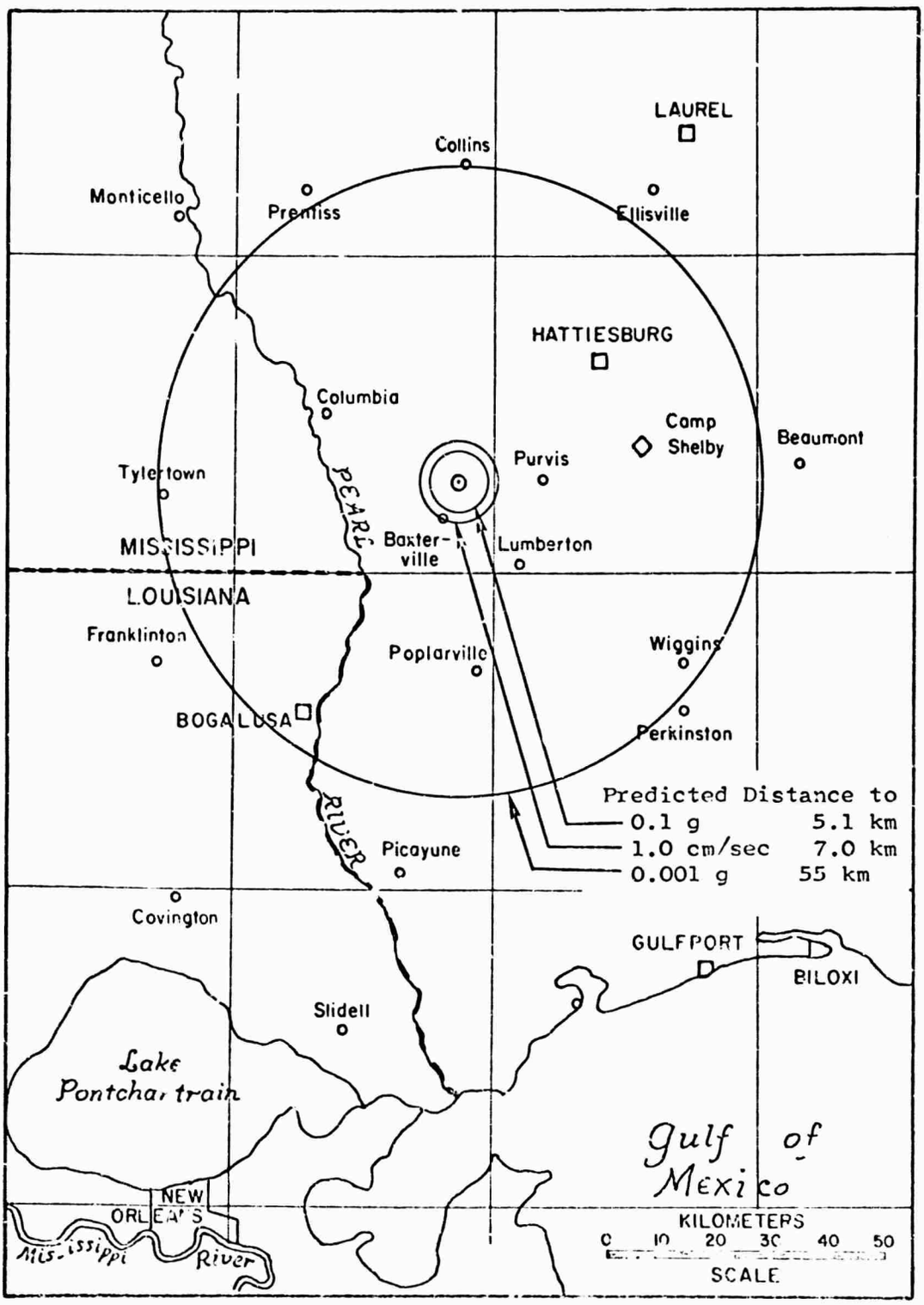

Figure 2.10. Predicted Distance to Significant Motions, Sterling Event Fully Tamped

displacement meters which record two horizontal components of particle displacement on paper.

The accelerographs were located at ten nearby structures within a radius from surface zero of about six kilometers. Location of these stations are shown on Figure 2.11.

The velocity meters and Wood-Anderson displacement meters were placed at selected points of interest such as nearby towns and cities. The locations are shown on Figure 2.12.

At two stations, 10S and 20S, the three-component set of NC-21 seismometers were supplemented by three additional vertical seismometers at 1000 foot intervals. At station 10S the vertical instruments were on a radial line in a direction away from ground zero while at Station 20S the vertical instruments were on a radial line toward ground zero. Further details concerning the instrumentation for the Sterling event may be found in Reference 2.12.

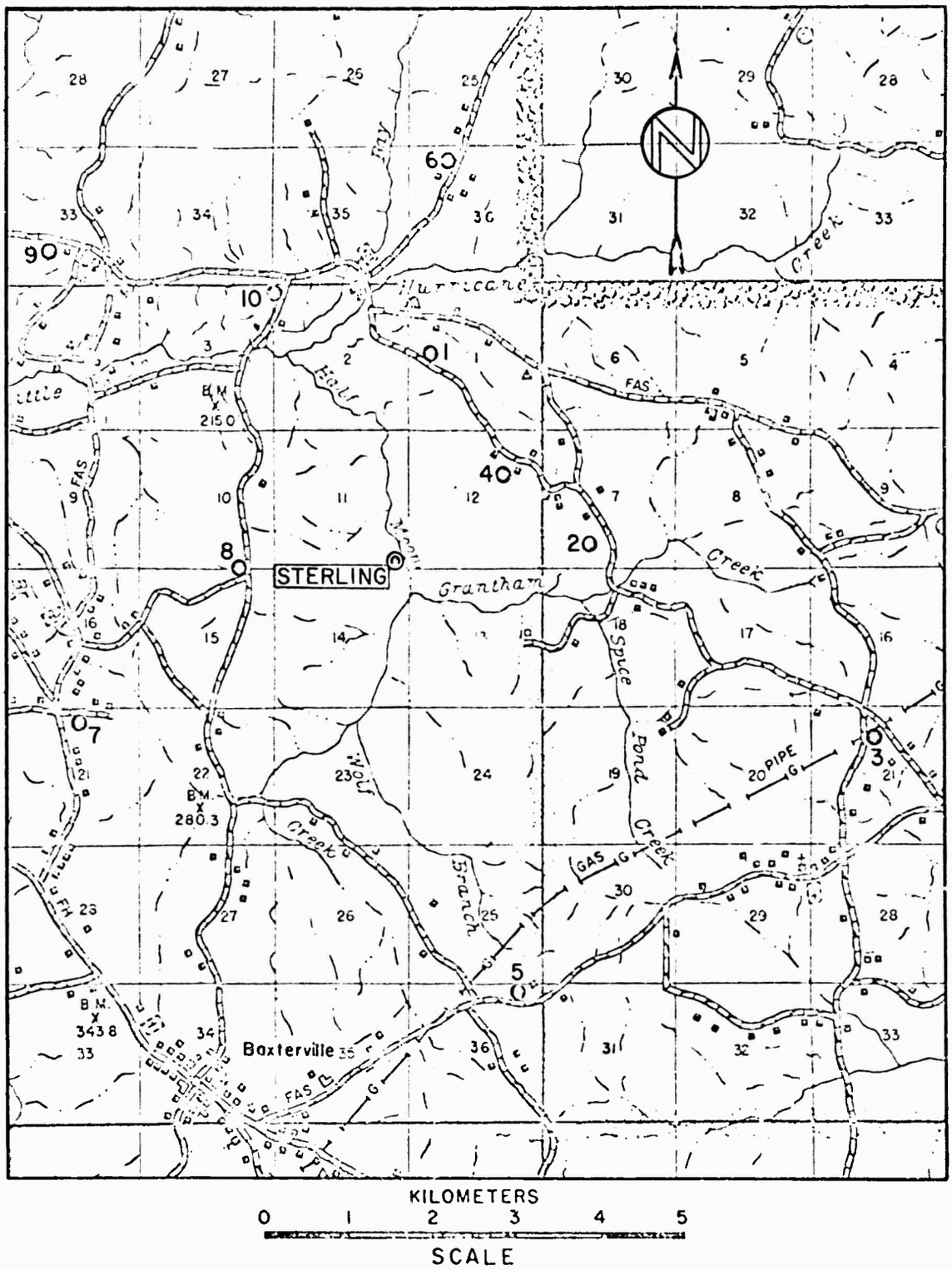

Figure 2.11 Map Showing Accelerograph Station Locations

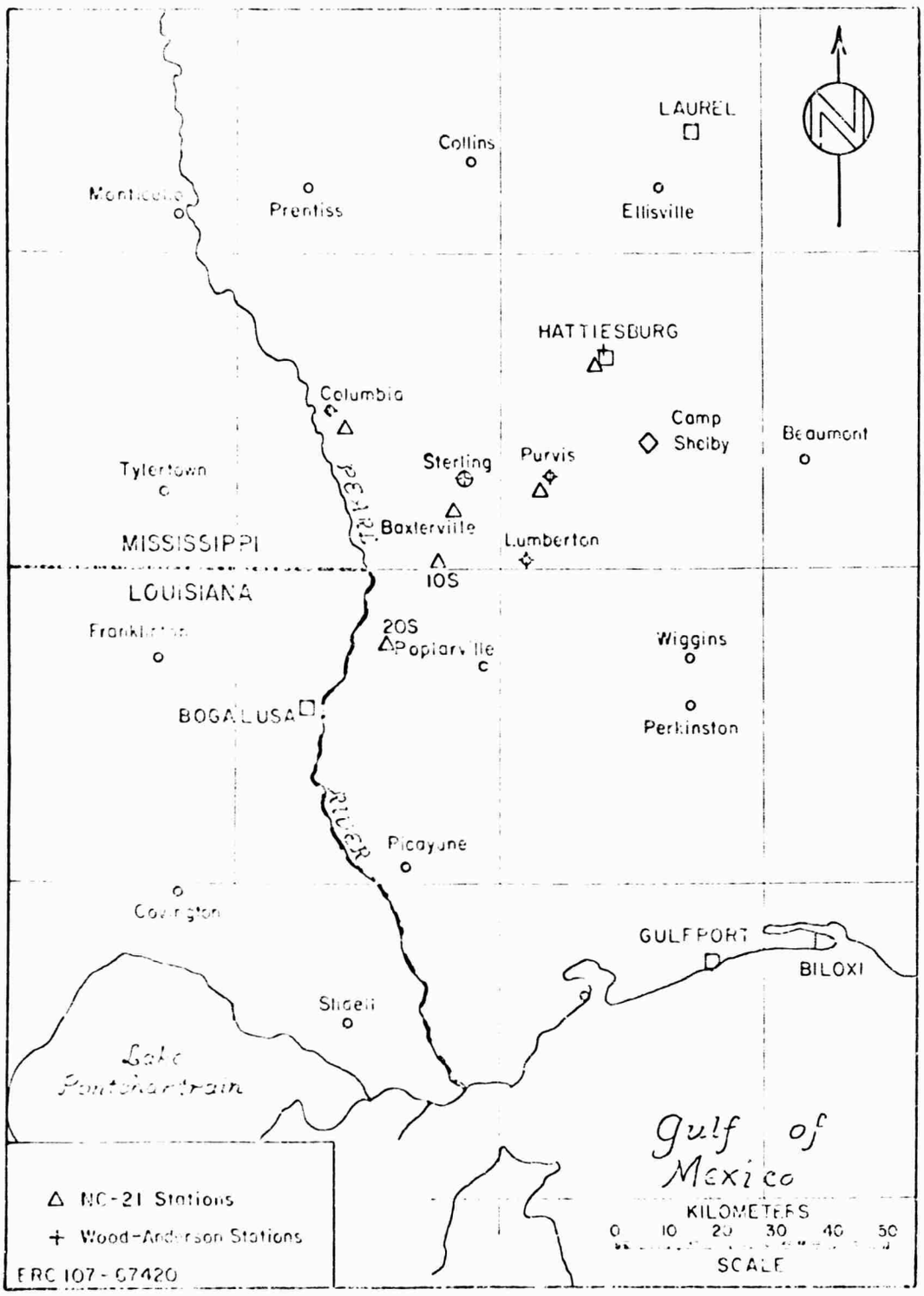

Figure 2.12 Area Map Showing Additional Station Locations

CHAPTER 3

RESULTS

3.1 PHENOMENOLOGY AND CONTAINMENT

The Sterling event was completely contained. Because there has been no post-shot drilling program to date, no other data are available.

3.2 SEISMIC

Seismic signals from the Sterling event were so weak that many of the instruments failed to record usable data. The best data are those recorded on magnetic tape with the NC-21 velocity meters. Of the eight NC-21 stations in operation, seven recorded usable data, although in some cases not all components (at a station) were usable. No usable data were obtained at Hattiesburg.

The NC-21 velocity meter data were processed by analog computer. Corrections were made for the frequency response characteristics of the instruments to obtain corrected velocity. Acceleration and displacement traces were derived by integration and differentiation of the corrected velocity traces. The velocity traces were also filtered with narrow band-pass filters at pre-selected center frequencies. The peak velocities at each frequency were plotted

versus frequency to provide amplitude-frequency relationships at each station. The center frequencies were selected so as to include, where possible, all frequencies which were of significant amplitude. At three stations; Columbia, Lumberton, and Bass Memorial School at Purvis; high cutoff filters of 16 hz were used during the field recording and at both Baxterville stations the cutoff was at 23 hz. Band-pass filtering was not carried beyond these frequencies. In general, the peak amplitude at these stations appeared to be occurring at frequencies lower than the high cutoff field filters, so it was possible to identify the significant frequencies.

Of the ten Accelerograph stations, only four produced traces with sufficient amplitudes for analysis. These were recorded with the accelerometers. The Carder displacement meters (the Accelerograph consists of three accelerometers and three Carder displacement meters) did not record any motion. The useable accelerometer traces exhibited very high frequency motions, generally well outside the flat portion of the response curve. These traces were digitized and corrected for the frequency response characteristics of the instruments. Particle velocity traces were derived from these corrected acceleration

data and were then band-pass filtered by digital methods to provide amplitude-frequency information comparable to that obtained from the NC-21 data. No readable motions were obtained at the Wood-Anderson displacement meter stations.

The peak values of ground motion are listed in Tables 3.1 through 3.3. The tables include the peak value for each component of motion and the peak resultant vector value. The resultant vectors were obtained by analyzing simultaneously the three components of motion at a station in order to determine the absolute value of ground motion. The resultant vectors are the instantaneous value of the square root of the sum of the squares of the individual components. Where only two components of motion were recorded, peak resultant vectors were also calculated. The peak resultant vector values are plotted versus slant distance on Figures 3.1 through 3.3. Least squares regression lines were fitted to the data and the standard errors of estimate calculated. These are given on the figures.

The amplitude-frequency curves, derived by filtering the velocity signals, are shown on Figures 3.4 through 3.16.

TABLE 3.1. PEAK SURFACE ACCELERATION

Station	Slant Distance (meters)	Peak Acceleration, g			
		Vertical	Radial	Transverse	Resultant
1	2,550	3.18×10^{-2}	1.35×10^{-2}(N-S)	—	3.18×10^{-2}
2	2,620	2.20×10^{-2}	9.25×10^{-3}(N-S)	1.68×10^{-2}(E-W)	2.28×10^{-2}
3	5,970	—	—	—	—
4	1,830	8.69×10^{-2}	3.10×10^{-2}(N-S)	3.03×10^{-2}(E-W)	8.99×10^{-2}
5	5,210	—	—	—	—
6	4,720	—	—	—	—
7	4,320	—	—	—	—
8	2,060	2.38×10^{-1}	8.81×10^{-2}(N-S)	—	2.38×10^{-1}
9	5,390	—	—	—	--
10	3,520	—	—	—	—
Baxterville Post Office*	6,100	1.61×10^{-3}	7.95×10^{-4}	6.35×10^{-4}	1.69×10^{-3}
School*	6,500	1.43×10^{-3}	8.74×10^{-4}	5.13×10^{-4}	1.55×10^{-3}
Purvis (Bass Memorial School)*	16,000	1.55×10^{-4}	4.94×10^{-5}	4.59×10^{-5}	1.56×10^{-4}
10 S*	17,800	2.22×10^{-4} 1.70×10^{-4} 2.02×10^{-4} 1.50×10^{-4}	7.28×10^{-5}	3.97×10^{-5}	2.22×10^{-4}
Lumberton*	19,000	3.85×10^{-5}	4.65×10^{-5}	2.69×10^{-5}	5.15×10^{-5}
Columbia*	26,000	—	—	—	—
20 S*	31,700	1.56×10^{-5} 1.72×10^{-5} 2.31×10^{-5} 1.84×10^{-5}	1.97×10^{-5}	1.06×10^{-5}	2.12×10^{-5}
Hattiesburg*	32,700	—	—	—	—

* Derived from corrected velocity.

TABLE 3.2. PEAK SURFACE DISPLACEMENT

Station	Slan Distance (meters)	Peak Displacement, cm			
		Vertical	Radial	Transverse	Resultant
1	2,550	—	—	—	—
2	2,620	—	—	—	—
3	5,970	—	—	—	—
4	1,830	—	—	—	—
5	5,210	—	—	—	—
6	4,720	—	—	—	—
7	4,320	—	—	—	—
8	2,060	—	—	—	—
9	5,390	—	—	—	—
10	3,520	—	—	—	—
Baxterville Post Office*	6,100	2.57×10^{-4}	2.26×10^{-4}	—	3.08×10^{-4}
School*	6,500	3.23×10^{-4}	1.83×10^{-4}	7.16×10^{-5}	3.24×10^{-4}
Purvis (Bass Memorial School)*	16,000	8.78×10^{-5}	3.45×10^{-5}	3.45×10^{-5}	1.02×10^{-4}
10 S*	17,800	8.50×10^{-5} 8.08×10^{-5} 1.13×10^{-4} 7.23×10^{-5}	9.24×10^{-5}	2.49×10^{-5}	9.57×10^{-4}
Lumberton*	19,000	4.90×10^{-5}	6.21×10^{-5}	3.09×10^{-5}	7.11×10^{-5}
Columbia*	26,000	—	—	—	—
20 S*	31,700	—	—	—	—
Hattiesburg*	32,700	—	—	—	—

* Derived from corrected velocity.

TABLE 3.3. PEAK SURFACE VELOCITY

Station	Slant Distance (meters)	Peak Velocity, cm/sec			
		Vertical	Radial	Transverse	Resultant
1*	2,550	1.65×10^{-1}	8.06×10^{-2}(N-S)	—	1.65×10^{-1}
2*	2,320	1.27×10^{-1}	5.95×10^{-2}(N-S)	8.05×10^{-2}(E-W)	1.34×10^{-1}
3	5,970	—	—	—	—
4*	1,830	3.48×10^{-1}	1.37×10^{-1}(N-S)	1.27×10^{-1}(E-W)	3.58×10^{-1}
5	5,210	—	—	—	—
6	4,720	—	—	—	—
7	4,320	—	—	—	—
8*	2,060	6.09×10^{-1}	1.50×10^{-1}(N-S)	—	6.09×10^{-1}
9	5,390	—	—	—	—
10	3,520	—	—	—	—
Baxterville Post Office	6,100	1.59×10^{-2}	1.24×10^{-2}	7.06×10^{-3}	1.68×10^{-2}
School	6,500	1.64×10^{-2}	1.31×10^{-2}	5.74×10^{-3}	1.69×10^{-2}
Purvis (Bass Memorial School)	16,000	3.08×10^{-3}	8.97×10^{-4}	7.59×10^{-4}	3.15×10^{-3}
10S	17,800	2.81×10^{-3} 2.07×10^{-3} 2.41×10^{-3} 1.74×10^{-3}	1.62×10^{-3}	5.98×10^{-4}	2.85×10^{-3}
Lumberton	19,000	1.00×10^{-3}	1.35×10^{-3}	7.59×10^{-4}	1.59×10^{-3}
Columbia	26,000	—	—	4.03×10^{-4}(E-W)	—
20S	31,700	5.48×10^{-4} 4.90×10^{-4} 5.52×10^{-4} 5.90×10^{-4}	6.83×10^{-4}	2.40×10^{-4}	6.93×10^{-4}
Hattiesburg	32,700	—	—	—	—

* Derived from corrected acceleration.

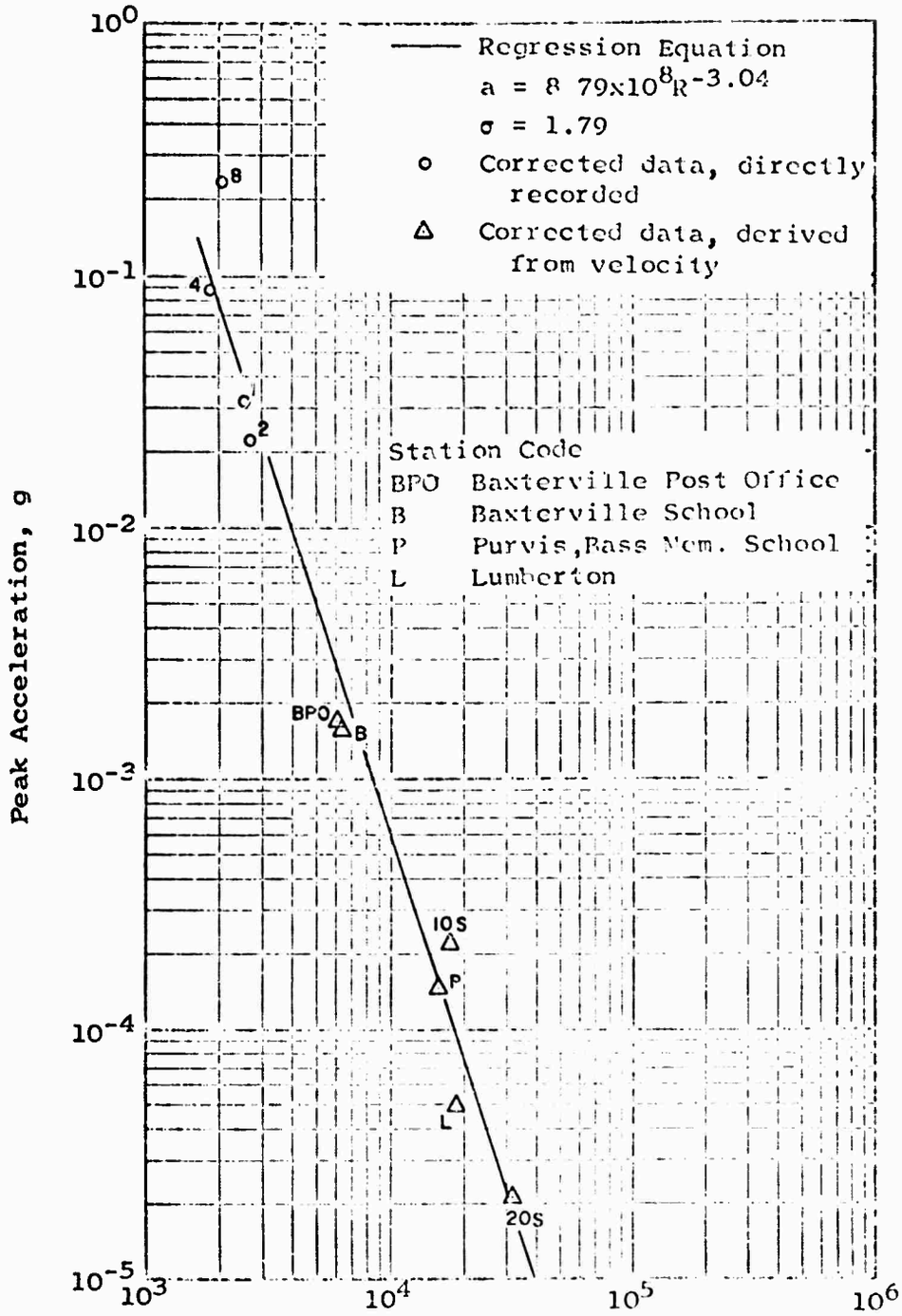

Figure 3.1 Observed Peak Resultant Vectors of Surface Particle Acceleration

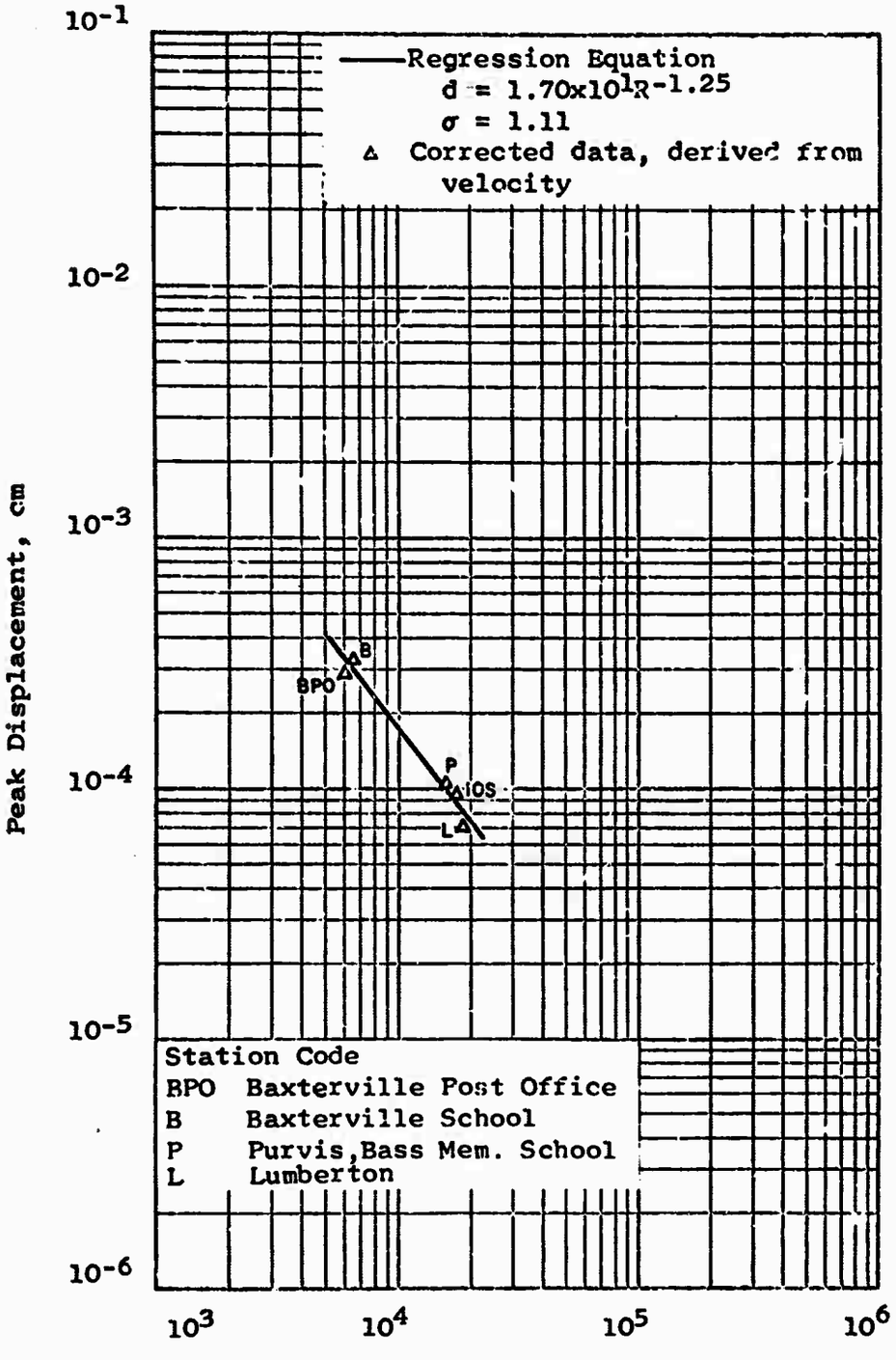

Figure 3.2 Observed Peak Resultant Vectors of Surface Particle Displacement

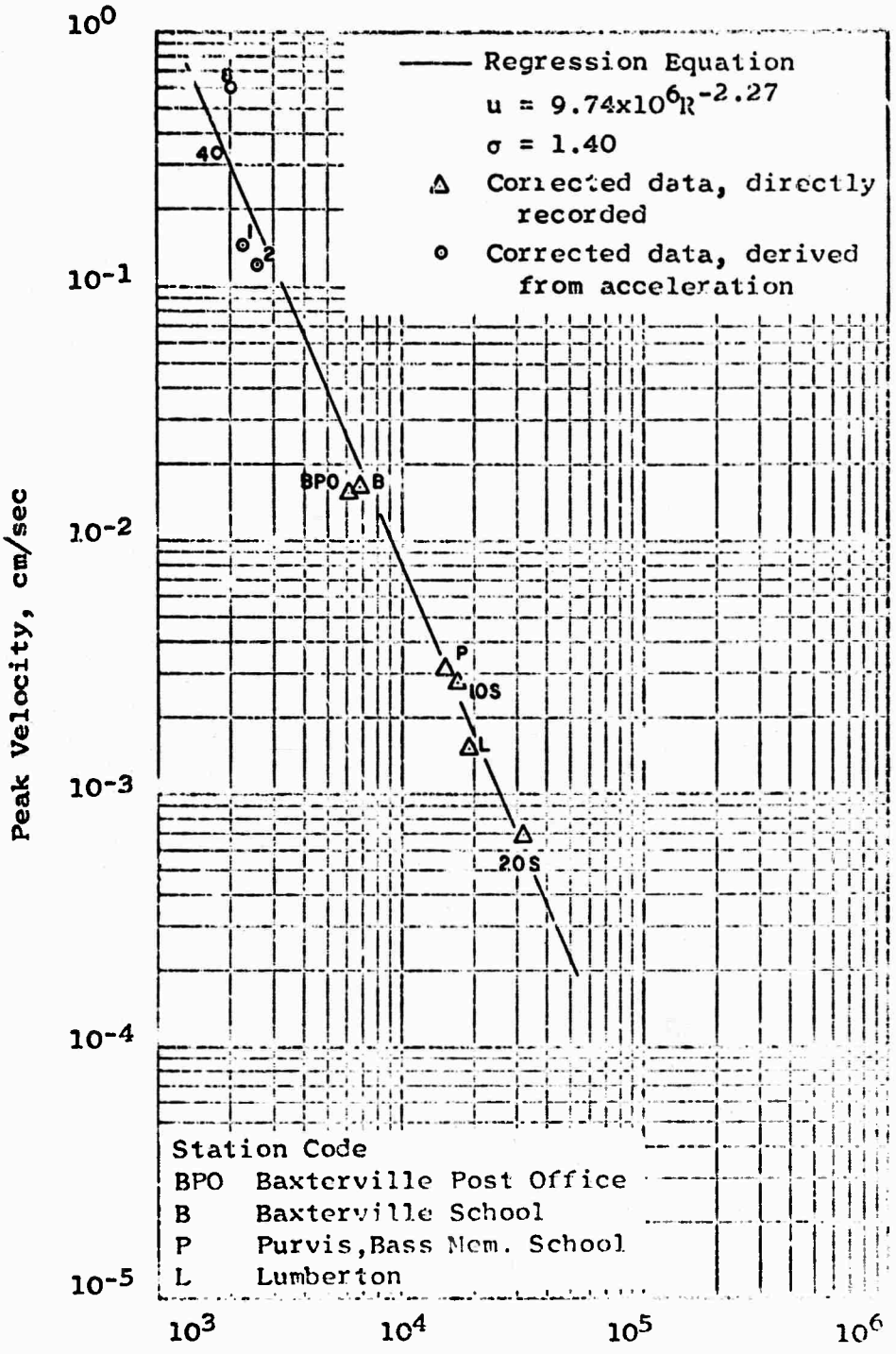

Figure 3.3 Observed Peak Resultant Vectors of Surface Particle Velocity

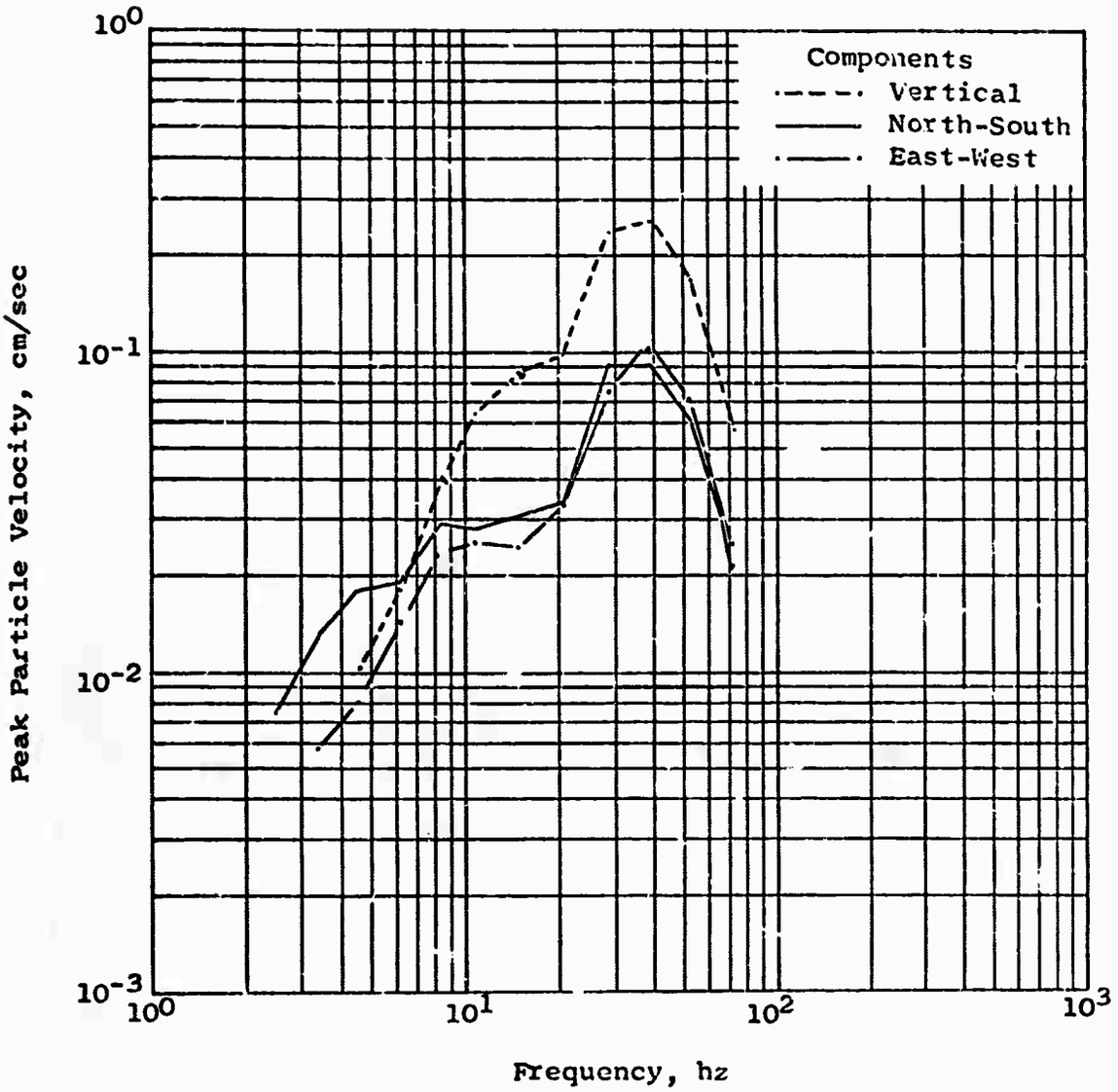

Figure 3.4 Peak Band-Pass Filtered Particle Velocity versus Frequency, Station 4

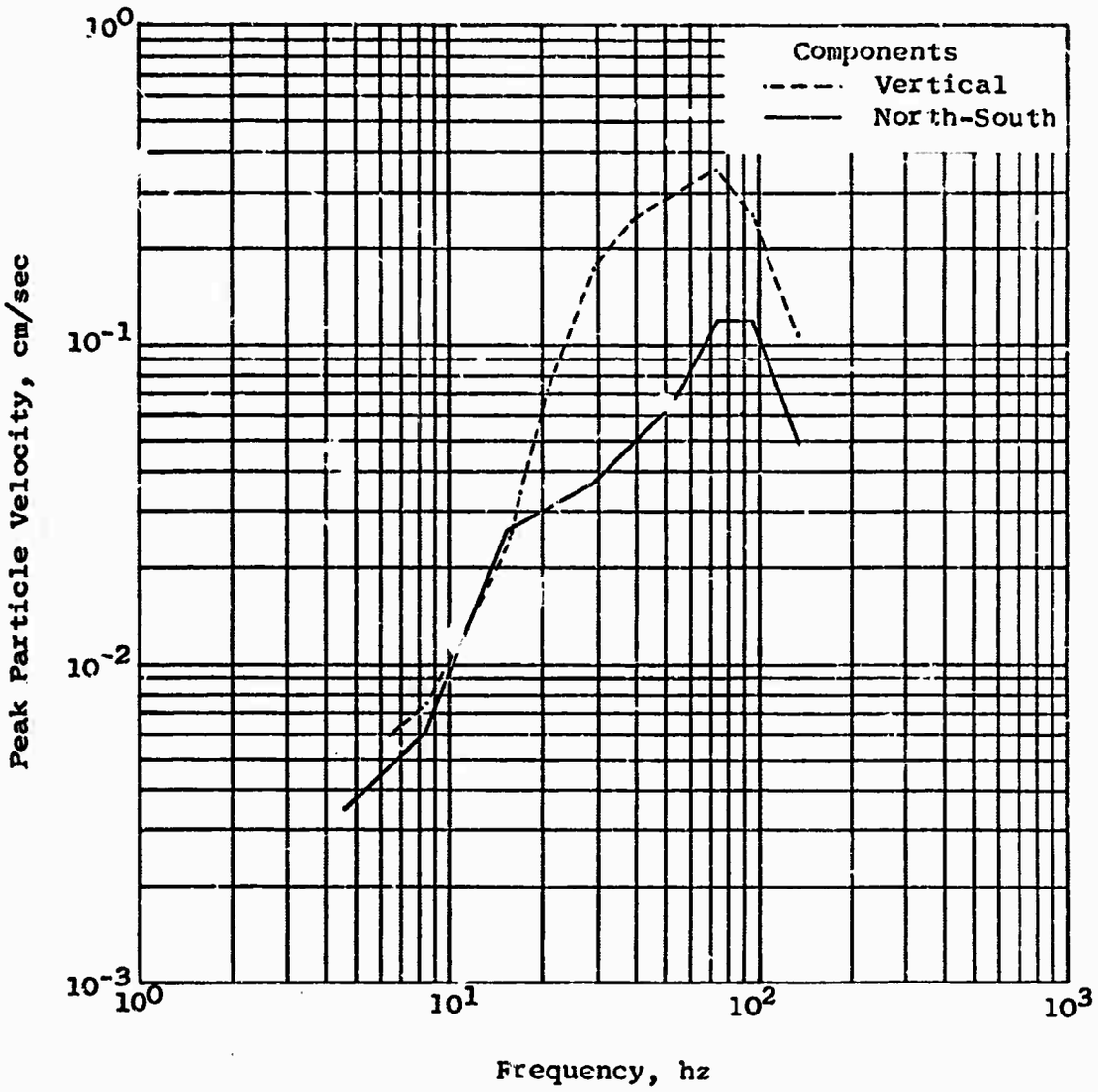

Figure 3.5 Peak Band-Pass Filtered Particle Velocity versus Frequency, Station 8

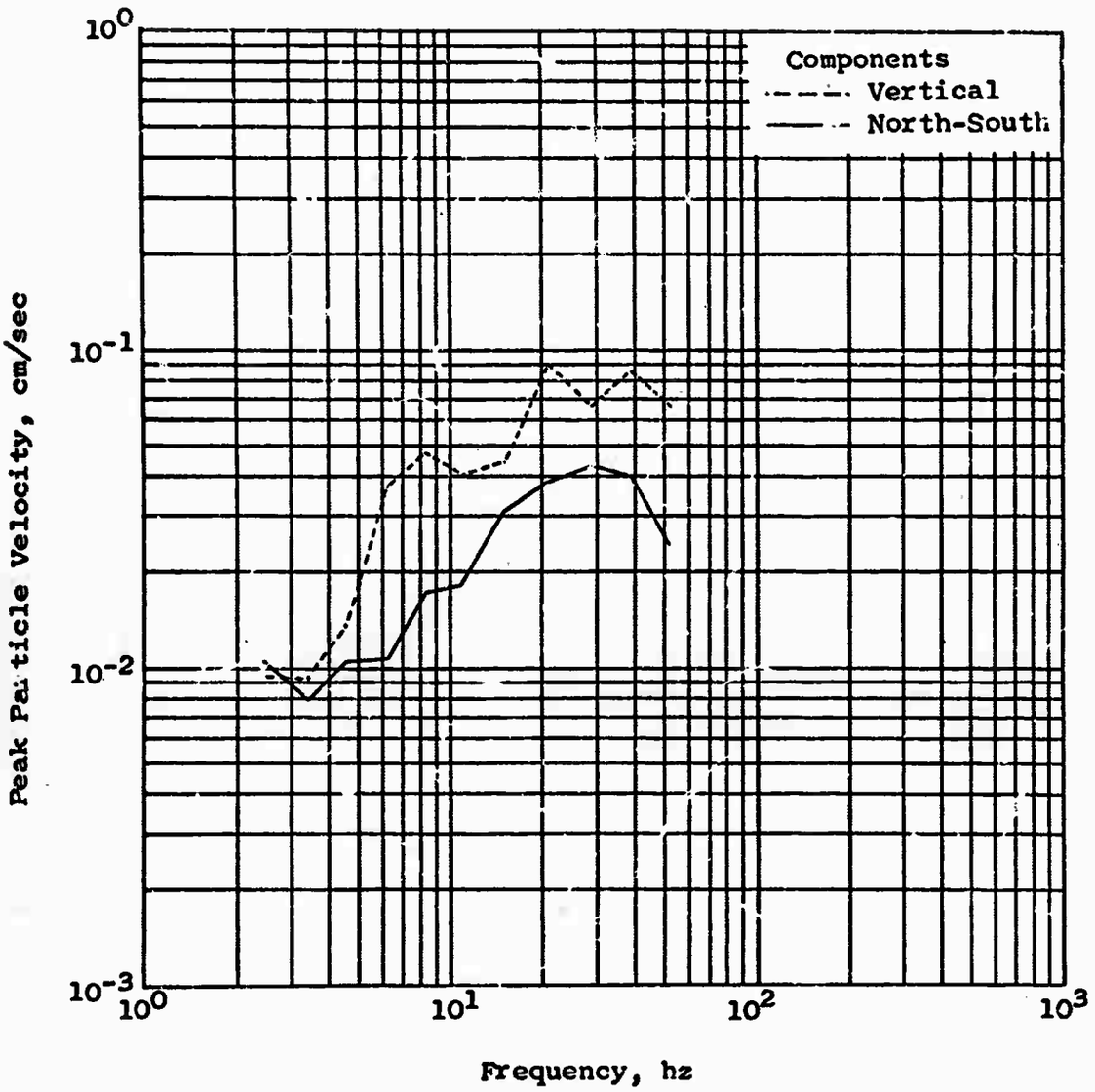

Figure 3.6 Peak Band-Pass Filtered Particle Velocity versus Frequency, Station 1

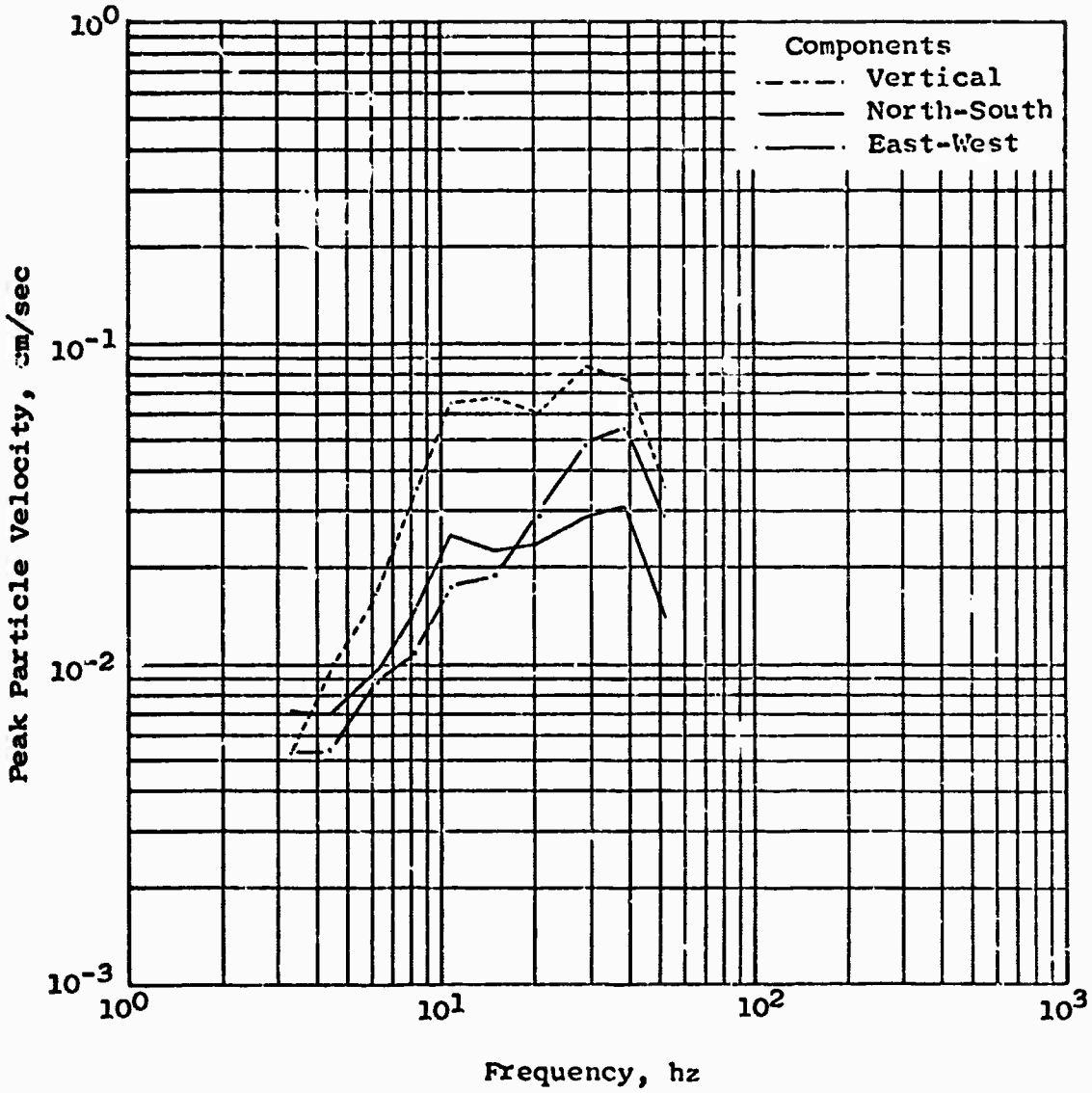

Figure 3.7 Peak Band-Pass Filtered Particle Velocity versus Frequency, Station 2

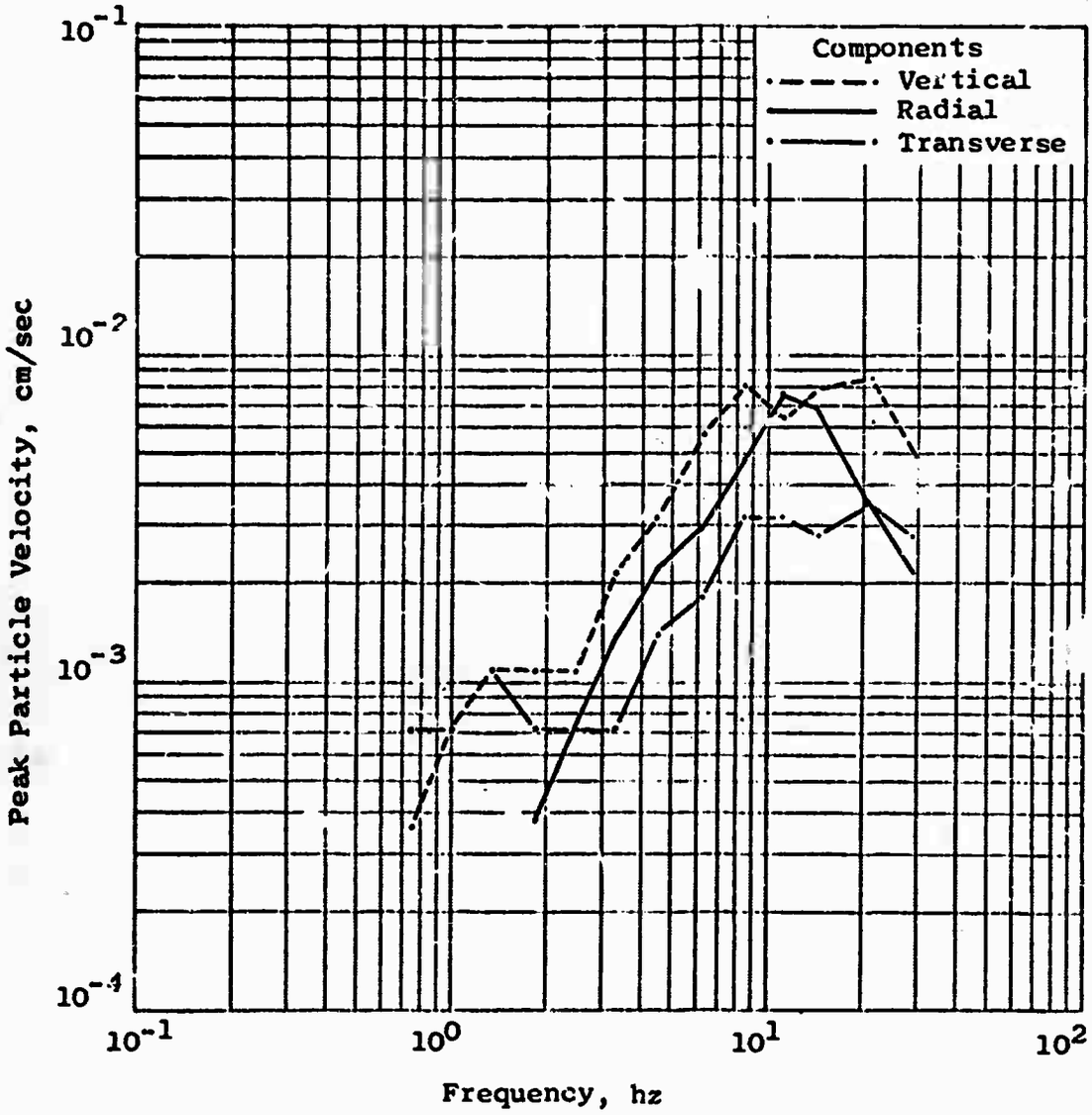

Figure 3.8 Peak Band-Pass Filtered Particle Velocity versus Frequency, Baxterville School

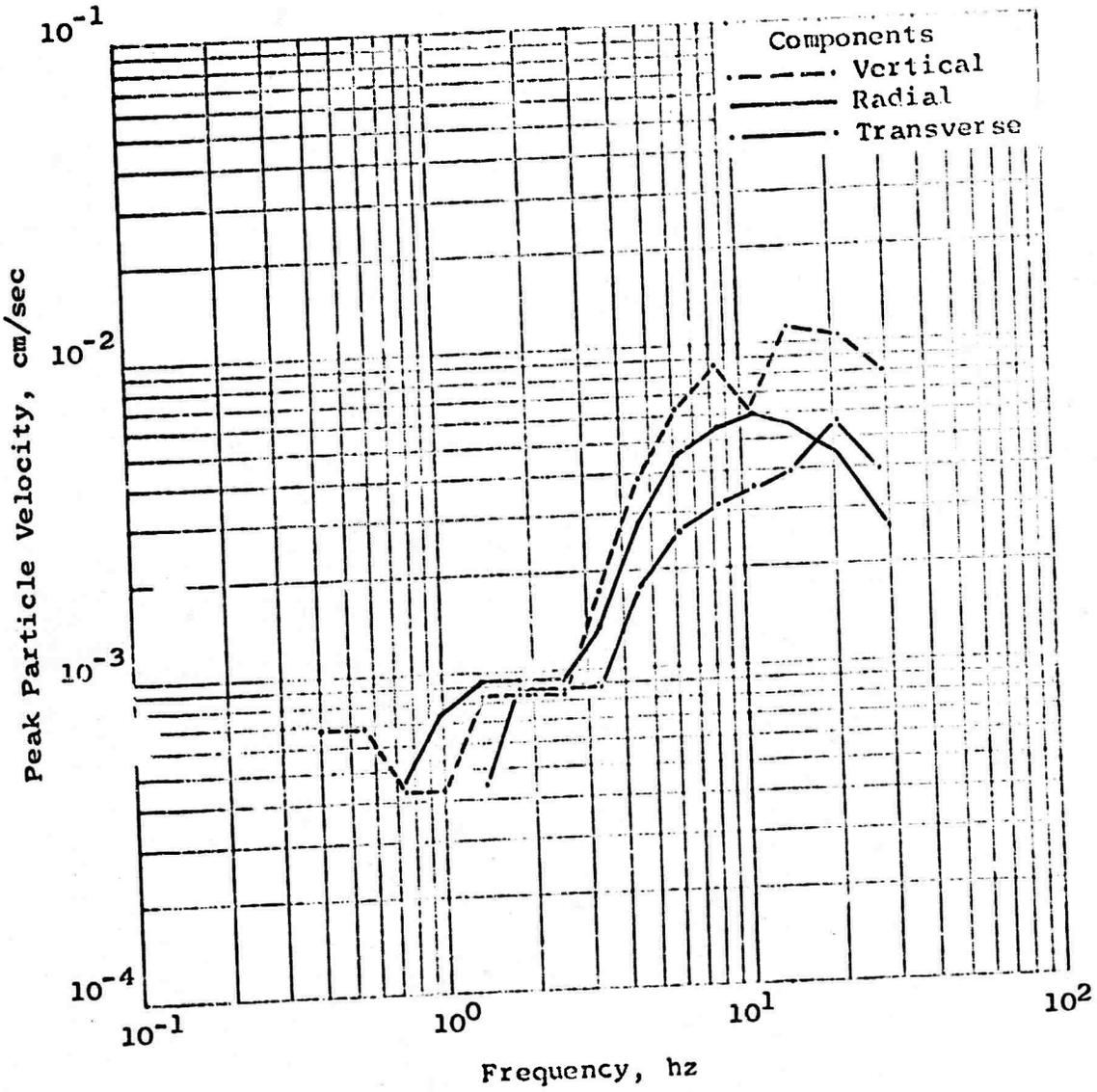

Figure 3.9 Peak Band-Pass Filtered Particle Velocity versus Frequency, Baxterville Post Office

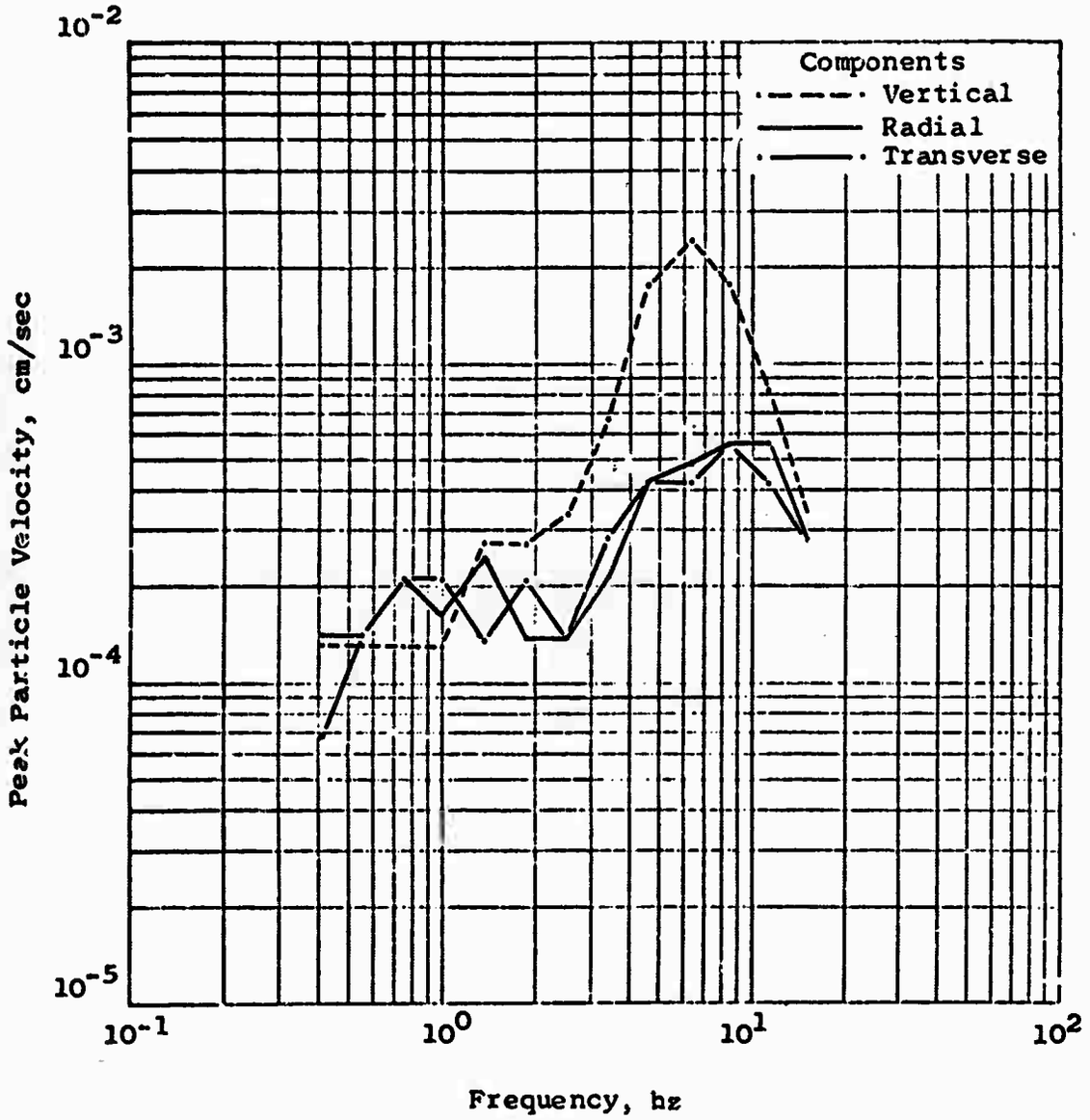

Figure 3.10 Peak Band-Pass Filtered Particle Velocity versus Frequency, Purvis

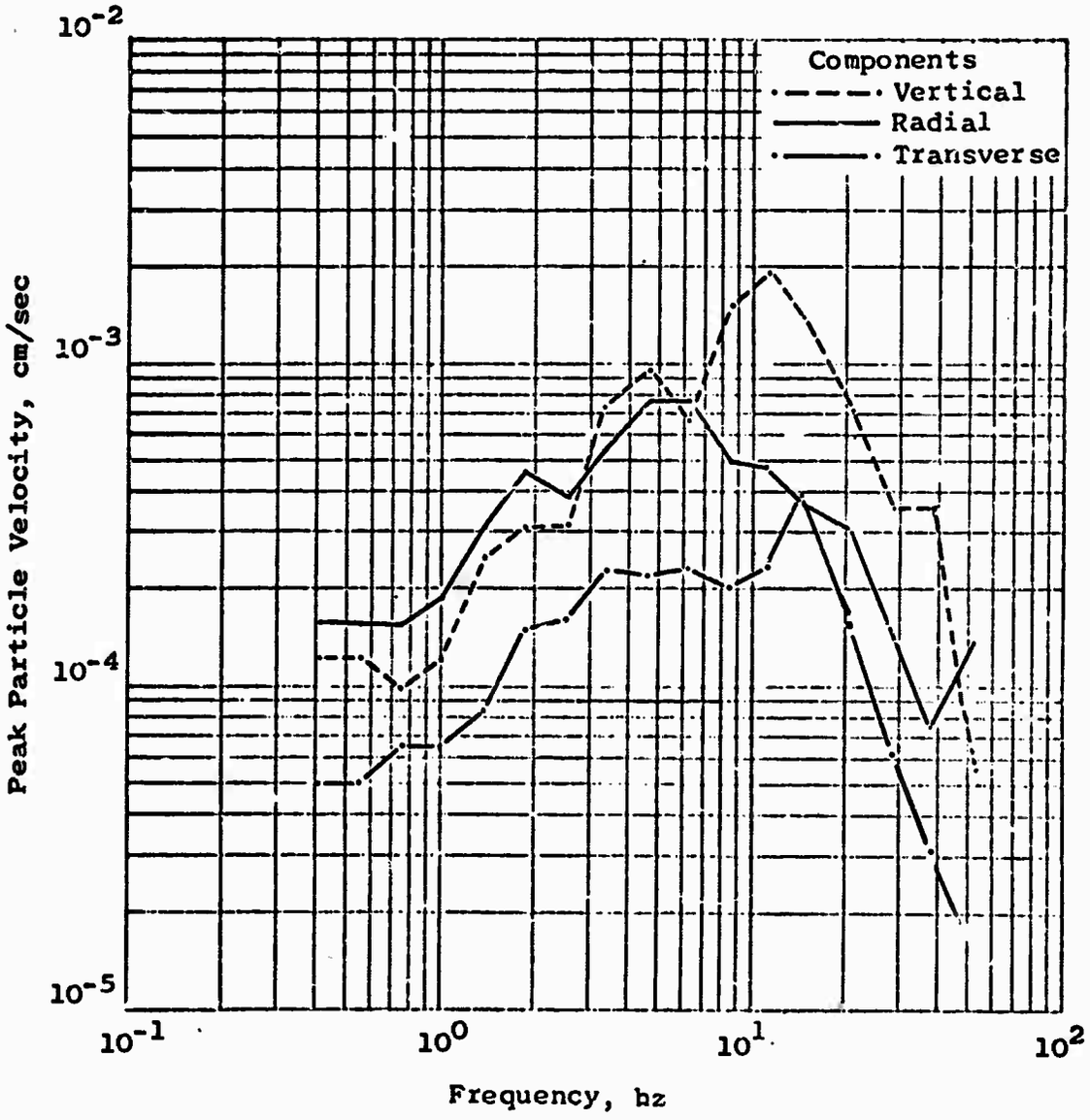

Figure 3.11 Peak Band-Pass Filtered Particle Velocity versus Frequency, Station 10S

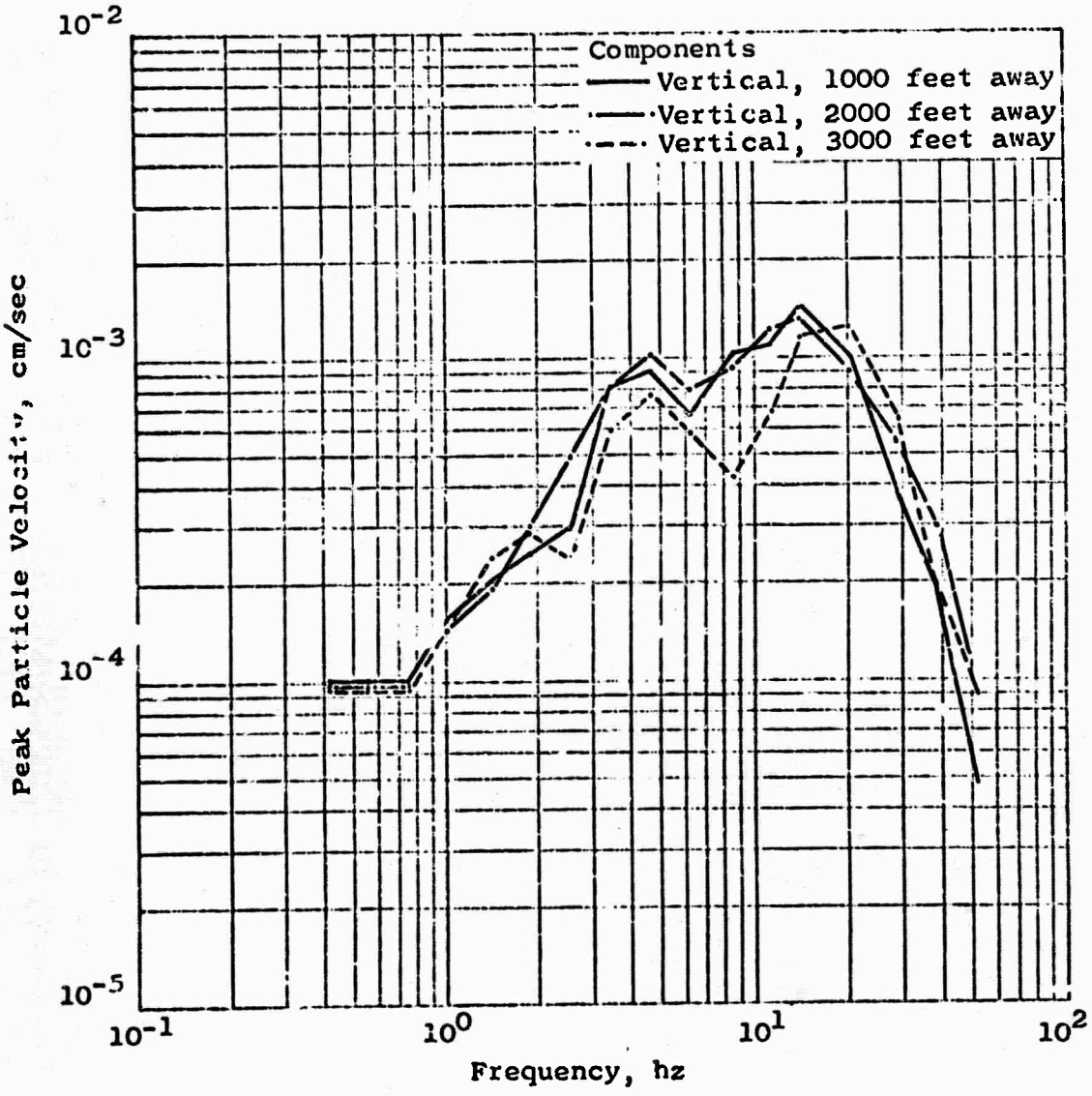

Figure 3.12 Peak Band-Pass Filtered Particle Velocity versus Frequency, Station 10S

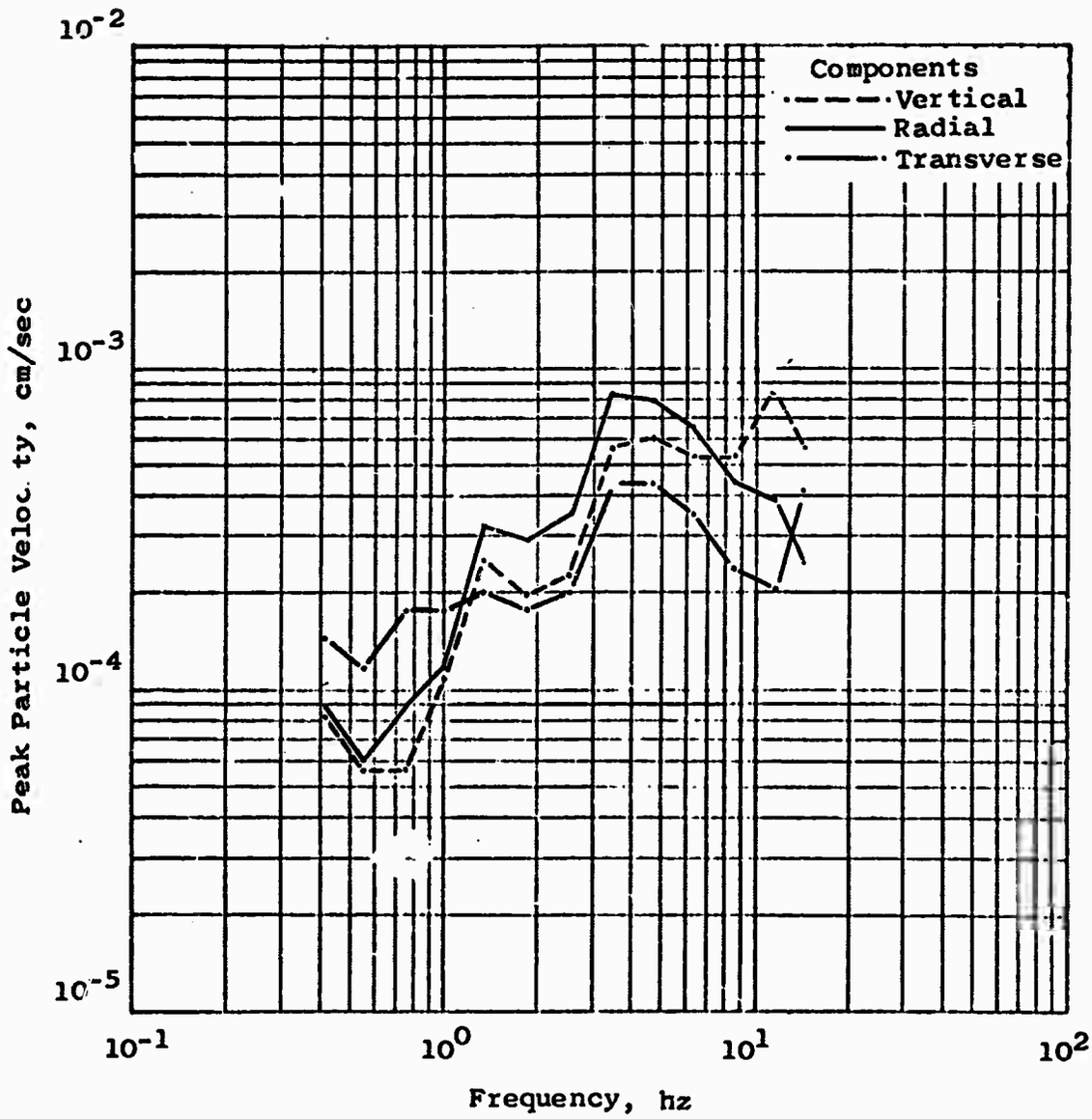

Figure 3.13 Peak Band-Pass Filtered Particle Velocity versus Frequency, Lumberton

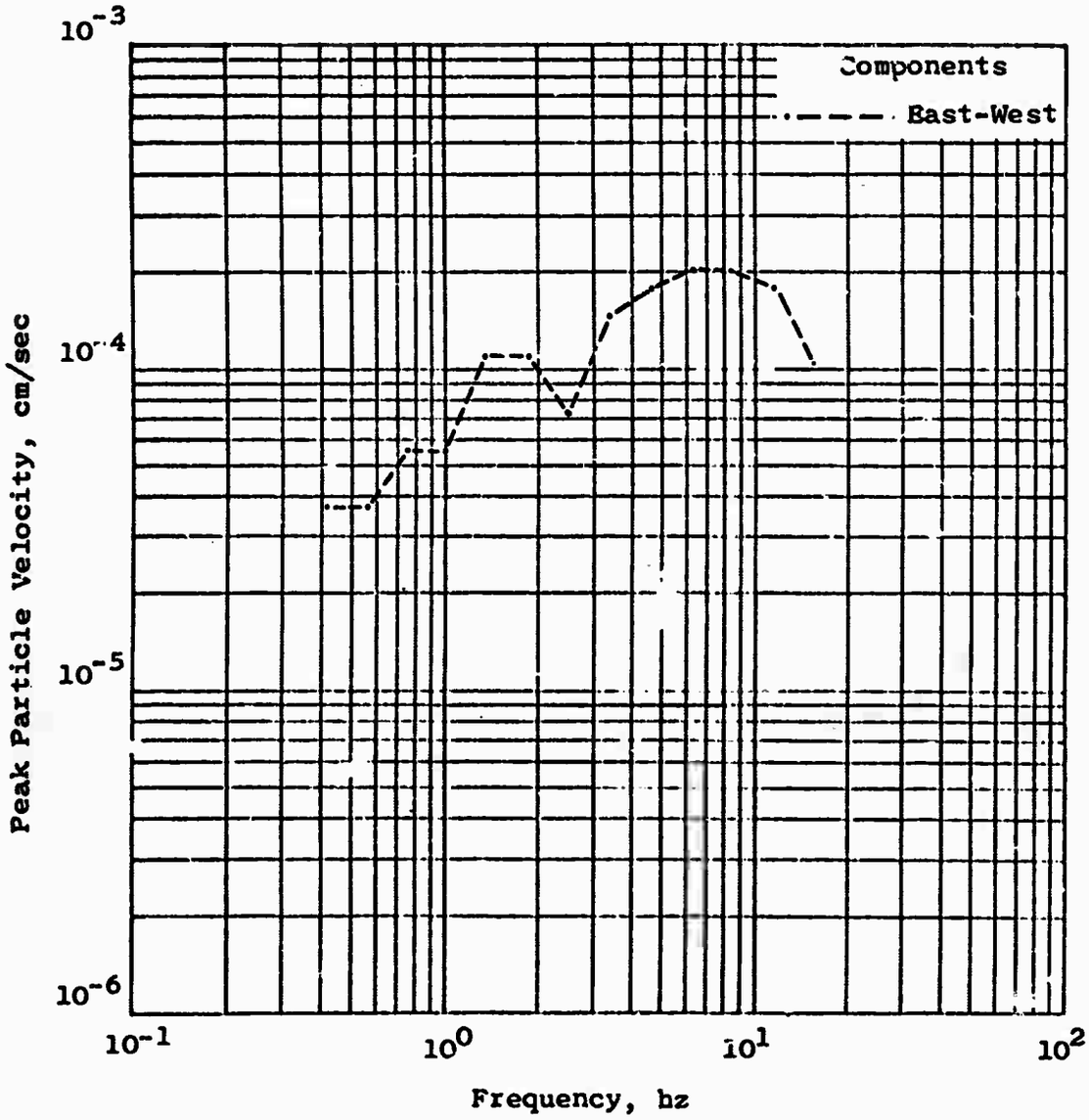

Figure 3.14 Peak Band-Pass Filtered Particle Velocity versus Frequency, Columbia

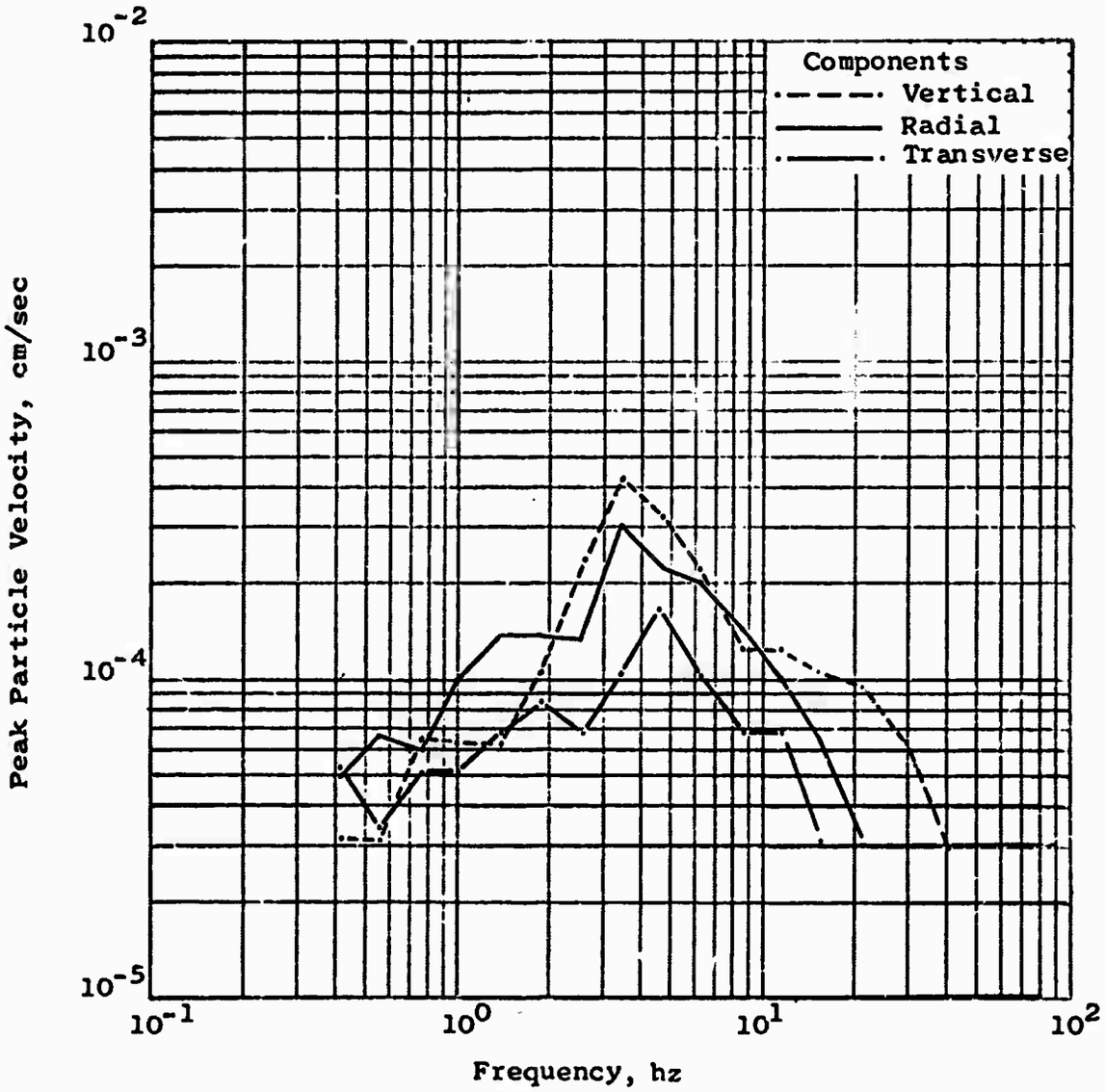

Figure 3.15 Peak Band-Pass Filtered Particle Velocity versus Frequency, Station 20S

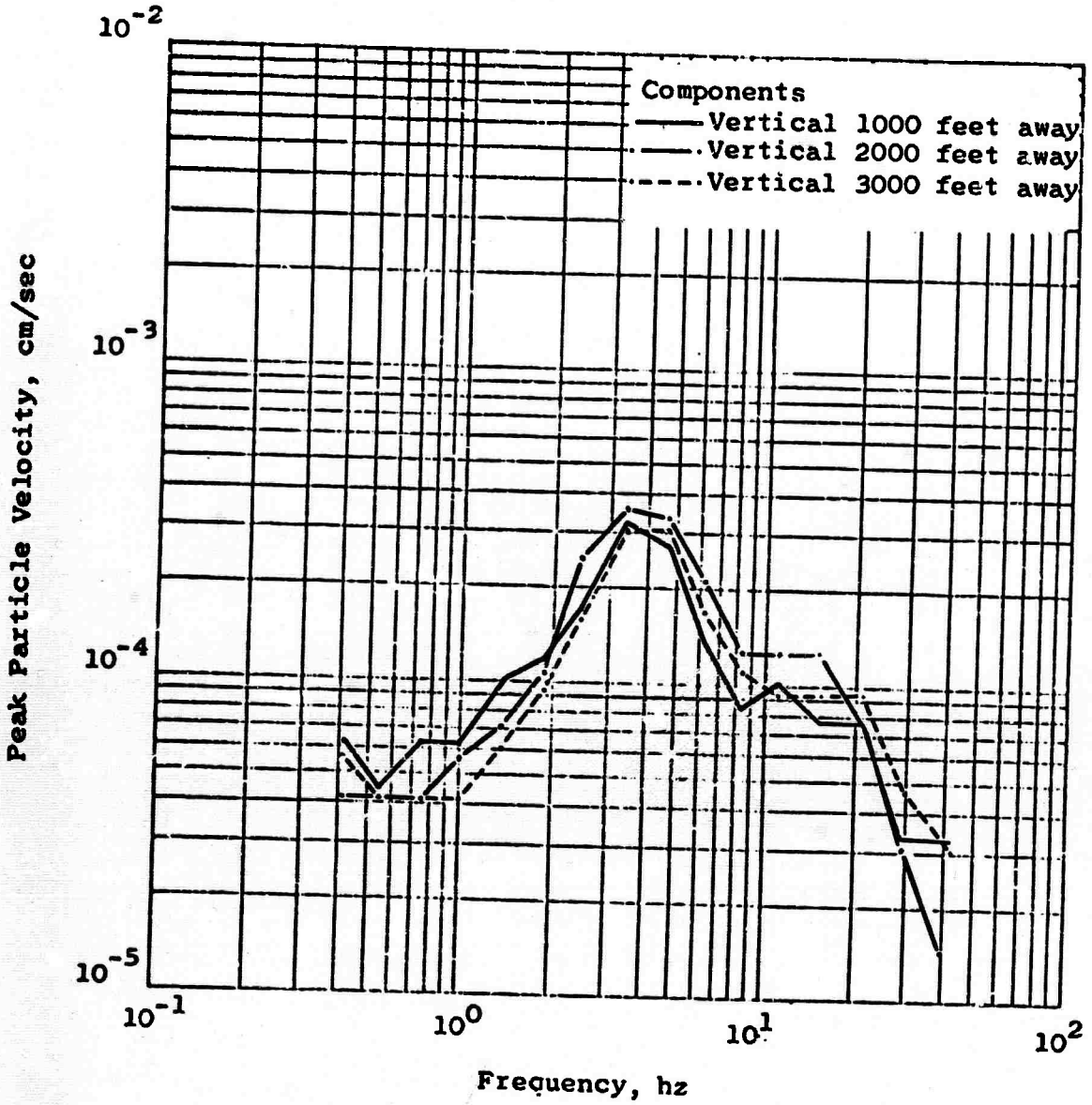

Figure 3.16 Peak Band-Pass Filtered Particle Velocity versus Frequency, Station 20S

CHAPTER 4

ANALYSIS AND DISCUSSION

4.1 PHENOMENOLOGY AND CONTAINMENT

As stated in Chapter 3, the only information available is that the event was completely contained as predicted. The prediction that containment would be achieved was based on the prediction and evaluation of the individual effects and their interrelation in terms of containment. Because Sterling was contained, there is a qualitative substantiation of ERC's evaluation of the adequacy of stemming and the depth of burial. However, none of the other predicted quantities can be compared with results, because there has been no post-shot exploratory program to date.

4.2 SEISMIC

Comparisons of predictions and results are shown on Figures 4.1 through 4.3 for acceleration, displacement, and velocity, respectively. Each figure shows the predictions, for 0.35 kt, for a fully tamped situation and for a decoupling factor of 20. For comparison with the predictions, the least squares regression lines which were fitted to the peak resultant vectors of motions are shown. In general, the observed motions from the Sterling event were associated with high frequencies, and the peak amplitudes attenuated

with distance much more rapidly than did the peak motions observed for the Salmon event.

4.2.1 Acceleration

The comparison between predicted and observed acceleration is shown on Figure 4.1. The regression equation through the data shows an attenuation rate proportional to $R^{-3.04}$, an extremely rapid attenuation when compared with the predicted rate of $R^{-1.95}$ which was based on Salmon data. The predictions using a decoupling factor of 20 are lower than the observed data at the close distances and higher at the long distances. The scatter in the observed data was measured by calculating the standard error of estimate, σ. For the acceleration data, the value of σ was 1.79 which indicates that 68% of the data points are within a factor of 1.79 of the regression equation, assuming normal distribution. By comparison, the standard error calculated for the Salmon acceleration data was 1.66 (Reference 2.11).

4.2.2 Displacement

The displacement comparison is shown on Figure 4.2. The predictions, using a decoupling factor of 20, were higher than observed by factors ranging from about 4 at

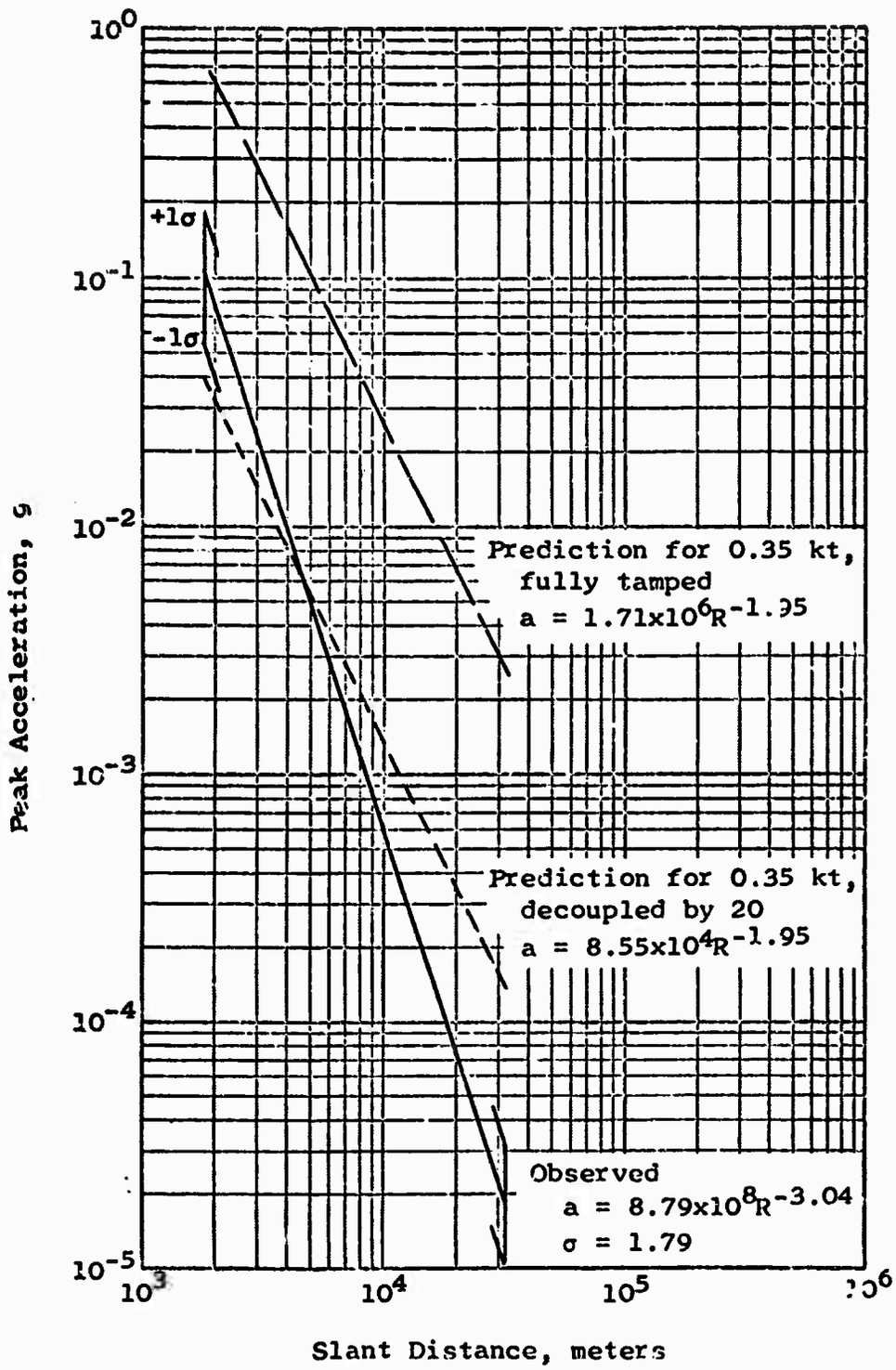

Figure 4.1 Comparison of Predicted and Observed Peak Surface Particle Acceleration.

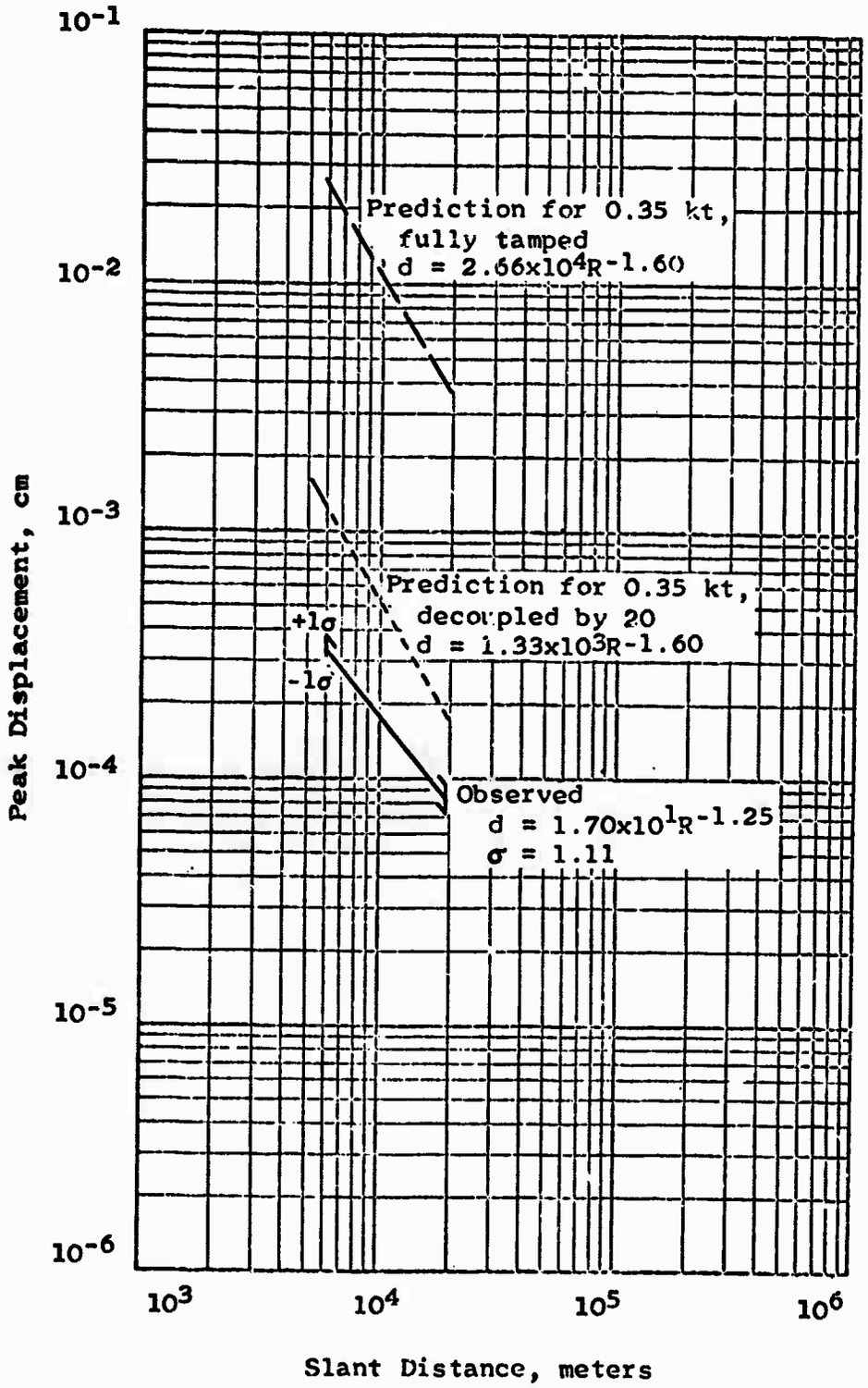

Figure 4.2 Comparison of Predicted and Observed Peak Surface Particle Displacement

the closest station to about 2.5 at the most distant. The data showed very little scatter; the standard error of estimate was a factor of 1.11 from the regression line. The attenuation rate indicated by the regression line through the data was $R^{-1.25}$ compared with the predicted rate of $R^{-1.60}$. However, only five displacement vectors were obtained. Therefore, the indicated scatter and the rate of attenuation of peak displacement, calculated statistically on a very small sample, are not necessarily representative of displacement behavior in general. For example, the Salmon data points showed a standard error of 1.66 (Reference 2.11).

4.2.3 Velocity

The comparison between predicted and observed particle velocity is shown on Figure 4.3. The scatter in the velocity data was small. The standard error was a factor of 1.40 compared with the factor of 1.66 associated with the Salmon data. The predictions using the decoupling factor 20 were higher than the observed velocities by factors ranging from about 1.1 to 6, from the closest to the most distant stations, respectively. The observed data showed a rate of attenuation with distance of $R^{-2.27}$ compared with the predicted rate of $R^{-1.64}$.

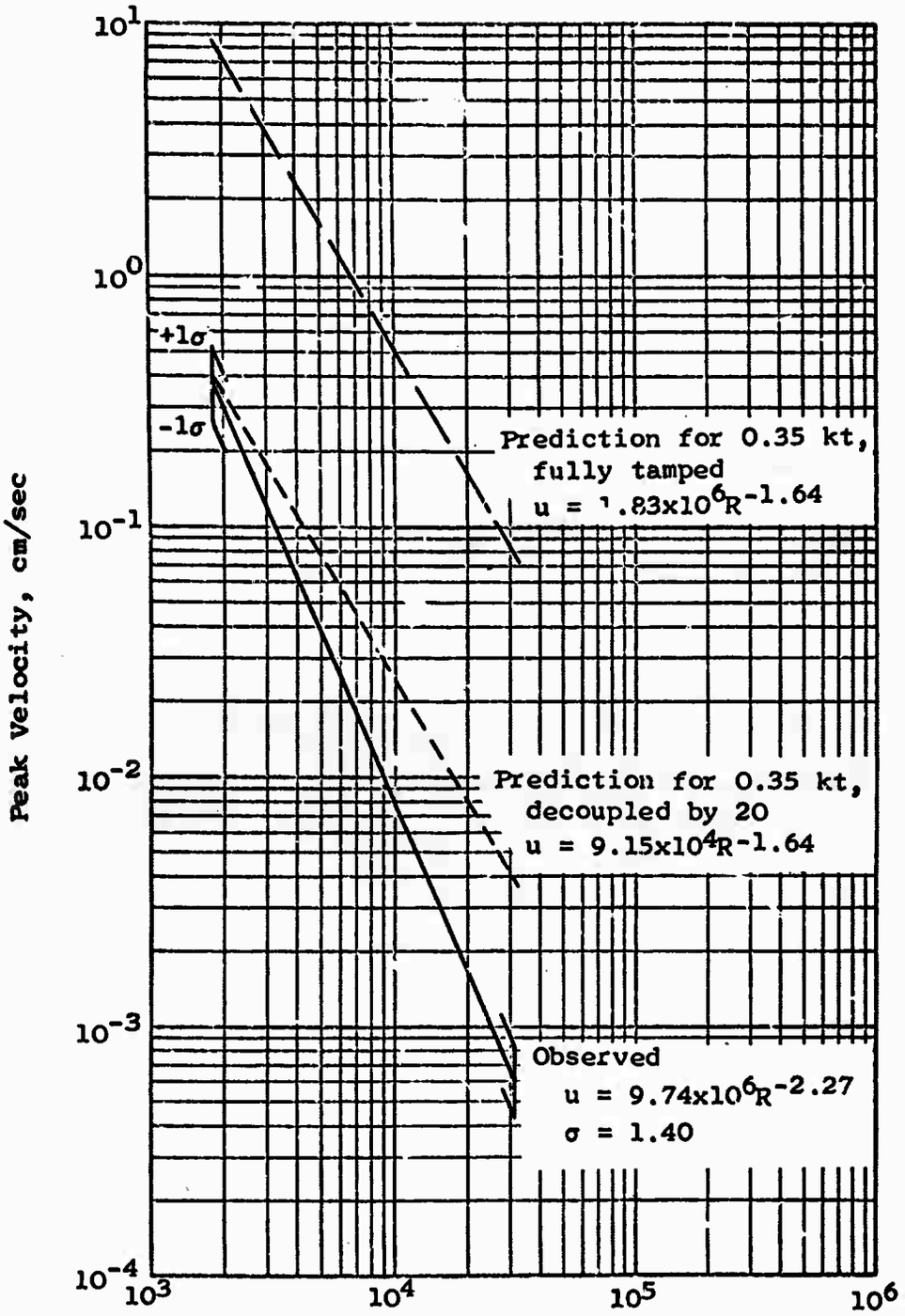

Figure 4.3 Comparison of Predicted and Observed Peak Surface Particle Velocity.

4.2.4 Azimuthal Distribution of Peak Amplitudes

The ground motions recorded from the Salmon event exhibited an asymmetrical distribution with azimuth (Reference 2.11). For comparison, the Sterling data were plotted and contours were drawn showing the azimuthal distribution of the peak amplitudes measured from the Sterling event. Peak vertical, radial and transverse components of particle velocity are shown on Figures 4.4 through 4.6 Peak accelerations are shown on Figures 4.7 through 4.9.

The azimuthal variations observed in the Sterling data were relatively minor compared with Salmon. The high motions at Station 8, about 2 km west of surface zero, indicated preferential propagation to the west. However, this might have been a local phenomenon because the one component of motion (transverse velocity) measured at Columbia (see Figure 4.6) appeared normal with respect to the motions at other stations. The distribution of the peak velocities and accelerations was generally similar if the same components were compared, but differences were noted between the distribution of vertical and horizontal components. The vertical components of both velocity and acceleration were slightly low at Lumberton indicating increased attenuation

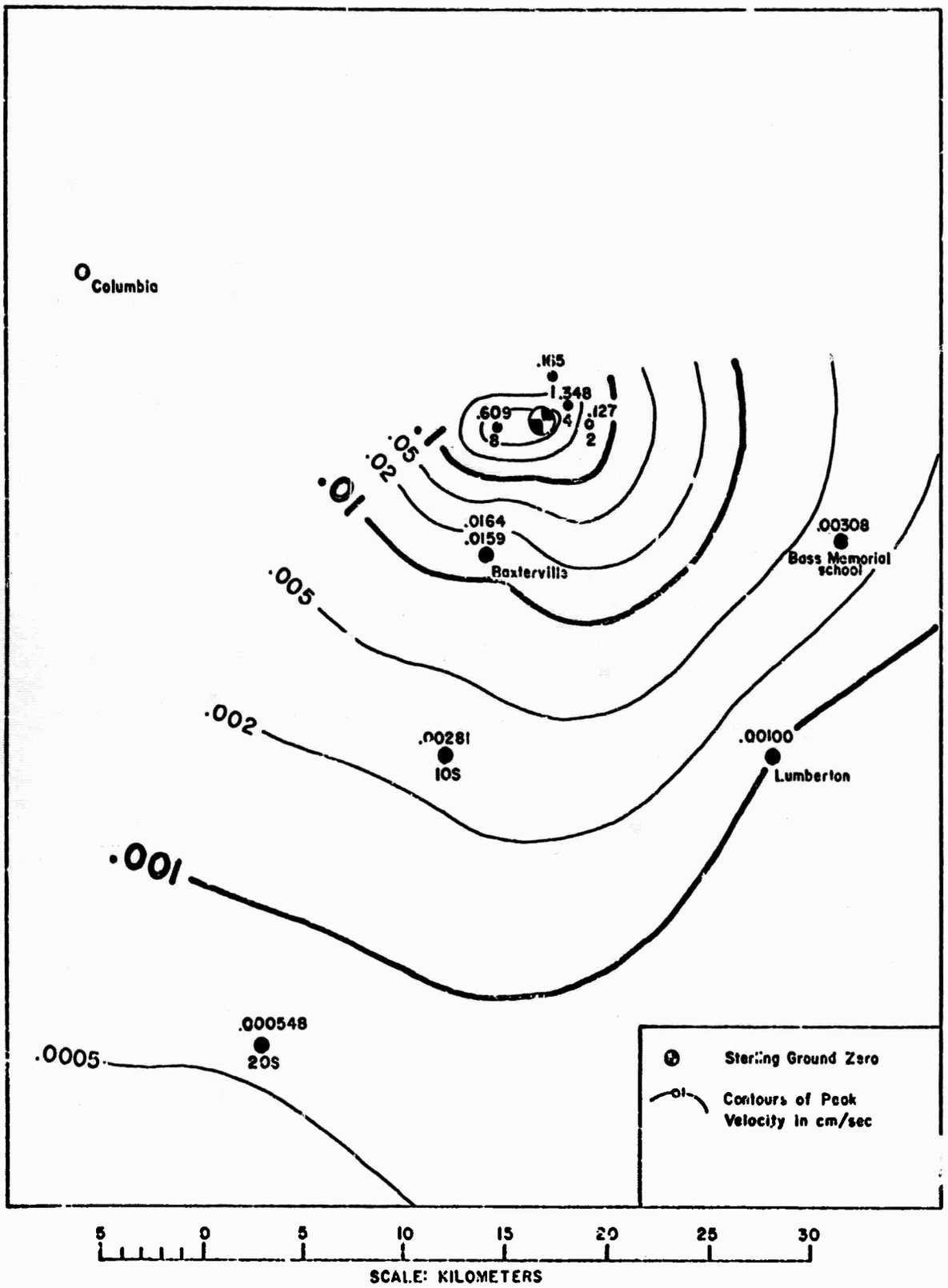

Figure 4.4 Azimuthal Distribution of Peak Vertical Particle Velocity

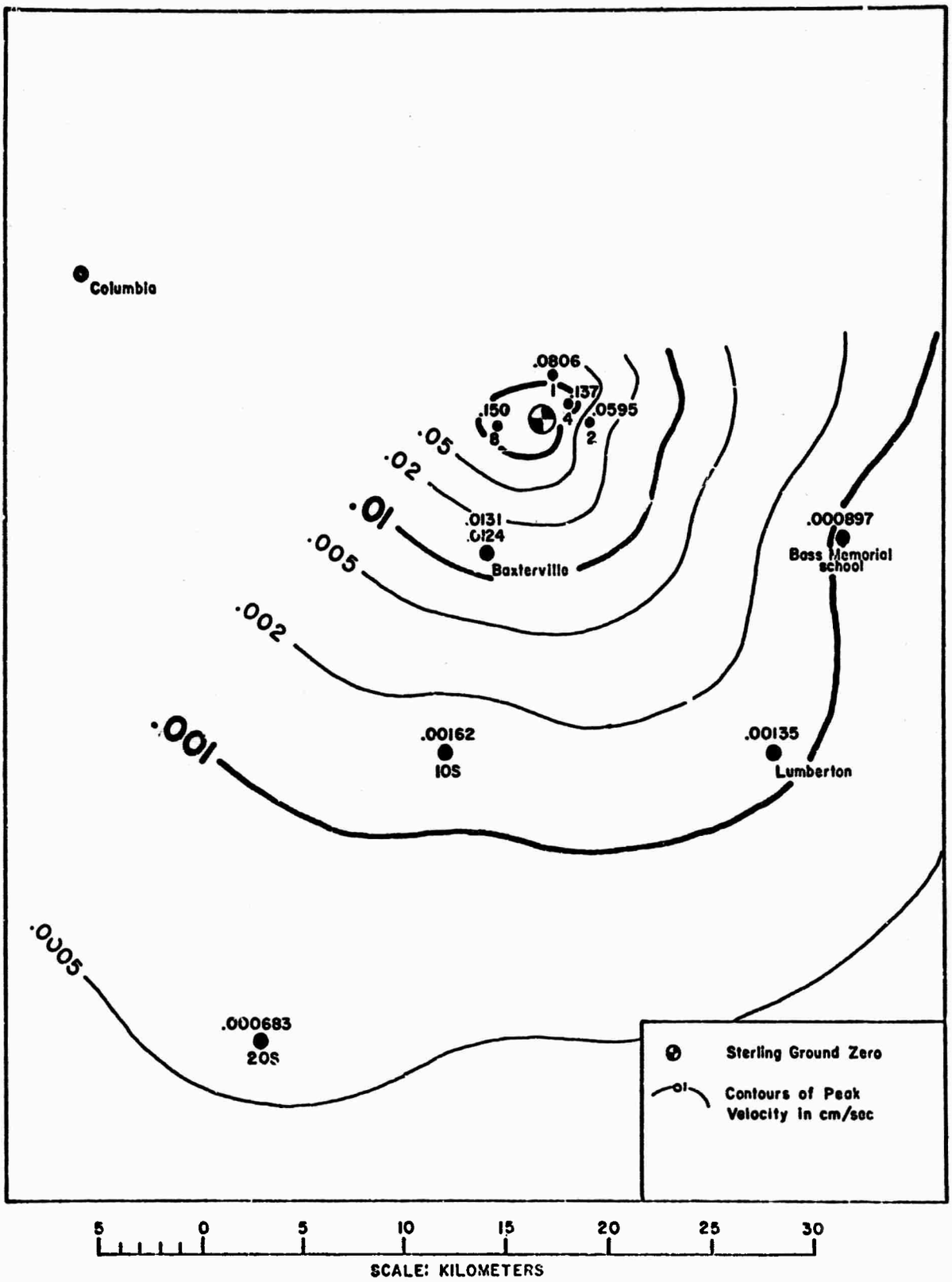

Figure 4.5 Azimuthal Distribution of Peak Radial Particle Velocity

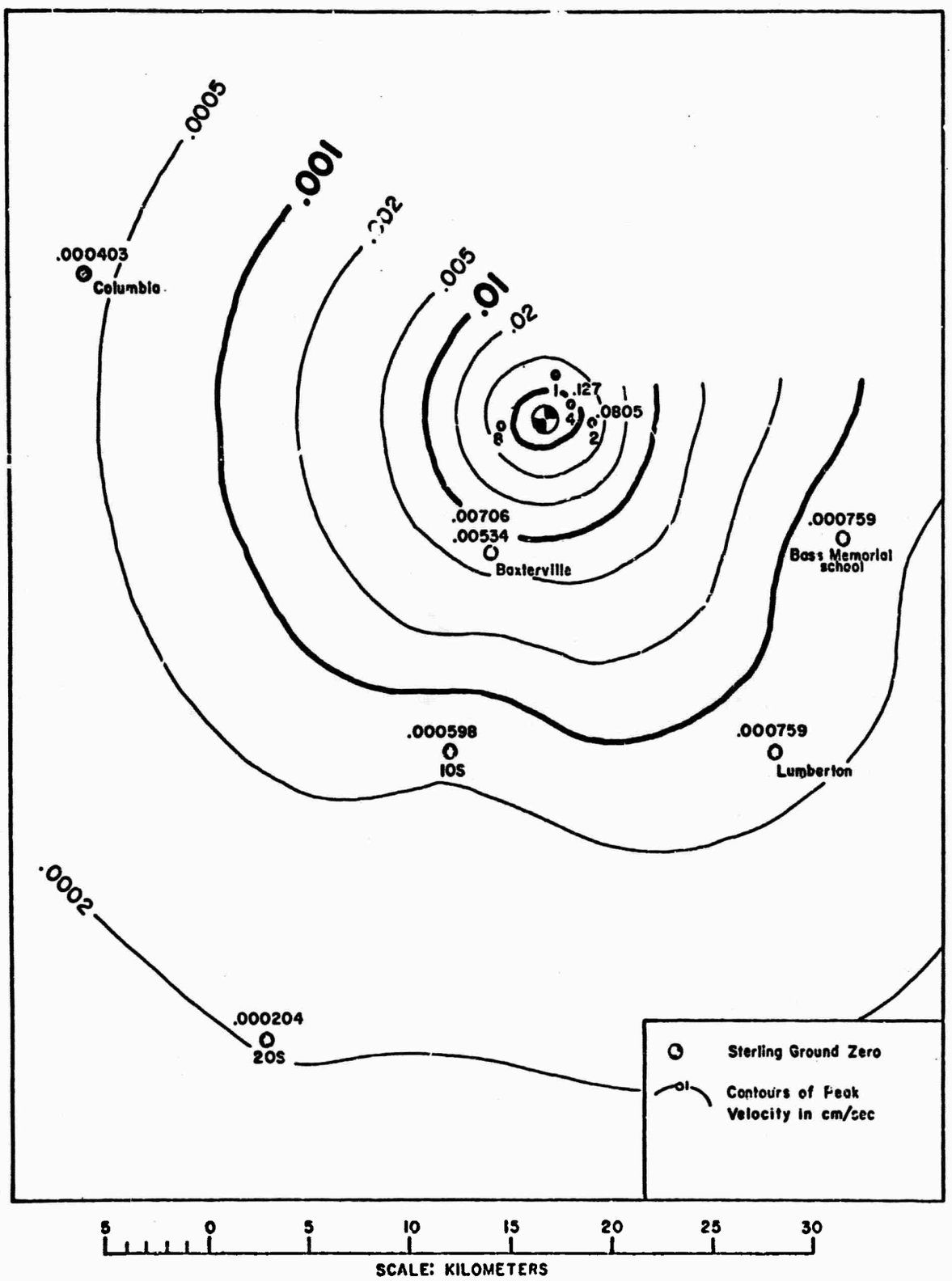

Figure 4.6 Azimuthal Distribution of Peak Transverse Particle Velocity

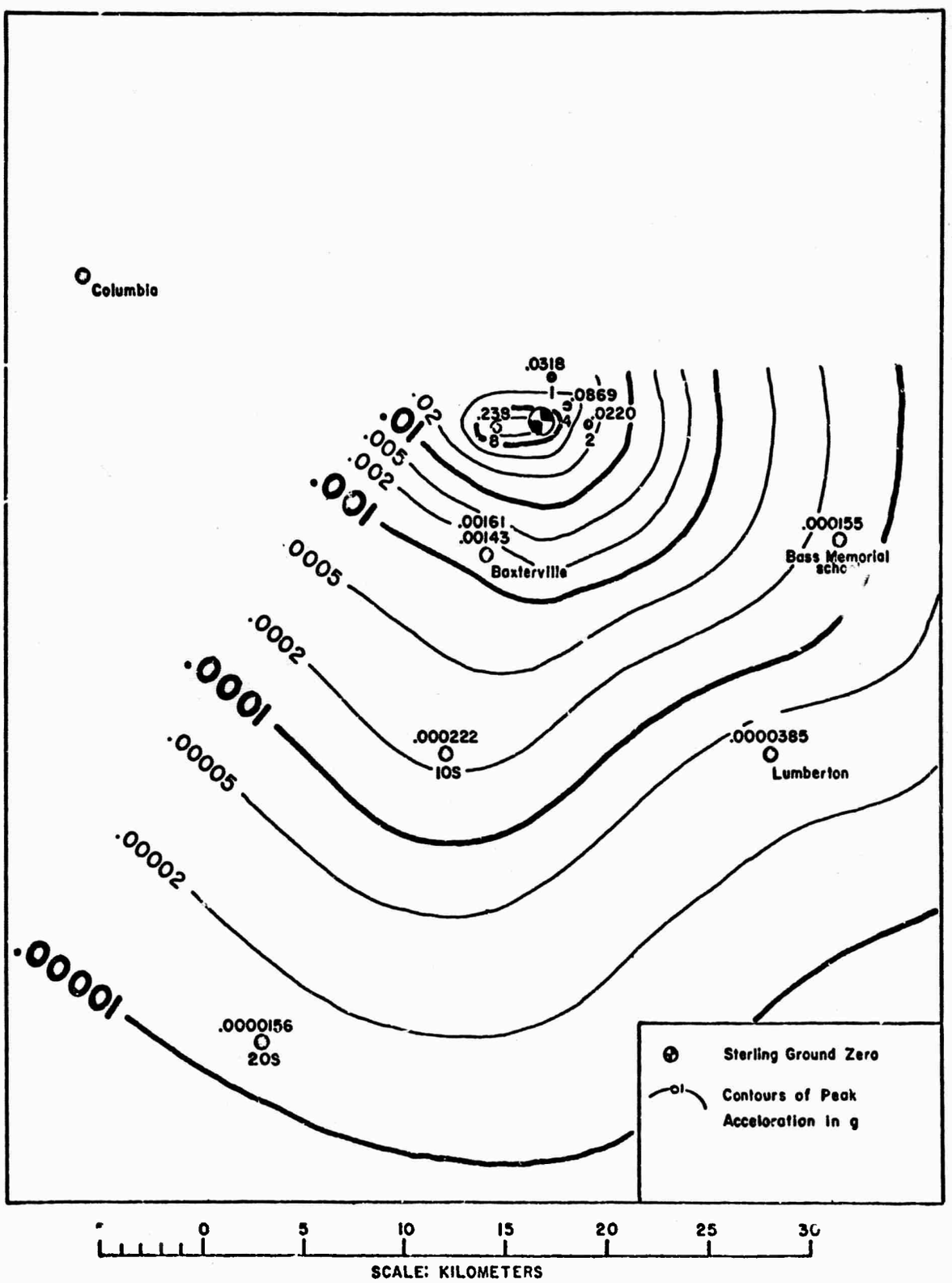

Figure 4.7 Azimuthal Distribution of Peak Vertical Particle Acceleration

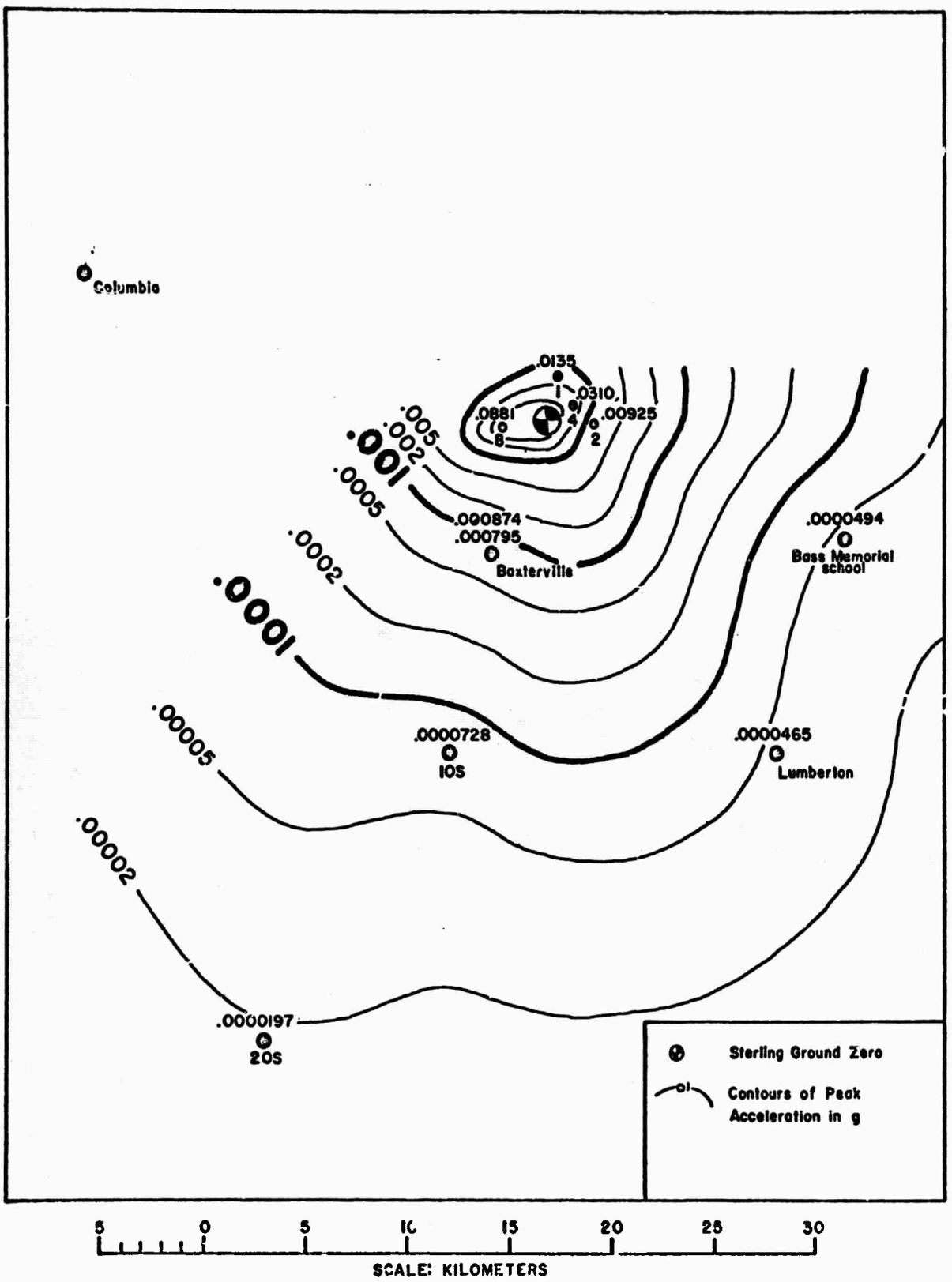

Figure 4.8 Azimuthal Distribution of Peak Radial Particle Acceleration

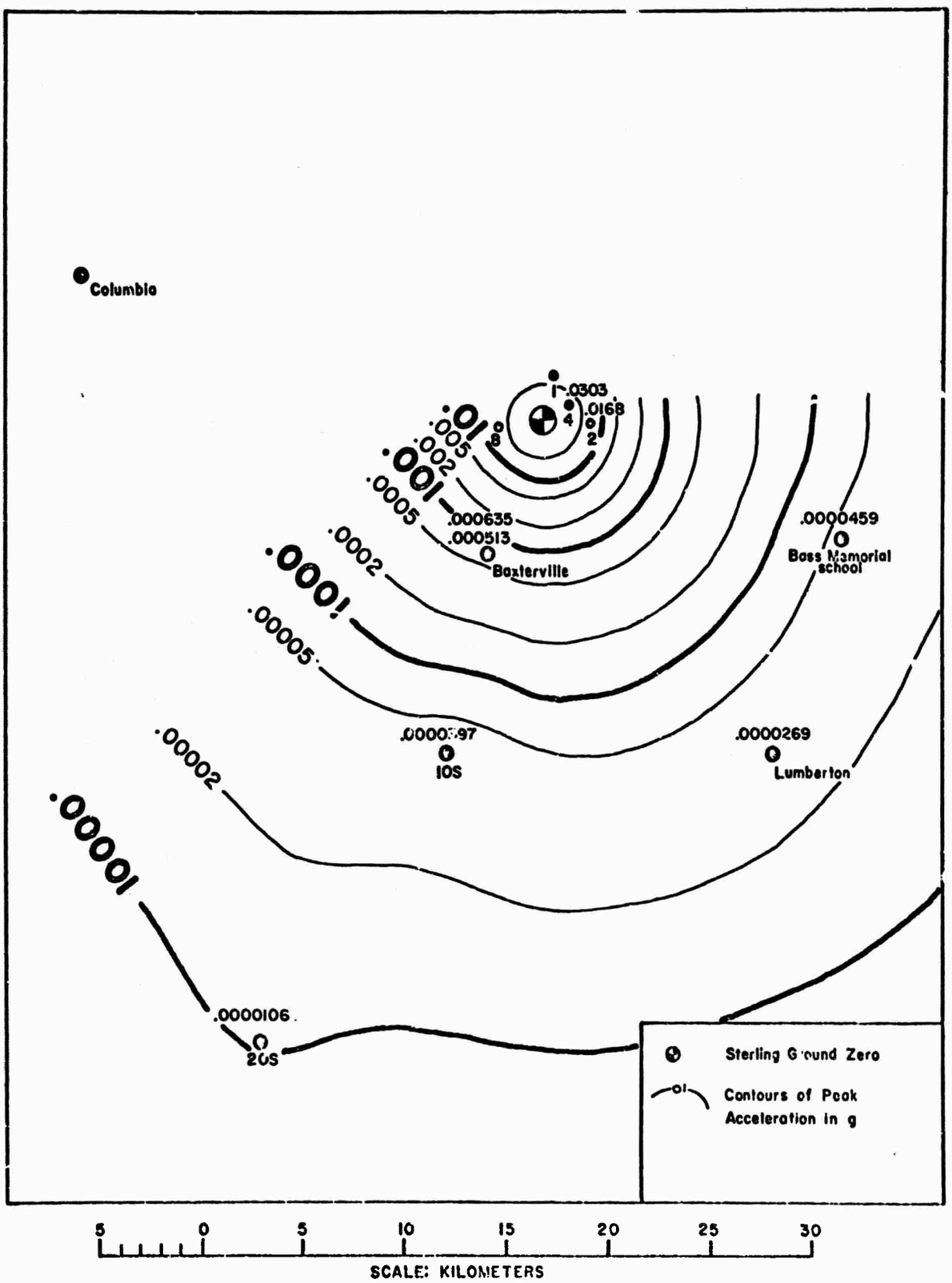

Figure 4.9 Azimuthal Distribution of Peak Transverse Particle Acceleration

of the vertical motion in the southeast direction. However, the horizontal components of velocity and acceleration were about normal at Lumberton but low at Purvis to the east, and Baxterville and 10S to the south.

4.2.5 Amplitude-Frequency

The amplitude-frequency curves shown on Figures 3.4 through 3.15 indicate that the peak amplitudes of ground motion were associated with relatively high frequencies.

The closest stations (Figures 3.4 through 3.7) show that the peak velocities were associated with very high frequency energy. The amplitude-frequency curves for Stations 1, 2 and 4 reach a maximum between 20 and 40 hz, while at Station 8 the peak occurs at about 80 hz.

With increasing distance the frequency at which the peak amplitudes occur tends to decrease. For example Baxterville Post Office (6.1 km), Baxterville School (6.5 km), Bass Memorial School near Purvis (16 km), and 10S (17.8 km) show peak amplitudes associated with frequencies between 10 and 20 hz.

Lumberton and Columbia, 19 and 26 km, respectively, received peak motions with frequencies between 3.5 and 10 hz while at Station 20S, 31.7 km, the peak motions were at frequencies between 3 and 5 hz.

The decrease in frequency with increasing distance is illustrated on Figure 4.10. The frequency of the largest band-pass filtered velocity is shown versus distance for each component. In a few cases, two frequencies had equal amplitudes so the average frequency was plotted. Least-squares regressions through these data show that the change in frequency was proportional to $R^{-.76}$ on the vertical component, $R^{-.92}$ on the radial, and $R^{-.77}$ on the transverse.

4.2.6 Observed Decoupling Factors

The level of the Sterling ground motions and the high rates of attenuation for particle acceleration and velocity (Figures 4.1 and 4.3) considered together with the frequency-distance relationships (Figure 4.10) indicate that the Sterling seismic signal was decoupled and that decoupling was frequency-dependent. A direct measure of the decoupling as a function of frequency results from comparison of the Salmon and Sterling band-pass-filtered particle velocities at Stations 10S and 20S where identical instrumentation was employed for both events. Five traces are available for comparison at Station 10S; one radial, one transverse and three vertical. Station 20S provided a radial, a transverse, and two vertical traces.

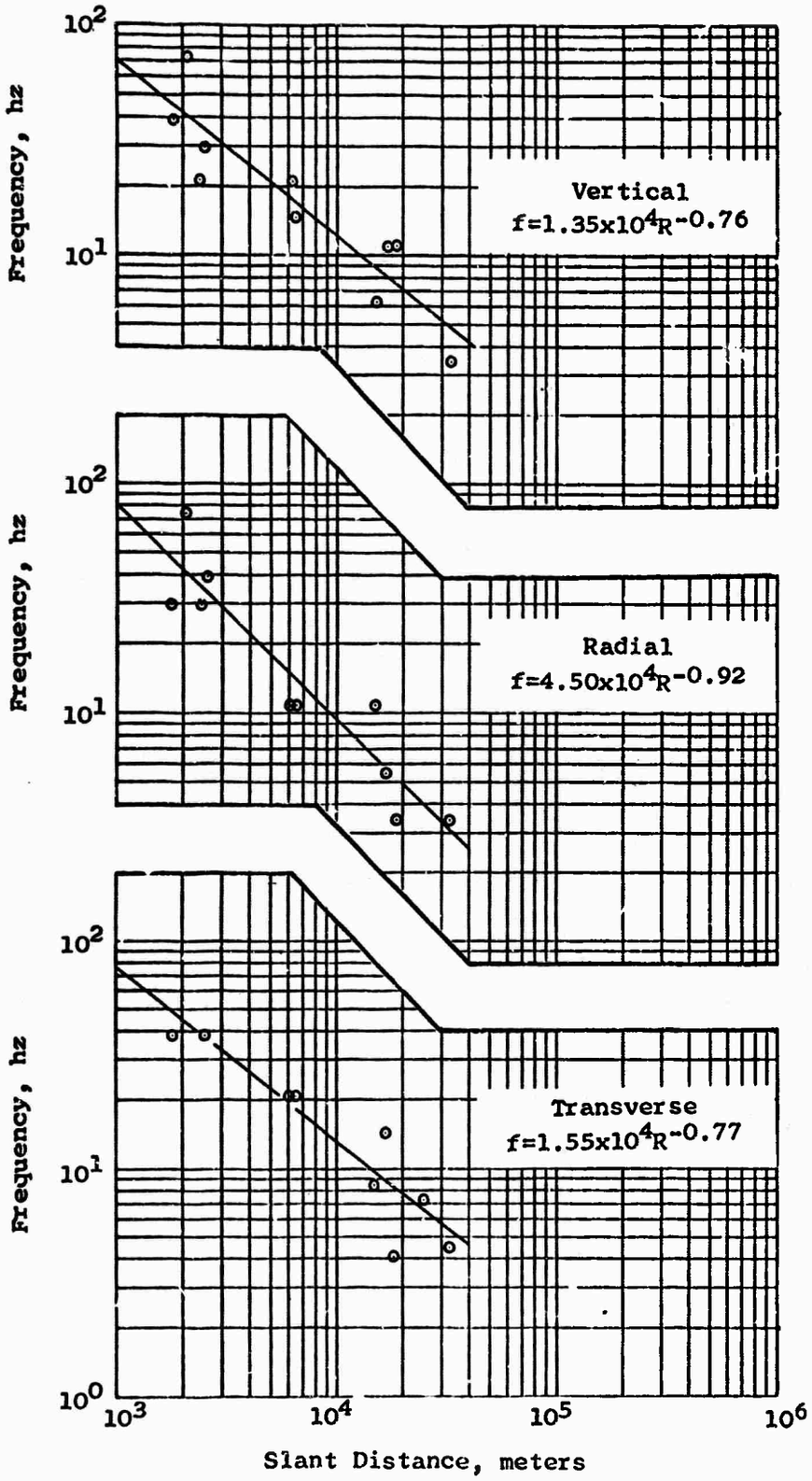

Figure 4.10 Frequency of the Peak Band-Pass Filtered Velocity versus Slant Distance

The Salmon band-pass-filtered velocities at each frequency were scaled to the Sterling yield of 0.35 kt using the frequency-dependent yield scaling exponents from the extrapolation method discussed in Reference 4.1. These scaled velocities were then compared at each frequency with the Sterling velocities. After scaling the Salmon data to the Sterling yield, the Salmon/Sterling ratios are the decoupling factors for particle velocity. Decoupling factors were calculated for fifteen different frequencies ranging from .41 to 29 hz. These values are listed in Table 4.1. Although the decoupling factors exhibit some scatter, there are no noticeable major differences between the factors observed at the two stations and the factors were averaged for each frequency. Separate averages were compiled for the vertical and horizontal components. These average factors are plotted versus frequency on Figure 4.11. The maximum decoupling (a factor of about 200) occurred for frequencies between 2 and 5 hz. The amount of decoupling decreased exponentially for both higher and lower frequencies, dropping to a factor of about 50 at .41 hz and to a factor of about 15 at 29 hz. The decoupling exceeded a factor of 100 for frequencies between 1 and 8 hz.

The observed dependency of decoupling on frequency provides an explanation for the high rates of attenuation

TABLE 4.1. OBSERVED DECOUPLING FACTORS AT STATIONS 10S AND 20S

f (hz)	Vertical Components					Average
	Station 10S			Station 20S		
	Z_o	$Z_{1000'}$	$Z_{2000'}$	$Z_{1000'}$	$Z_{3000'}$	
.41	48	189	57	52	57	81
.55	30	117	44	83	81	71
.75	80	86	70	71	126	87
1.0	150	99	113	151	235	150
1.35	125	91	120	90	223	130
1.85	122	144	118	141	215	148
2.5	269	176	177	282	358	252
3.4	232	224	175	276	268	235
4.6	217	240	175	311	191	227
6.2	210	188	158	310	163	206
8.4	57	90	63	180	88	96
11.3	37	66	35	58	63	52
15.5	17	22	12	30	22	21
21	16	29	11	26	19	20
29	7.4	24	9.4	—	—	14

	Horizontal Components				
	Station 10S		Station 20S		Average
	Radial	Transverse	Radial	Transverse	
.41	24	73	50	20	42
.55	36	93	51	65	61
.75	52	82	63	35	58
1.0	124	149	62	72	102
1.35	127	181	117	118	136
1.85	161	163	215	140	170
2.5	228	251	378	282	285
3.4	177	266	255	227	231
4.6	112	232	208	149	175
6.2	116	190	165	170	160
8.4	105	143	89	130	117
11.3	63	66	79	50	65
15.5	25	12	39	55	33
21	19	14	39	33	26
29	13.	16	—	—	15

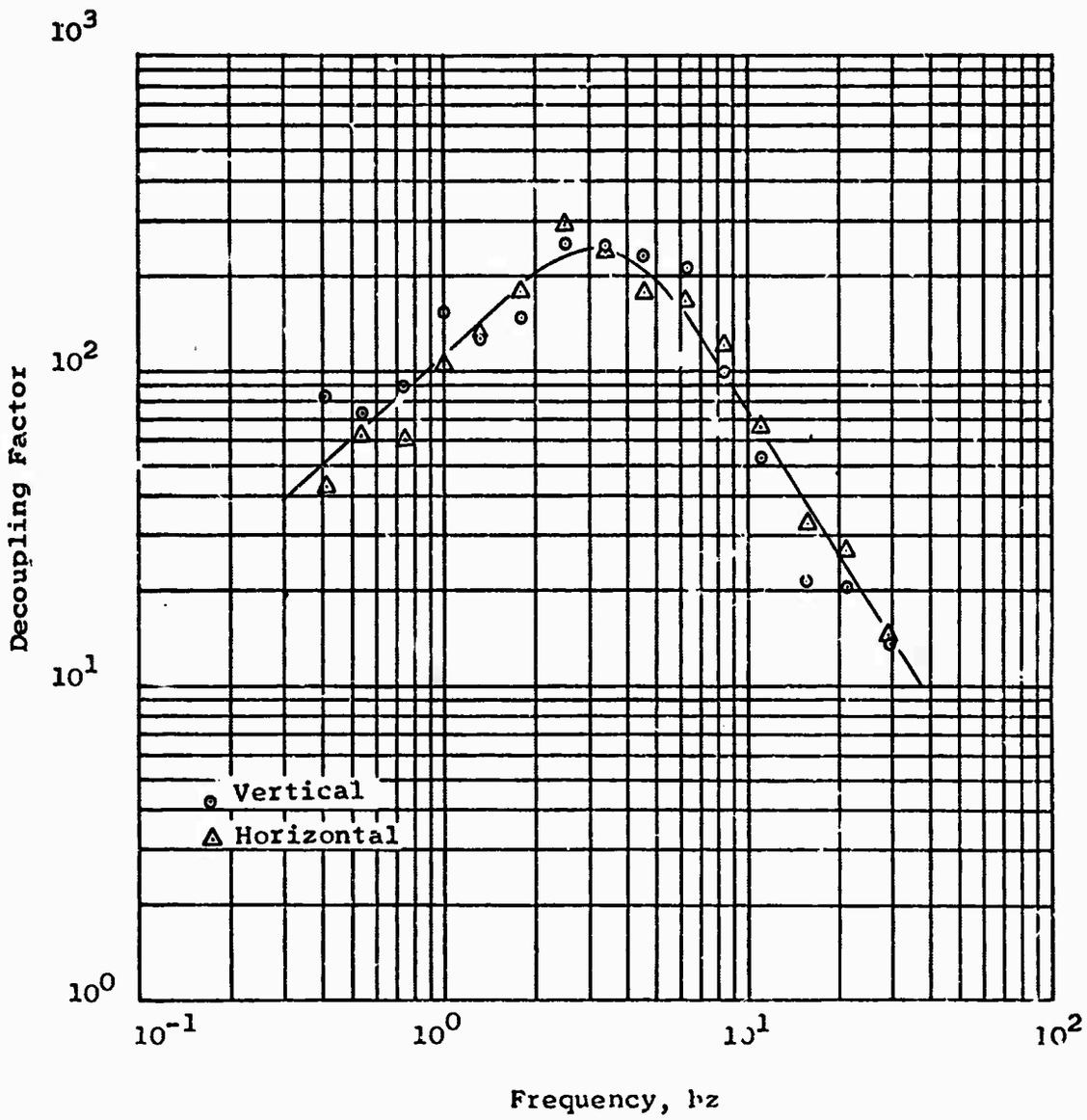

Figure 4.11 Particle Velocity Decoupling Factors Calculated from observed Salmon and Sterling Band Pass Filtered Velocities at Stations 10 S and 20 S

which were observed for the Sterling peak motions. On Figure 4.3, the peak velocities at the closest distances are below the fully coupled prediction by a factor of about 20. These stations recorded relatively more high frequency energy (30 to 50 hz) than more distant stations.

As distance increases, peak amplitudes of particle velocity occur at progressively lower frequencies. Moreover, departures of recorded peak values from the Salmon-derived attenuation rates follow a similar trend. The results of this analysis (Table 4.1, Figure 4.11) show the variation in decoupling factor with frequency of the peak amplitudes.

In summary, the particle velocities from the Sterling event were decoupled by as much as a factor of ' , but only for frequencies in the 2 to 5 hz range. The observed decoupling steadily decreased at frequencies outside this range. The decoupling factor was over 100 throughout the 1 to 8 hz interval. (See Figure 4.11.)

4.2.7 Comparison of Theoretical and Observed Decoupling Factors*

The frequency dependence of the decoupling factor noted in the previous section suggested a study of the decoupling

---

* This section contributed by J. R. Murphy

theory presented by Latter et. al., to determine if the theory is compatible with the observations at the distances under consideration.

The Fourier transform of the displacement at a distance R from a tamped shot is given by (Reference 4.1):

$$(1) \qquad \hat{\zeta}_T(\omega) = \frac{p(\omega)a'}{4\mu}\left(\frac{1}{R^2} + \frac{i\omega}{Rc}\right)\frac{c^2}{\omega_o'^2 + i\omega_o'\omega - \frac{\lambda+2\mu}{4\mu}\omega^2}$$

where c is the compressional wave velocity in the medium, a' is the radius at which the medium begins to behave elastically, $p(\omega)$ is the Fourier transform of the pressure that acts at a' and $\omega_o' = c/a'$. With $R >> c/\omega$, Equation (1) reduces to:

$$(1a) \qquad \hat{\zeta}_T(\omega) = \frac{p(\omega)a'(i\omega)}{4\mu R}\,\frac{c}{\omega_o'^2 + i\omega_o'\omega - \frac{\lambda+2\mu}{4\mu}\omega^2}$$

Similarly, the Fourier transform of the elastic displacement produced by a step pressure p, at a distance R for a decoupled shot is given by (Reference 4.2):

$$(2) \qquad \hat{\zeta}_D(\omega) = \frac{pa}{8\pi\mu R}\,\frac{c}{\omega_o^2 + i\omega_o\omega - \frac{\lambda+2\mu}{4\mu}\omega^2}$$

where a is the radius of the spherical cavity sufficiently large that the pressure developed on the wall does not exceed the elastic limit of the medium and $\omega_o = c/a$.

Thus, the decoupling factor as a function of frequency is given by

$$\left| \frac{\hat{\zeta}_T(\omega)}{\hat{\zeta}_D(\omega)} \right| .$$

We now calculate this decoupling factor for several physically realizable pressure profiles at R = a'.

Step Function

First, let the pressure profile at R = a' be given by p H(t) where H(t) is the unit step function. Then p(ω) is given by:

$$p(\omega) = \frac{p}{2\pi} \int_{-\infty}^{\infty} H(t) e^{-i\omega t}\, dt = \frac{p}{2\pi} \left[\frac{\delta(\omega)}{2} - \frac{i}{\omega} \right]$$

or, for

$$\omega \neq 0, \quad p(\omega) = \frac{-ip}{2\pi\omega} .$$

Letting λ = u and substituting for p(ω) in Equation (1a);

$$\frac{\hat{\zeta}_T(\omega)}{\hat{\zeta}_D(\omega)} = \frac{a'(\omega_o^2 + \omega_o i\omega_o \omega - 3/4\omega^2)}{a(\omega_o'^2 + i\omega_o'\omega - 3/4\omega^2)} .$$

Setting $\alpha = (\omega_o^2 - 3/4\omega^2)$, $\beta = (\omega_o'^2 - 3/4\omega^2)$, this gives a decoupling factor

$$(3) \qquad \left| \frac{\hat{\zeta}_T(\omega)}{\hat{\zeta}_D(\omega)} \right| = \frac{a' \sqrt{\alpha^2 + \omega_o^2 \omega^2}}{a \sqrt{\beta^2 + \omega_o'^2\, \omega^2}} .$$

Interpolation Function

Next, let the pressure profile at R = a' be given by

$$p(t) = p \operatorname{sinc} \tau \, H(\tau)$$

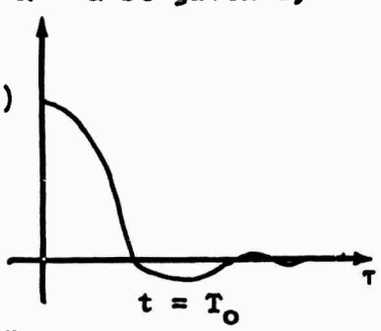

where

$$\operatorname{sinc} \tau = \frac{\sin \pi \tau}{\pi \tau}$$

and

$$\tau = \frac{t}{T_o} \quad . \quad \text{Then} \quad p(\omega) = \frac{pT_o}{2\pi} \int_{-\infty}^{\infty} \operatorname{sinc} \tau \, H(\tau) e^{-i\omega T_o \tau} \, d\tau$$

$$= \frac{pT_o}{2\pi} \left[\frac{\Pi\left(\frac{\omega T_o}{2\pi}\right)}{2} - \frac{i}{2\pi} \log \left| \frac{\frac{\omega T_o}{2\pi} + 1/2}{\frac{\omega T_o}{2\pi} - 1/2} \right| \right]$$

where Π is the rectangle function given by

$$\Pi\left(\frac{\omega T_o}{2\pi}\right) = \begin{cases} 0, & \left| \frac{\omega T_o}{2\pi} \right| > 1/2 \\ 1, & \left| \frac{\omega T_o}{2\pi} \right| < 1/2 \end{cases}$$

Letting $n = \frac{\Pi\left(\frac{\omega T_o}{2\pi}\right)}{2}$, $\gamma = \frac{\log \left| \frac{\frac{\omega T_o}{2\pi} + 1/2}{\frac{\omega T_o}{2\pi} - 1/2} \right|}{2\pi}$;

$$p(\omega) = \frac{pT_o}{2\pi} (n - i\gamma) \, .$$

Therefore,

$$\frac{\hat{\zeta}_T(\omega)}{\hat{\zeta}_D(\omega)} = \frac{a' T_o \omega \left[(\gamma\alpha - n\omega_o\omega) + i(n\alpha + \gamma\omega_o\omega) \right]}{a \, (\beta + i\omega_o'\omega)} \, .$$

This gives a decoupling factor

$$(4) \qquad \left| \frac{\hat{\zeta}_T(\omega)}{\hat{\zeta}_D(\omega)} \right| = \frac{a' T_o \omega \sqrt{(\gamma\alpha - n\omega_o\omega)^2 + (n\alpha + \gamma\omega_o\omega)^2}}{a\sqrt{\beta 2 + \omega_o'^2 \omega^2}}$$

Exponential Function

Finally, let the pressure profile at R = a' be given by

$$p(t) = pe^{-|\tau|} \quad H(\tau)$$

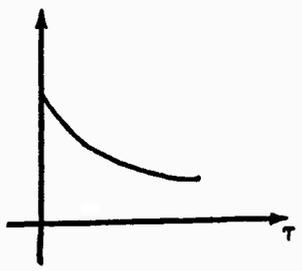

where again, $\tau = \frac{t}{T_o}$

Then

$$p(\omega) = \frac{pT_o}{2\pi} \int_{-\infty}^{\infty} e^{-|\tau|} \quad H(\tau)\ e^{-i\omega T_o \tau}\ d\tau$$

$$= \frac{pT_o}{2\pi} \left[\frac{1 - i\omega T_o}{1 + (\omega T_o)^2} \right]$$

Letting

$$n' = \frac{1}{1+(\omega T_o)^2}, \quad \gamma' \quad \frac{\omega T_o}{1+(\omega T_o)^2} \quad ;$$

$$p(\omega) = \frac{pT_o}{2\pi} \quad (n' - i\gamma')$$

Therefore, the decoupling factor in this case is given by:

$$(5) \qquad \left| \frac{\hat{f}_T(\omega)}{\hat{f}_D(\omega)} \right| = \frac{a' T_o \omega \sqrt{(\gamma'\alpha - n'\omega_o\omega)^2 + (n'\alpha + \gamma'\omega_o\omega)^2}}{a \sqrt{\beta^2 + \omega_o'^2 \omega^2}}$$

In evaluating Equations (3) through (5), the following constants were used; c = 4267 m/sec, a = 16.8 m, T_o = 0.02 seconds. The elastic radius of Salmon, a', was taken to be 300 m and 400 m respectively in accordance with the lower and upper bounds determined by other investigators (Reference 4.3).

The decoupling factors corresponding to Equations (3), (4), and (5) with a' = 300 m are shown in Figures 4.12, 4.13, and 4.14 respectively, and those corresponding to the same equations with a' = 400 m are shown in Figures 4.15-4.17. No attempts have been made to obtain realistic magnitudes of the pressures acting at a and a', and therefore the magnitudes appearing on the ordinates are not necessarily representative of the values to be expected. It can be seen, however, that the shapes of the curves corresponding to Equations (4) and (5) are very similar to the shape of the decoupling curve from the observed BPF data. In all cases, the calculated curves roll off at the high frequency end as does the observed.

In conclusion, it may be said, that the theory predicts a frequency dependence of the decoupling factor which is in good agreement with the measured data.

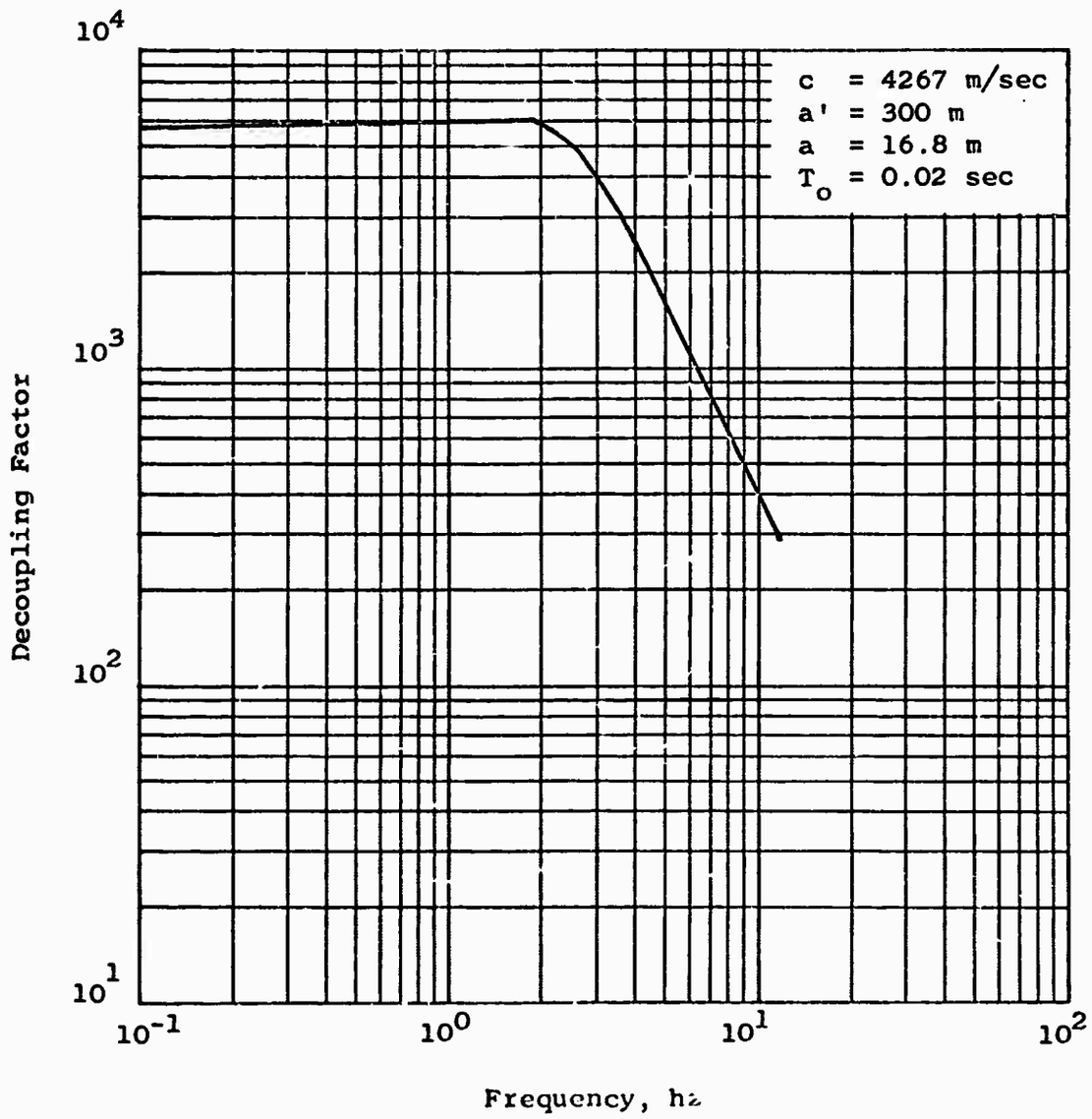

Figure 4.12 Decoupling Factor for Step Function Pressure Profile, p(t) = p H(t).

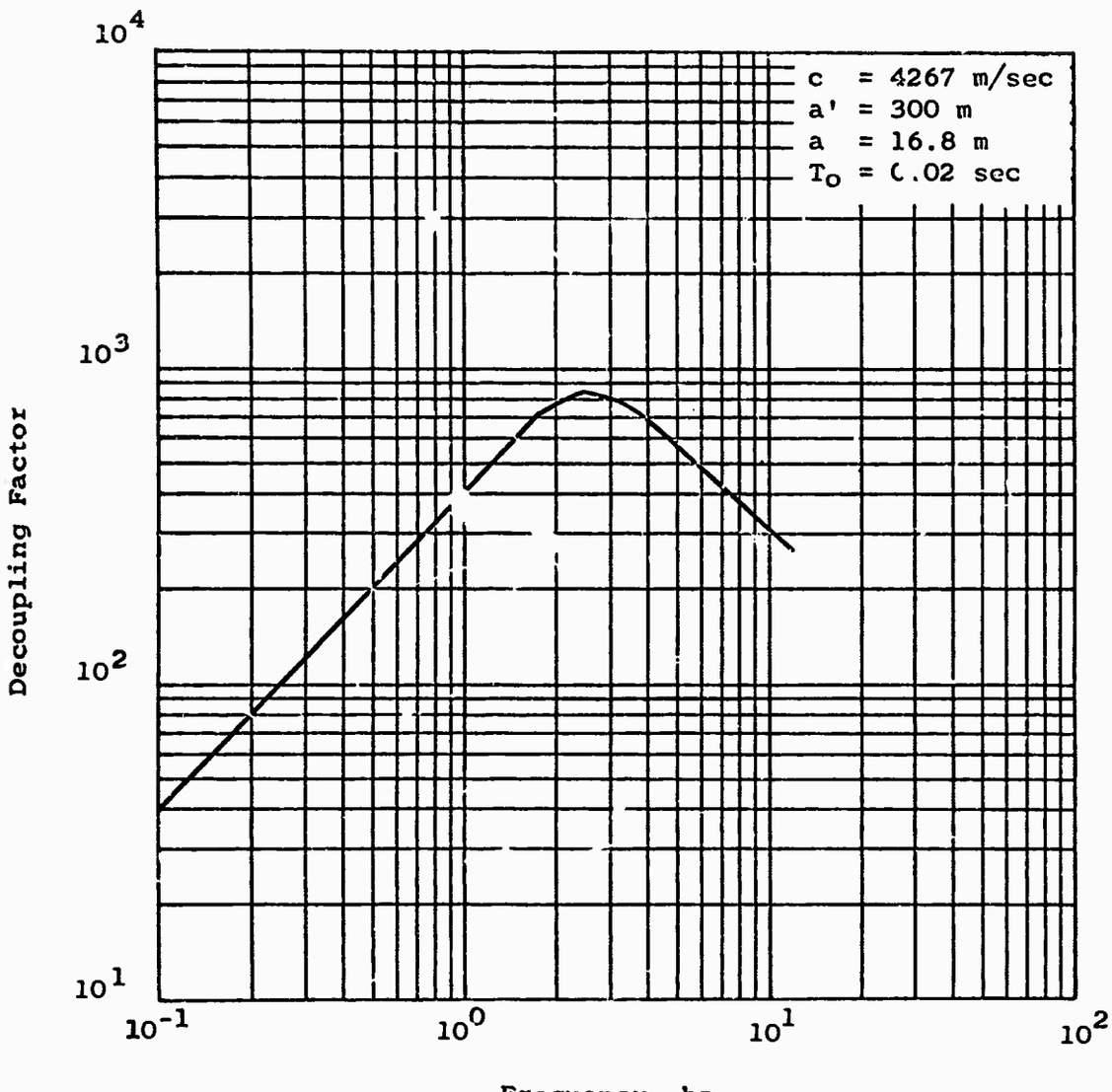

Figure 4.13 Decoupling Factor for Interpolation Function Pressure Profile, $p(t) = p \operatorname{sinc} \tau H(\cdot)$

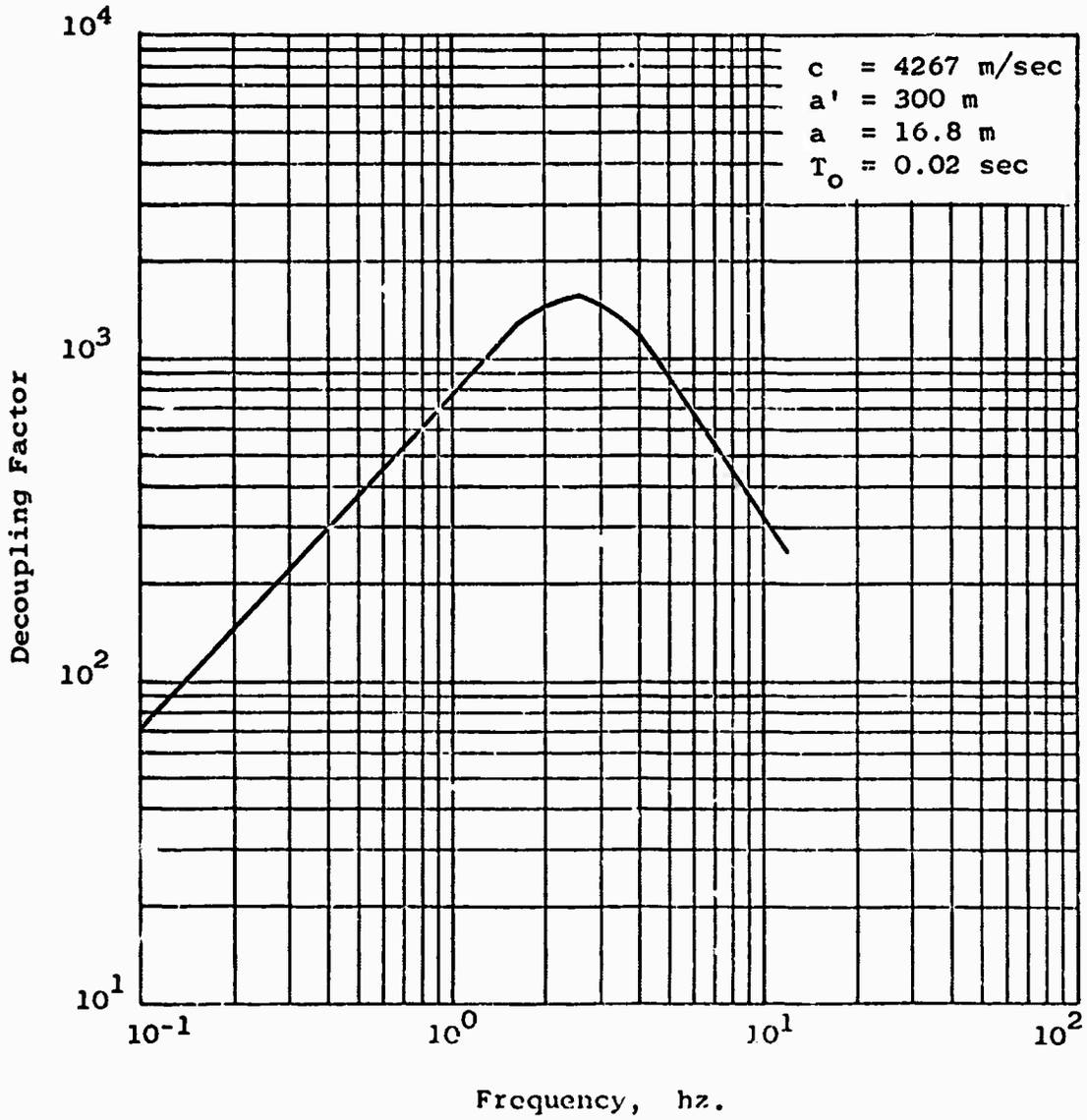

Figure 4.14 Decoupling Factor for Exponential Function Pressure Profile $p(t) = p\, e^{-|\tau|} H(\tau)$.

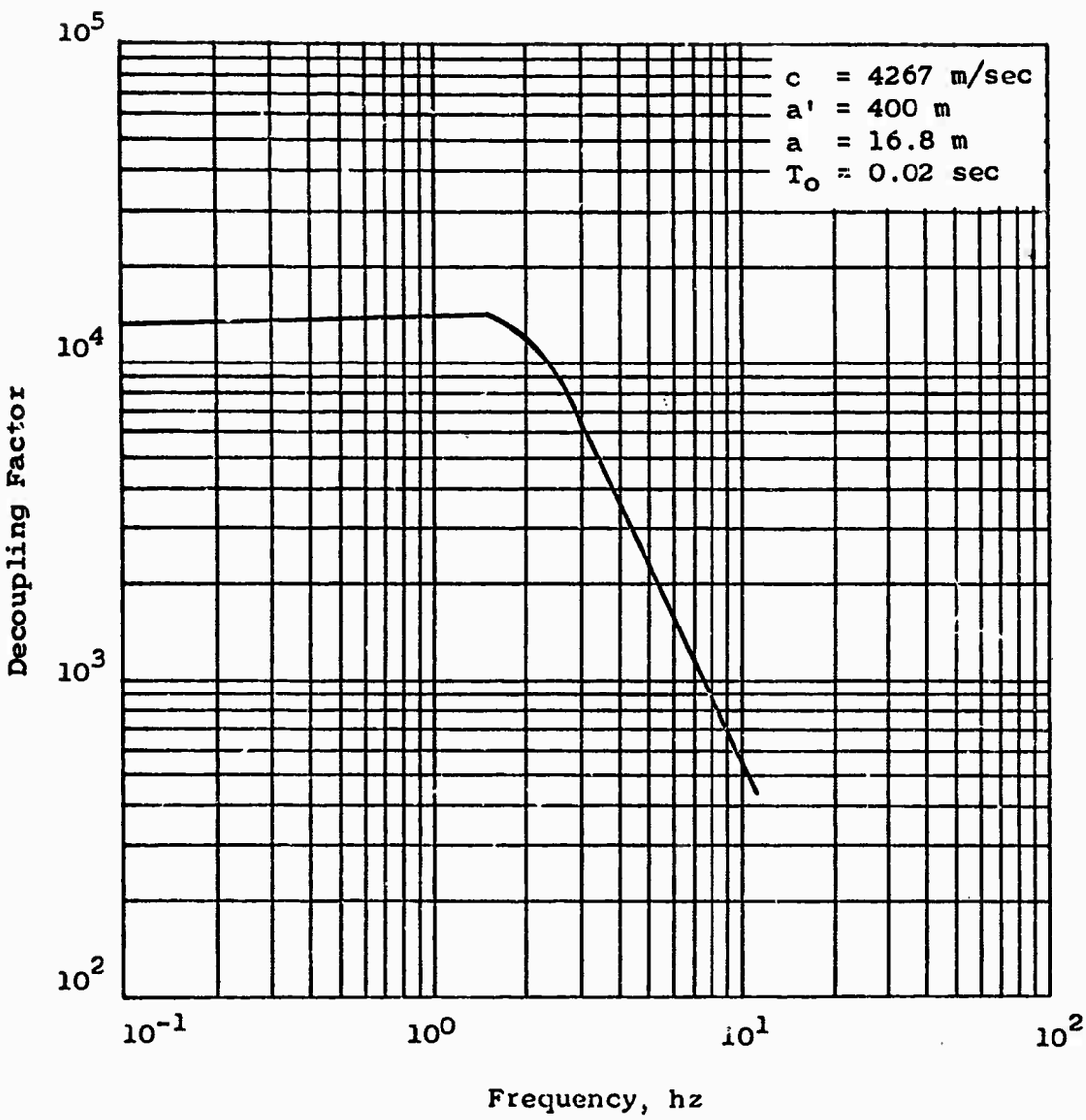

Figure 4.15 Decoupling Factor for Step Function Pressure Profile $p(t) = p\,H(t)$.

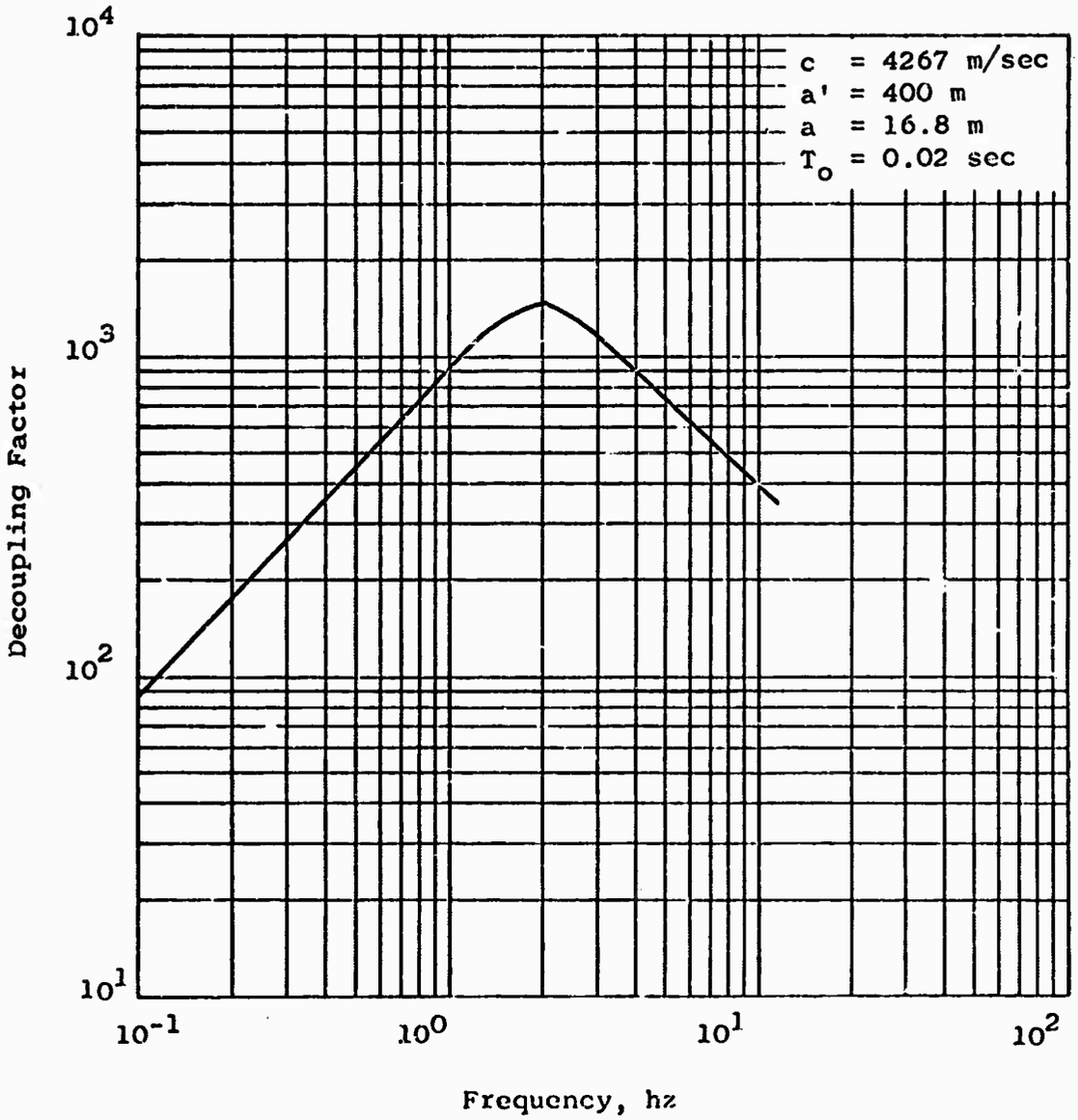

Figure 4.16 Decoupling Factor for Interpolation Function Pressure Profile, $p(t) = p \operatorname{sinc} \tau H(\tau)$.

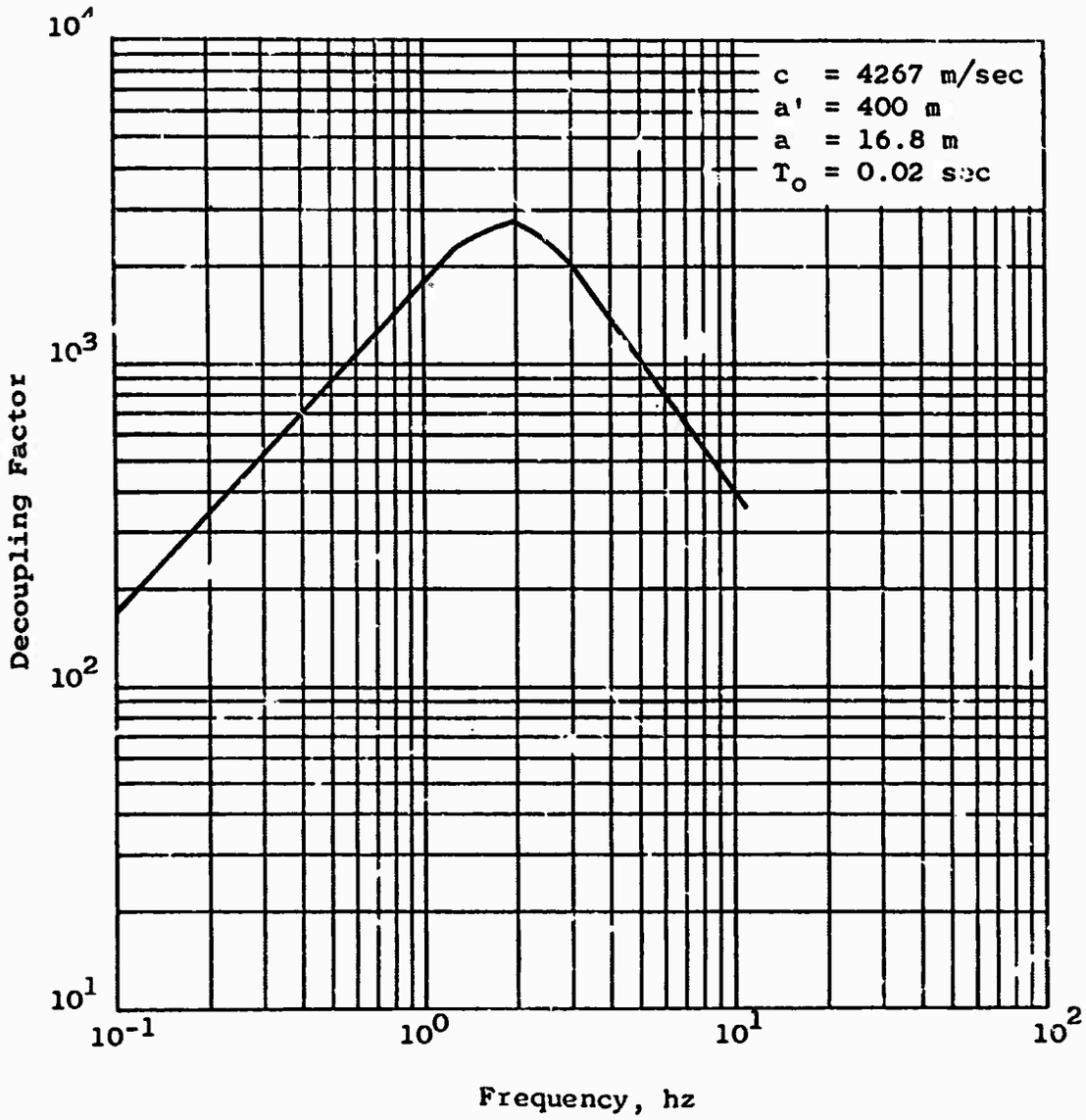

Figure 4.17 Decoupling Factor for Exponential Function Pressure Profile, $p(t)=p\ e^{-|\tau|}\ H(\tau)$.

CHAPTER 5

CONCLUSIONS

5.1 CONTAINMENT

The prediction that the Sterling event would be contained was substantiated. Although no post-shot drilling program has yet been conducted, the fact that Sterling was contained substantiated ERC's evaluation of such items as the adequacy of stemming and the depth of burial.

5.2 SEISMIC

All observed peak motions were less than predicted for a fully tamped event of this yield. Compared with the predictions using a decoupling factor of 20, the observed peak displacements and velocities were less than predicted at all stations, and peak accelerations were larger than predicted at stations within 1 km and less at more distant stations. The observed rates of attenuation of particle acceleration and velocity were considerably greater than the predicted rates which were based on Salmon data.

The data did not show abnormal scatter. Some azimuthal variations were observed, but the variations were small in comparison to the observed azimuthal variations in the Salmon data.

The frequency content was defined at eleven locations. Peak amplitudes were associated with frequencies ranging

from 3 to 80 hz. A general decrease in frequency with increasing distance was observed.

The seismic signal from the Sterling event was decoupled and the amount of decoupling was dependent on frequency. Between 2 and 5 hz, the particle velocities were decoupled by a factor of about 200. Between 1 and 8 hz, the decoupling factor was 100 or greater. An expontential decrease in decoupling was observed for frequencies outside the 2 to 5 hz range. The frequency dependence of the observed decoupling factors, i.e., the shape of the decoupling factor versus frequency curve, agreed very closely with calculations made using the decoupling theory.

REFERENCES

1.1 Memorandum from R. H. Johnston, Jr., Classification Officer, NVOO; Subject: "Declassified Yields of Continental Test Events," PAA-JHP-79; March 16, 1967.

1.2 Memorandum from W. R. Cooper, Plans Division, NVOO; Subject: "Unclassified Excerpt from LRL's Sterling Technical Concept," PDA:KNJ-501; July 15, 1966.

2.1 Bureau of Mines; "Salt Disposal Study, Project Dribble, Tatum Dome Area, Lamar County, Mississippi"; July 1962.

2.2 Harvey, C. J. and R. V. Chafin; "Geology and Hydrology of the Tatum Salt Dome, Lamar County, Mississippi," Technical Letter: Dribble-34; USGS; April 29, 1963.

2.3 Taylor, R. E.; "Geologic Section and Hydrologic Observations at Station 1A, Tatum Salt Dome, Lamar County, Mississippi," Technical Letter: Dribble-49; USGS; February 25, 1966.

2.4 Eargle, D. H.; "Geology of Core Hole WP-4, Tatum Dome, Lamar County, Mississippi," Technical Letter: Dribble-19; USGS; April 25, 1962.

2.5 Roland F. Beers, Inc.; "Summary Report of Predictions, Dribble Series," NVO-1163-10(R); June 15, 1964.

2.6 LRL Drawing AAA-66-116277-0, "Project Sterling Station 1A Stemming Plan," Ward; September 27, 1966.

2.7 Hazleton-Nuclear Science Corporation; "Ground Water Safety - Salmon Event, Project Dribble," VUF-1027; December 13, 1965.

2.8 Roland F. Beers, Inc.; "An Empirical Data Summary of Underground Nuclear Events (U)," NVO-1163-5, Rev. 1; April 8, 1966; SECRET/RD.

2.9 Preston, R. G. and W. M. Adams; "Progress Report #2, Predicted Phenomenology and Effects for Project Dribble Test Detonations," UOPAC 61-134; University of California, Lawrence Radiation Laboratory; May 1961.

2.10 Rawson, D. and P. Randolph; "Post-Explosion Environment Resulting from the Salmon Event," UCRL-14280, Rev. II; University of California, Lawrence Radiation Laboratory.

2.11 Roland F. Beers, Inc.; "Analysis of Ground Motion and Containment - Salmon Event, Project Dribble," VUF-1026; August 26, 1965.

2.12 "Event Sterling Seismic Report," CGS-101-Em; U. S. Coast and Geodetic Survey, Special Projects Party, Las Vegas, Nevada.

4.1 Latter, A. L., E. A. Martinelli, and E. Teller; "A Seismic Scaling Law for Underground Explosions," Physics of Fluids, Vol. 2, No. 1, pp 280-282; 1959.

4.2 Latter, A. L., R E. LeLevier, E. A. Martinelli, and W. G. McMillan; "A Method of Concealing Underground Nuclear Explosions," Journal of Geophysical Research, Vol. 66, No. 3, pp 943-946; 1961.

4.3 Boardman, C.; Memorandum to O. H. Roehlk, AEC/NVOO, SDK 65-11; Lawrence Radiation Laboratory, Livermore, California; August 11, 1965.

APPENDIX "A"

Table A-1. Internal Energy Table (Reference 2.9)

$T^{o}K$	E k cals/kg
300	51.18
700	122.6
2,400	513.6
3,800	1,083.
4,200	1,320.
5,000	1,772.
6,000	2,278.
7,000	3,025.
8,500	5,400.
10,000	7,699.
11,000	9,071.
12,000	10,070.
14,000	11,900.
15,849	13,420.
17,783	15,750.
25,119	28,500.
28,184	33,820.
31,623	29,080.
35,481	44,010.
39,811	50,260.
44,668	59,470.
50,000	72,000.
70,000	123,000.
90,000	186,000.

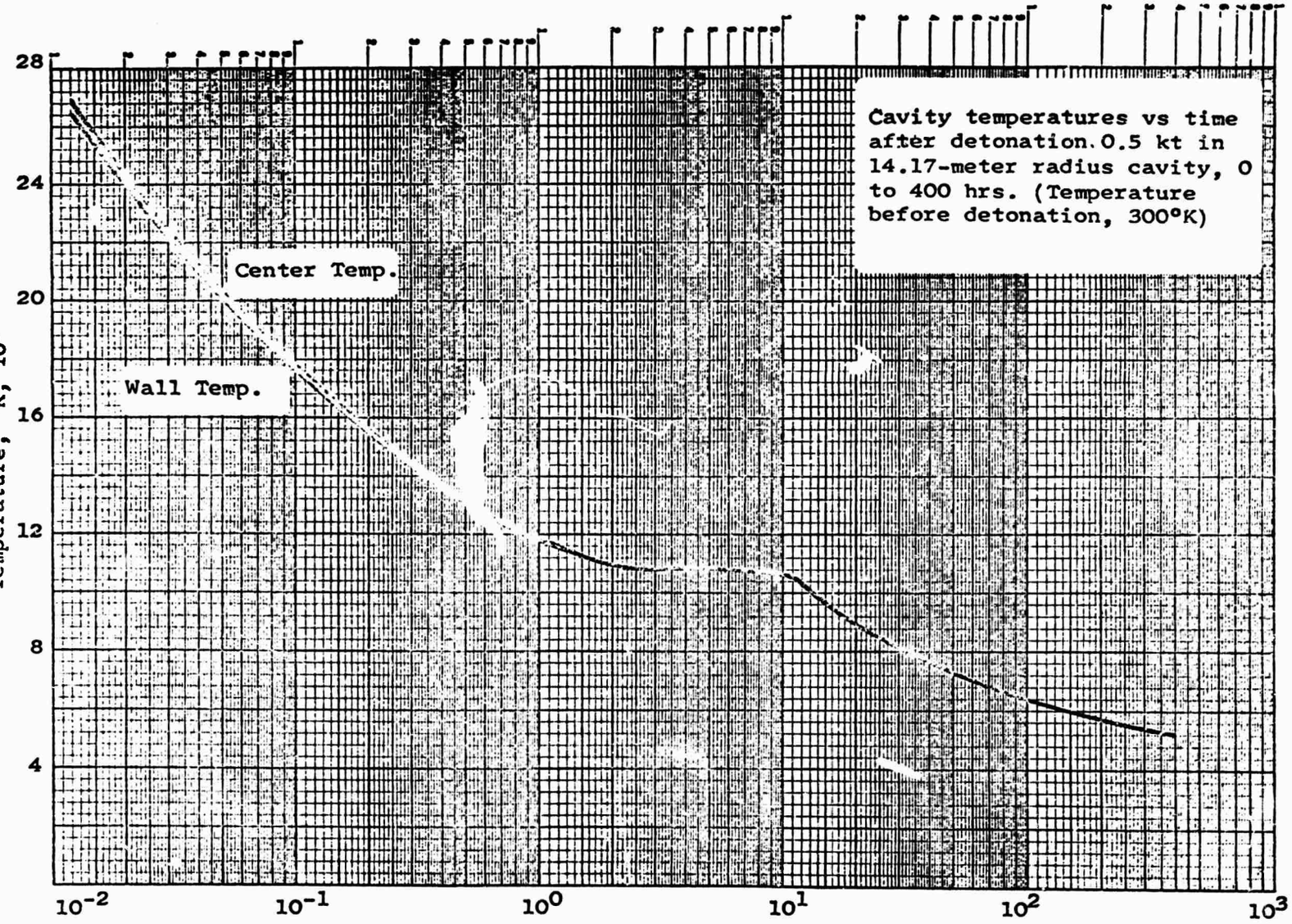

Figure A1 (Redrawn for Reproduction from Fig. D-2B Reference 2.9 with permission of LRL)

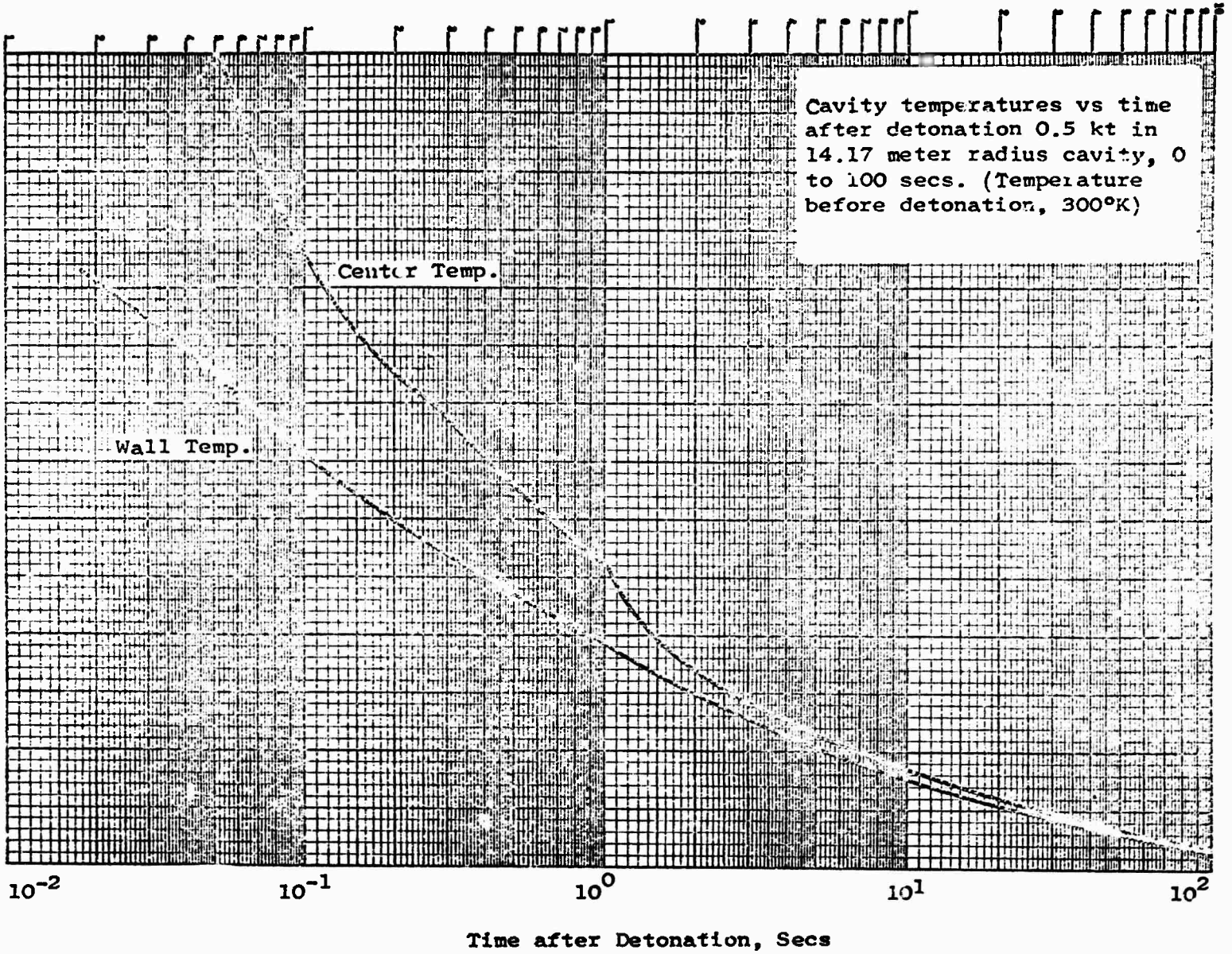

Figure A2 (Redrawn for reproduction from Fig. D-2A Reference 2.9 with permission of LRL)

PROJECT STERLING REPORTS

SAFETY REPORTS

Report No.	Agency	Title
ERC	VUF-1035	Analyses of Ground Motion and Containment
USPHS	VUF-1036	Off-Site Surveillance
ESSA/ARFRO	VUF-1037	Weather & Radiation Predictions
REECo	VUF-1038	On-Site Health and Safety
FAA	VUF-1039	Federal Aviation Agency Airspace Advisory
H-NSC	VUF-1040	Hydrologic Safety Evaluation
USBM	VUF-1041	Pre- and Post-Shot Safety Inspections of Oil and Gas Facilities
USGS	VUF-1042	Well Aquifer Response to the Sterling Event, Tatum Dome
USGS	VUF-1043	Chemical and Radio-Chemical Quality of Water Following the Sterling Event
JAB	VUF-1044	Structural Response

TECHNICAL REPORTS

LRL, SC	VUF-3025	Subsurface Phenomenology Measurements Near a Decoupled Nuclear Event
USC&GS USGS GEO TECH LRL	VUF-3026	Decoupling of Seismic Waves By a Shot-Generated Cavity
TI	VIF-3027	Radioactive Gas Analysis
II	VUF-3028	Detection of Radionuclides

List of Abbreviations for Technical Agencies
Participating in Project Sterling

ERC	Environmental Research Corporation Alexandria, Virginia
ESSA/ARFRO	Environmental Science Services Administration Air Resources Field Research Office Las Vegas, Nevada
FAA	Federal Aviation Agency Los Angeles, California
GEO TECH	Geotechnical Corporation Garland, Texas
H-NSC	Hazelton-Nuclear Science Corporation Palo Alto, California
II	Isotopes, Inc. Westwood, New Jersey
JAB	John A. Blume San Francisco, California
LRL	Lawrence Radiation Laboratory Livermore, California
REECo	Reynolds Electrical & Engineering Co., Inc. Las Vegas, Nevada
S[illegible]	Sandia Corporation Albuquerque, N. M.
TI	Texas Instruments, Inc. Dallas, Texas
USBM	U. S. Bureau of Mines
USC&GS	U. S. Coast & Geodetic Survey Las Vegas, Nevada
USGS	U. S. Geologic Survey Denver, Colorado
USPHS	U. S. Public Health Service Las Vegas, Nevada